Enhanced Calibration of Steady-State Wake Models for Innovative Helix Control in Wind Farms

Exploring the Influence of the Helix Approach on Model Parameters Calibration

Margherita Perrero

Delft University of Technology

Enhanced Calibration of Steady-State Wake Models for Innovative Helix Control in Wind Farms

Exploring the Influence of the Helix Approach on Model Parameters Calibration

by

Margherita Perrero

Student Name	Student Number
Margherita Perrero	5855888

Instructor:	Jan-Willem Van Wingerden
Teaching Assistant:	Tim Dammann
Project Duration:	November, 2023 - August, 2024
Faculty:	Faculty of EECMS (Electrical Engineering , Mathematics and Computer Science), Delft

TU Delft

Acknowledgements

The past months dedicated to writing this thesis have been a profound learning experience that I will always carry with me. I developed patience, dedication, and a sense of fulfillment, while also deepening my understanding of aerodynamic modeling and wind farm optimization. This journey would not have been possible without the continuous guidance and support of many people.

I would like to express my deepest gratitude to Jan-Willem Van Wingerden for his invaluable guidance, support, and insightful feedback. Your advice helped me stay focused and find the right direction throughout this process. I am truly grateful for the opportunity to work with and learn from you. I also wish to sincerely thank my daily supervisor, Tim Dammann, for introducing me to this topic and for always being available to answer my questions and address my doubts. I have gained a lot from your guidance, and your advice will remain with me. I would also like to express my gratitude to Marcus Becker and Wei Yu for their willingness to be part of my final evaluation committee.

Last but not least, I am deeply grateful for the immense support and warmth of my family and friends. This journey would have been far more difficult without you. Thank you for believing in me when I doubted myself and for lifting me up every time I stumbled. You will always be my happy place and my greatest achievement.

Abstract

The global demand for renewable energy is driving the rapid growth of the wind energy sector, with wind farms increasingly preferred over stand-alone turbines due to their operational and economic benefits, such as reduced deployment costs, operational efficiencies, and minimized land use. Effective wind farm operation depends on optimizing energy extraction, necessitating accurate energy yield predictions. Traditional wind turbine operation focuses on maximizing individual performance, often overlooking interactions within wind farms that can lead to suboptimal overall performance due to wake effects. Wakes are characterized by reduced wind speeds and increased turbulence downstream of turbines, negatively impacting the performance of downstream turbines. Managing these wakes is crucial for improving overall wind farm efficiency. Wind Farm Flow Control (WFFC) aims to enhance wind farm performance by managing wake effects through dedicated control strategies. Aerodynamic effects are accounted for by the controller using specific models.

This thesis addresses the need for integrating advanced control techniques, such as Individual Pitch Control (Helix Approach), into engineering wake models to improve wind farm simulations and real-time control applications. To achieve this, the research identifies the most suitable wake model by examining the performance of various models implemented in PyWake, selecting the Super Gaussian model for its superior accuracy in representing near-wake behavior. A robust calibration framework is developed, balancing precision and computation time. The thesis investigates the stability of the calibration process, addressing common optimization challenges such as local minima, and identifies strategies to ensure the global optimum configuration.

The sensitivity of model parameters to different inflow conditions is analyzed, allowing the calibration process to be generalized across a range of wind speeds within the partial load region of the power curve. This generalization reduces the need for frequent recalibration, streamlining the process.

The research further explores the responsiveness of different helix approach configurations to establish correlations between control signal amplitudes and model parameters. The newly extended model incorporates helix approach information through parameter calibration for varying pitch angle amplitudes, demonstrating a polynomial relationship between model parameters and control signal amplitudes. This integration reduces the calibration requirement to a single procedure, enhancing model adaptability.
Finally, the extended model is tested for optimizing online wind farm performance across different external environmental conditions. The helix approach shows significant improvements in reducing wake losses and increasing overall wind farm efficiency, particularly in turbine clusters. Comparisons with traditional "greedy control" highlight the helix approach's advantage, with power output increasing by up to 17% in clusters of five turbines when upstream turbines utilize helix control.

This thesis contributes to the field by providing a comprehensive approach to wind farm modeling and control, facilitating the practical application of advanced control strategies. The integration of control data into engineering wake models not only enhances calibration processes but also broadens their practical applications, paving the way for more efficient and sustainable wind farm operations.

Contents

Nomenclature

The terms and definitions used throughout this work are listed below to ensure clarity and consistency.

Abbreviations

Abbreviation	Definition
NS	Navier-Stokes
RANS	Reynolds-Averaged Navier-Stokes
LES	Large Eddy Simulation
CFD	Computational Fluid Dynamics
DNS	Direct Numerical Simulations
LIDAR	Light Detection And Ranging
SCADA	Supervisory Control And Data Acquisition
OF	Objective Function
DE	Differential Evolution
ES	Evolution Strategies
PSO	Particle Swarm Optimization
ML	Machine Learning
AI	artificial Intelligence
WFFC	Wind Farm Flow Control
DIC	Dynamic Induction Control
DIPC	Dynamic Individual Pitch Control
BEM	Blade Element Momentum
RMSE	Room Mean Square Error
FAST	Fourier Amplitude Sensitivity Testing

Symbols

Symbol	Definition	Unit
U_∞	Free Stream Velocity	[m/s]
D	Turbine Diameter	[m]
D_w	Wake Outer Diameter	[m]
a	Induction Factor	[-]
C_T	Thrust Coefficient	[-]
C_P	Power Coefficient	[-]
I_0	Atmospheric Turbulence	[-]
I_w	Wake generated Turbulence	[-]
α	Expansion constant in Jensen model	[-]
A	Nygaard and Turbo Gaussian model parameter	[-]
c_1	Nygaard and Turbo Gaussian model parameter	[-]
c_2	Nygaard and Turbo Gaussian model parameter	[-]
k	growth rate in Bastankhah model	[-]
a_1	Niayifar model parameter	[-]
a_2	Niayifar model parameter	[-]
a_s	Super Gaussian model parameter	[-]
b_s	Super Gaussian model parameter	[-]
c_s	Super Gaussian model parameter	[-]

Symbol	Definition	Unit
b_f	Super Gaussian model parameter	[-]
c_f	Super Gaussian model parameter	[-]

1 Introduction

The global demand for renewable energy is fueling the rapid growth of the wind energy sector, emerging as a fundamental contributor to meeting growing electricity demands. Stand-alone wind turbines are becoming increasingly rare due to the advantages of clustering turbines in wind farms. These benefits include reduced deployment costs of the turbines and electricity grids, reduced operation and maintenance costs, and reduced land use and impact [12]. However, grouping turbines together leads to a significant decrease in performance due to the interactions between them. When a turbine extracts kinetic energy from the wind, it creates a wake downstream, characterized by reduced wind speeds, increased turbulence, and vortex formation. Downstream turbines will then experience different inflow conditions which lead to lower energy production and higher mechanical load and fatigue.
Essential to maximizing the effectiveness of wind farms are robust strategies for optimizing energy extraction and employing advanced control methods. Accurate prediction of energy yield plays a key role in these efforts, facilitating efficient resource management and enhancing overall operational performance. Currently, the primary focus in wind turbine design and operation is on maximizing the performance of individual turbines, often neglecting their interactions and the presence of wakes, which can lead to suboptimal overall performance [12]. These wakes not only affect downstream turbines but also interact with each other, significantly complicating wind farm dynamics and necessitating a shift towards comprehensive wind farm-level control.

Wind Farm Flow Control (WFFC) aims to increase wind farm performance by determining control actions based on measurements and potentially using an internal model to simulate the airflow ([12]). Wake effects can be managed through control strategies that adjust the wind turbine operational configuration, reducing the shadowing effect turbines have on each other and decreasing wake losses. It has been an active research topic since 1988 when Steinbuch et al. [66] proposed the first attempt to control the wind farm flow through axial induction control to enhance energy capture. Today, in addition to axial induction control, wake steering is playing a major role and is the most developed and commercialized strategy in the industry. Recently, research has focused on manipulating wakes to increase wind farm energy production directly influencing wake mixing and turbulence. The most promising strategies include Dynamic Induction Control ([32]) and Dynamic Individual Pitch Control ([26]) which both have been intensively studied when sinusoidal actuation signals are applied (Dynamic Individual Pitch Control is often referred as helix approach due to the helical wake pattern produced). The former produces a larger structural loading on the turbine compared to Individual Pitch control due to the rapid changes in the induction factor, bringing the latter to being very appealing.

In order to design an effective control system for wind farms, it is crucial to represent both individual turbines and the overall wind farm flow behavior accurately. This involves using appropriate turbine models, wind farm flow aerodynamic models, and control systems [2]. Wind farm flow aerodynamic models are generally classified into three categories: high fidelity, medium fidelity, and engineering models (also referred to as low fidelity models). Each category offers a different balance between accuracy and computational efficiency, addressing various stages of wind farm design and operation. In initial wind farm design stages, high-fidelity models are typically preferred for their precision despite their higher computational demands. However, during operational phases requiring rapid and online responses, engineering models prove to be more practical [12]. When external conditions change (revealed by sensors or external information), a message to the wind turbine controller must be sent to track the new situation. This action must be quick if the farm wants to react promptly to variations. Adjusting the control state requires real-time insights into the flow field, accessible from dedicated engineering models.

The key objective of wind farm modeling and control is to account for interactions within the wind farm and use control variables to ensure a specific level of performance. Engineering models, with appropriate formulations, can encompass a broad spectrum of operational conditions influenced by diverse control strategies. Moreover, their adjustable parameters enable high accuracy across varying external environmental conditions. They can be fine-tuned to match the specific environmental settings. In literature it is possible to find several engineering models with standard parameter values which were retrieved for particular ranges of applications ([40], [53], [5], [51], [81], [55], [11]). However a further calibration is recommended for specific purposes. Parameters can be calibrated using SCADA data, as demonstrated by [24]. Lidar measurements ([17], [80]) and wind tunnel experiments ([43]) can also be employed for calibration. Additionally, also high fidelity simulations such as large eddy simulations are used for the purpose ([5],[11],[51]). Current literature primarily focuses on extending existing models by incorporating correlations with external and operational parameters such as turbulence intensity and thrust coefficient (Nyayifar and Portè-Agel [51] expanded upon [5] to incorporate turbulence effects). However, there remains a notable scarcity of research into the calibration procedures themselves and the potential complexities that may arise during their application.

Moreover, engineering models have never been calibrated under conditions where wake mixing is induced through dynamic individual pitch control, and this issue has not received sufficient attention. To accurately represent such scenarios, model calibration is necessary for each specific control configuration, even if external factors like wind speed and turbulence remain constant. Although this process is crucial for improving engineering models, it is also highly labor-intensive and repetitive. Consequently, incorporating control information into existing engineering models could streamline the calibration process and expand their practical use by significantly reducing the need for repeated calibrations.

1.1. Research Gap and Research Question

Extensive research has been conducted on wake models, with calibration playing a key role in refining and validating them for specific conditions. These models vary in their emphasis on different dependencies related to wind inflow and operational conditions. Given advancements in wind farm control technology, there is an undeniable need for wake models capable of accommodating these factors.

The unsolved question is therefore:

What is the relationship between control inputs and the calibrated parameters in engineering models? And how can this relationship be utilized to expand existing models to have a comprehensive simulation of the wind farm for real control applications?

The aim of this work is trying to answer to this question or at least expand the knowledge of the correlations between the interacting parameters. To achieve this, various sub-questions derived from the main research question will be addressed sequentially.

- What is the most suitable wake engineering model for this analysis?
  The main wake models implemented in PyWake ([56]) are investigated and the most appropriates for the analysis at hand are selected. Many of these models are specifically designed for certain atmospheric conditions, limiting their applicability. At the end a single wake model will be selected for its higher accuracy and adaptability.
- What calibration methods can be used to effectively capture fine details?
  The main focus in this thesis is building a robust framework for the calibration. By examining various optimization algorithms, a solution is identified that balances precision and computation time. The analysis is conducted for all the wake models tested to highlight the superiority of the selected algorithm, which consistently outperforms the others.
- How stable is the model formulated?

A straightforward question is whether the implemented procedure identifies the optimal configuration of results. The issue of local minima, a common challenge in optimization, is addressed, and various strategies are outlined to mitigate and reduce its negative impact on the results. Fine-tuning the optimizer's hyperparameters directs the computational effort towards the region where the optimal solution is likely to be found, thereby helping to avoid local minima.

- How sensitive are the parameters depending on different inflow conditions?
  The analysis is designed to be as universal as possible, aiming to identify the range of environmental conditions under which it remains valid. To achieve this, the impact of various incoming wind fields is examined across different wind speeds to observe their effects on the calibrated parameters. The goal is to determine whether the procedure can be generalized within the selected range. This approach may ultimately reduce the need for calibration and streamline the overall process.
- Which control techniques and control settings are the most responsive to find such a correlation?
  Due to the newly identified advantage of the helix approach as a control strategy, its characteristics aim to be captured by calibration of the parameters. The main question has been addressed by establishing correlations between model parameters and the amplitude of the control signal by keeping the signal frequency constant.

Finally, the model can be applied by incorporating control information to demonstrate its effectiveness in optimizing wind farm operations. This application not only highlights the benefits of a comprehensive engineering model for improving performance but also underscores the potential of the helix approach in increasing energy extraction. This reinforces the need to integrate the helix method into the latest advancements in the field.

- What benefits does control bring to wind farm simulations?
  The new extended model that takes into account the helix approach information in its formulation is finally tested for its intended purpose: optimizing on-line wind farm performance for different wind speeds and wind directions. The benefit of the helix approach is showed comparing its performance to normal ”greedy control” where the turbines are operating to maximize their own singular performance.

2
The State-of-the-Art in Dynamic Control and Wake Models

Engineering models play a crucial role in the wind industry and research, serving as the backbone for the design, optimization, and performance prediction of wind energy systems. These models are indispensable because they allow engineers and researchers to simulate and analyze the complex interactions within a wind farm, which influence the efficiency and reliability of wind turbines. The complexity of these models arises from the need to accurately represent a multitude of interacting factors. Engineering models typically comprise wake models (which account for the effects generated by turbines on downstream performance), turbulence models, superposition models (which analyze the interaction of different wind flows produced by the turbines), deflection models and blockage models (to evaluate the impact of physical obstructions on wind patterns)[56]. These models not only assist in optimizing the design and layout of wind farms but also play a crucial role in the operation of turbines. The operation of wind turbines follows sophisticated control strategies that manage blade pitch, rotor speed, and yaw angle to adapt to varying wind conditions. By integrating these control systems, engineering models enhance the precision of simulations, enabling real-time optimization of turbine performance.
This thesis primarily focuses on engineering wake models using the open-source software ”PyWake” for modeling and simulating wind farms. Section 2.1 focuses on the state of the art of wind farm control describing the main techniques both already commercialized and in phase of development. Section 2.2 gives as overview of the main engineering wake models and 2.3 the necessity of calibration for correct level of description. Finally 2.4 gives a small overview of the software *PyWake* used for the overall analysis.

2.1. Wind Farm control

The importance of control in wind farms extends across various aspects, each contributing to the efficient and reliable generation of wind energy ([46], [23]). To begin with, control systems play a crucial role in maximizing energy capture by finely tuning the alignment of turbine blades with the prevailing wind direction. This deliberate optimization enhances kinetic energy capture and, consequently, improves overall energy production efficiency. The integration of advanced control algorithms facilitates real-time adjustments to the pitch and yaw of turbine blades, ensuring optimal performance in response to diverse wind conditions ([46]). Coordinating the individual turbines is essential for achieving optimal performance at the power plant level. Furthermore, the importance of control systems is evident in ensuring grid stability and integration of wind energy into the broader electrical grid. The intermittent and variable nature of wind energy can introduce challenges to grid stability. Control systems address this by smoothing out fluctuations, managing the output of individual turbines, and coordinating their operation. This, in turn, guarantees a stable and reliable power supply, facilitating the integration of wind energy into the electrical grid. Control systems also play a crucial role in load mitigation and structural health monitoring of wind turbines. Given the varying wind speeds and turbulent conditions to which turbines are exposed, mechanical stresses can occur. Control systems incorporate features for load mitigation, dynamically adjusting turbine operations to reduce mechanical loads during extreme conditions.The problem is clearly a multi-objective optimization that is still in the phase of actuation because of its complexity. The research and development is now focusing on the impact control technologies have on wake effects and consequently on power production and structural loading ([2],[46]).

Evolution of Controls in Wind Farms

Wind turbine control can be analyzed at two levels: individual turbine level and farm level.
Turbine level control aims to optimize the power extracted by a single turbine while considering its operational limits. The monitoring during normal operation is entrusted to the operational or turbine-level control ([52]). Four main regions can be distinguished depending on the turbine mode of operation and they can be easily observed through a variable-speed wind turbine power curve (Figure 2.1). Every region has a different purpose accomplished by different control objectives.

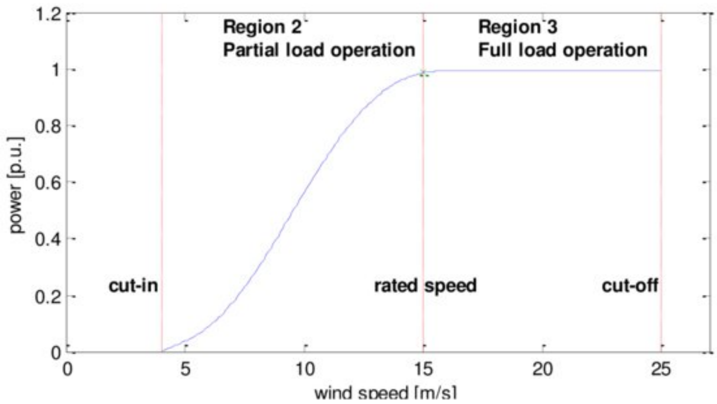

Figure 2.1: Wind Turbine power curve (normalized in the range from 0 to 1) from [33]. Partition in different operational regions depending on the incoming wind speed.

Region I covers the wind speeds below cut-in where the turbine is not operating because of the large losses experienced by low wind speeds. Region II, which is also called partial load region, maximize the power produced by the turbine while Region III (full load region) limits the power produced at the rated value to avoid mechanical and electrical damage. Partial region transition towards a full load region happens at the rated wind speed and particular attention must be brought to this operational area where the operational mode is changed. Region IV starts after cut-off wind speed where the turbine is stopped (shutdown process). When wind speed is higher than cut-in but lower than rated value (Region II), power extraction is maximized by a generator torque controller. The turbine is operated at the point of optimum power efficiency which corresponds to a certain optimal value for blade pitch angle. The generator torque is used to track the maximum power point (C_P, max) by changing the rotor speed depending on the incoming wind speed. After rated wind speed the power is not maximized anymore but limited to its rated value. This is performed by keeping the generator torque constant while pitch control is activated in order to set the generator speed to the rated value ([54],[52]).
However, stand-alone turbines are increasingly rare, so research on control has shifted towards a farm level control where the overall performance is taken into account. When the comprehensive operation is considered, turbine's performances affect each others and phenomena like wakes and blockage start playing an essential role. The simplest control that can be applied from turbine to farm level is also known as greedy control. Every turbine is adjusted to operate at its maximum point regardless other turbines' operational conditions. However, even though this practice is optimal for stand-alone turbines, it does not take into consideration the influence single performances have on each other. A second distinction can be done while talking about wind farm flow control (WFFC) [46]: (quasi) static WFFC and dynamic WFFC. A (quasi) static control adapt turbine operational points to all background phenomena that have the same developing time range as the flow physics. Faster occurrences can be captured by dynamic WFFCs which can be further used to influence the wake mixing and the turbulence produced.
The first effort to regulate the impact of wake effects involved the use of static axial induction control

and static yaw angles control. Static induction control (or derating control) aims at reducing the axial induction set point of upstream turbines which are operated away from their optimum resulting in smaller power production but also in lower wind deficit in the wake. Downstream turbines' energy extraction is therefore increased and the overall performance of the wind farm can benefit from it if the control implementation is properly optimized. However, down-rating the turbines also yield to a slower recovery of the wake and the benefit of this technique has been found to be very little compared to the original expectations [46]. Static yaw control, also called wake steering refers to a control strategy that operates on yaw angles to improve wind farm performance. The wake behind a turbine is deflected from its original trail (aligned with the wind direction to extract the maximum quantity of energy) in order to redirect the wake not towards downstream rotors. A challenge in this implementation is the structural loading, which increases when the turbine operational point is moved from the optimum. This technique is already implemented by Siemens Gamesa leading the way for industrial applications [28].
The new frontier of research is dynamic wind farm control through manipulation of the wake. The main purpose is increasing wake mixing by varying turbine's operational set points over time. Because of mixing, the wind turbine wake is restored faster, leading to higher incoming wind velocity for downstream turbines. Recently two main methods have gained interest in the scientific field: Dynamic induction control and dynamic individual pitch control.
Dynamic induction control (DIC) has been widely studied and tested in wind tunnels and through large eddy simulations. Goit and Meyers ([32]) first tried to implement the new method using a receding horizon control. However, it ended up being too complex and other solutions including sinusoidal variations of the thrust set point were investigated ([47]). The potential of periodic dynamic induction is then proved through simulation environments and in wind tunnel experiments with the work of Frederik et al. [27]. The new approach overtakes the traditional induction control by varying the induction factor over time and causing a turbulent flow that enhance wake mixing and recovery. Munters and Meyers proposed [47] this excitation to be sinusoidal and respective optimal amplitude and frequency have been evaluated that maximize the energy extraction. The optimal frequency corresponds to a Strouhal number (St) of 0.25 where $St = \frac{fD}{U_\infty}$(f, D and U_∞ are frequency, rotor diameter and inflow velocity respectively). Nevertheless, because of the varying induction factor, the thrust force on the rotor varies significantly causing load fluctuations.
Dynamic individual pitch control (DIPC) aims at controlling blade pitch angles individually through periodic signals and manipulating the wake to induce wake mixing ([26]). It comes from the already known concept of individual pitch control to reduce loads [13] proposed by Bossanyi and combined with dynamic excitation. Frederik et al. ([26]) proposed to dynamically manipulate the wake by altering individual pitch angles to generate directional moments on the rotor. The direction of the forces exerted on the rotor continuously change, varying the direction of the wake and inducing mixing. The propagation in space results in a helical shape, therefore this approach has been named *helix approach*. The wake motion is both in horizontal and vertical directions that correspond to yaw and tilt moment components respectively. The effect of periodic excitation has been studied. Tilt and yaw pitch angle components are excited with the same frequency which is much lower than the rotational frequency. Depending on the angle shift between the two components, the motion can correspond to clockwise or counterclockwise motions. If there is an offset of 90° between tilt and yaw pitch angle, a counterclockwise motion can be observed, while if the offset is of 270°, the rotation is clockwise. It is also been observed that the counterclockwise motion is much more effective than clockwise, leading to a faster recovery of the velocity and higher energy gain with respect to a baseline implementation with only a greedy control applied.

2.2. Engineering Wake Models

As mentioned before, WFFC relies on the aerodynamic flow within the wind farm and particularly on the presence of wakes, which must be modeled accurately. Wake models can be divided in two main categories: empirical models and computational models ([63]).
Empirical models, or low-fidelity models, describe the wake through analytical expressions based on conservation of mass and momentum ignoring the exact nature of the flow field.
On the other hand, computational models solve physical equations also known as Navier-Stokes (NS) equations. While this set of equations offers a comprehensive model for describing turbulent flows, solving them is challenging. The complexity arises from the non-linear convective term, which intro-

duces a broad spectrum of time and length scales, making turbulent flows particularly difficult to address. Therefore it is necessary combine them with the aid of additional models and simplifications for the smaller scales [60]. NS equations can be time-averaged and decomposed using Reynolds decomposition, which separates the flow into mean and fluctuating components, obtaining at the end a set of averaged equations called RANS (Reynolds-Averaged Navier-Stokes). Turbulence effects are represented in RANS by introducing additional equations such as mixing length model, k-eps model or Reynolds stress model. Large eddy simulations (LES) are another approach in computational fluid dynamics (CFD) used to describe the fluid flow, resolving large turbulent structures while modelling the effect of smaller scales. This technique requires higher computational resources than RANS but is more accurate. While in RANS a turbulence model was needed, direct numerical simulations (DNS) are solved directly from NS equations capturing all turbulent structures. DNS provide the most accurate representation of the turbulent flow but it also requires a very high computational cost, not suitable for the analysis of atmospheric flows.

Because of the higher computational effort required by CFD approaches and the necessity of rapid information for on-line control, investigation is focusing more and more on the development of highly accurate empirical wake models [12]. Empirical or engineering wake models respect mass and momentum conservation laws and are tailor-made for every situation that wants to be described through additional parameters added to fit empirical observations. These models not only describe the wake velocity deficit, but also the underlying physics and interactions between different wakes. A more detailed explanation will be provided in Section 2.4 where the simulation tool PyWake is introduced and its functionalities are explained.

Wind turbine wake's description can be divided in two regions depending on power losses and loading: near wake and far wake ([3],[63]). In the near wake, characteristics of the flow are directly influenced by turbine geometry. Pressure gradient is very significant and strong turbulence is created at the blade edges. In the far wake, the pressure gradient is less relevant and flow conditions are dominated by convection and turbulence diffusion. Atmospheric and topographic effects start having a bigger impact. It's important to model accurately both near and far wake. The far wake of a turbine can still affect the incoming wind of downstream turbines, while the near wake establishes boundary conditions during the transition to the far wake.
Not every engineering wake model accurately describes both regions due to its underlying structure and assumptions. Therefore, a comprehensive analysis is required to identify models that can more rigorously represent the flow.

As previously mentioned, engineering models are based on analytical expressions that describe the flow field. The field strongly depends on topographic characteristics of the site, technical and operational characteristics of the turbine, layout of the farm and wind inflow conditions, which need to be taken into account in the model. This is done by tuning the parameters that compose the model. Every engineering model has different parameters depending on the equations that describe the phenomena. A description of the main engineering wake models will follow with a graphical representation of the wake modelled. The plots are generated through Pywake following each model's default definition and with an incoming wind speed (U_∞) of 9 m/s. In order to distinguish every model, they are named after the main author of the respective research.

2.2.1. Niels Otto Jensen (NOJ)

Jensen assumed the wake to be comparable to a negative jet and the wake expansion is assumed to be linear ([40]). The cross-wind variation is described by a top-hat distribution, which means that at each downstream location the velocity is uniform within the wake region. The model also assumes that the wake expands freely, not taking into account earth surface roughness which causes an overestimation of recovery rate in the wake. The velocity behind a single turbine can be obtained from mass conservation as:

$$U(x) = U_\infty(1 - 2a(\frac{D/2}{D/2 + \alpha x})^2) \tag{2.1}$$

D is the rotor diameter and α is the expansion constant, whose value is tuned at approximately 0.1 in the present work. A more detailed description would require a calibration of the parameter for different testing situations. The induction factor a is related to the thrust coefficient through $C_T = 4a(1 - a)$ and it is assumed to be 1/3 as it is for optimal rotors. The analysis could be extended to multiple (N) wind turbines place in the wake of one another ([1]):

$$U_N(x) = U_\infty(1 - 2\frac{k}{3}\frac{1-(\frac{k}{3})^N}{1-\frac{k}{3}}) \tag{2.2}$$

$$k = (\frac{D/2}{D/2 + \alpha_N S})^2 \tag{2.3}$$

Where S is the normalised turbine spacing in turbine radii and α_N the expansion factor for multiple turbine. Optimal rotor is a strong assumption far from being realistic, but the non-ideality is included while calibrating the expansion constant. For a large number of turbines (N), the term $(\frac{k}{3})^N$ will tend to asymptotically vanish as k is around the unity.

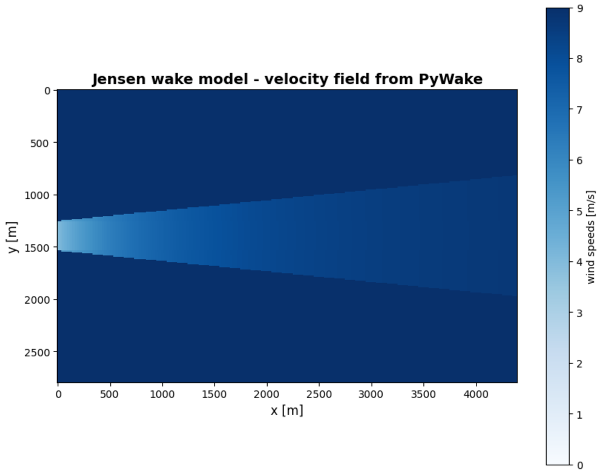

Figure 2.2: Wind velocity field generated from PyWake for Jensen model. The incoming wind speed is 9 m/s.

2.2.2. Nygaard (Turbo NOJ)

Based on the work of [40] and [42], in order not to overestimate the wake recovery rate, Nygaard et al. ([53]) proposed a new model coupling the wake expansion to the local turbulence intensity at hub height which comprises both atmospheric and wake-generated turbulence. The wake profile still has a top-hat shape but the wake expansion is no more only linearly dependent on the distance from the rotor. Equation 2.1 can be rewritten as 2.4 where D_w is the wake cone diameter.

$$1 - \frac{U}{U_\infty} = (1 - \frac{U_{in}}{U_\infty}\sqrt{1 - C_T(U_{in})})(\frac{D}{D_w(x)})^2 \tag{2.4}$$

U_{in} is rotor-averaged inflow wind speed.
Wake expansion is supposed to be locally linearly dependent on the turbulence intensity, as can be seen in Equation 2.5. The turbulence is modelled through Frandsen wake turbulence model ([25]). Total turbulence intensity and additional turbulence intensity (I_w) are defined in 2.6 and 2.7 respectively where I_0 is the atmospheric turbulence. The additional turbulence decays with distance and asymptotically vanishes, emphasizing the largest turbulence contribution closest to the turbine where the shear and wake edge is more relevant.

$$\frac{dD_w}{dx} = AI(x) \tag{2.5}$$

$$I(x) = \sqrt{I_0^2 + I_w^2} \tag{2.6}$$

$$I_w(x) = \frac{1}{c_1 + c_2 \frac{x/D}{\sqrt{C_T(U_{in})}}} \quad (2.7)$$

A, c_1 and $c2$ are calibration parameters. Integrating Equation 2.5, expression 2.8 for the wake diameter can be obtained.

$$D_w(x) = D + \frac{AI_0D}{\beta}(\sqrt{(\alpha+\beta x/D)^2+1} - \sqrt{1+\alpha^2} - \ln(\frac{(\sqrt{(\alpha+\beta x/D)^2+1}+1)\alpha}{(\sqrt{1+\alpha^2}+1)(\alpha+\beta x/D)})) \quad (2.8)$$

Two auxiliary variables have been introduced: $\alpha = c_1 I_0$ and $\beta = (c_2 I_0)/\sqrt{C_T(U_{in})}$ which are both positive.
In this model the wake recovers slower leading to larger losses for downstream turbines.

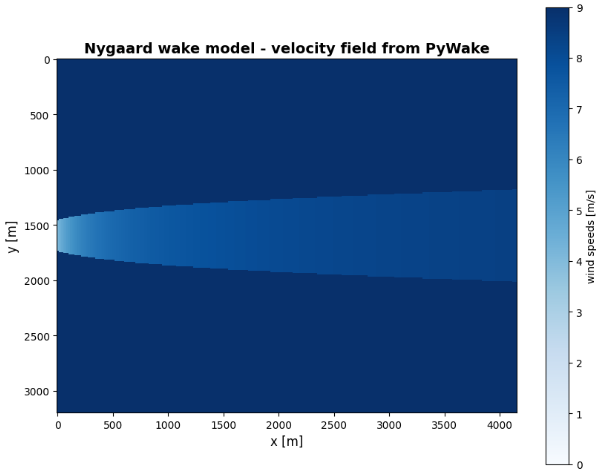

Figure 2.3: Wind velocity field generated from PyWake for Nygaard model. The incoming wind speed is 9 m/s.

2.2.3. Bastankhah

Jensen and Nygaard models both assume a uniform velocity distribution in the cross-wind plane. This assumption is highly unrealistic and the authors themselves found out that a Gaussian shape better describes the distribution for the wake velocity deficit in the wake ([40]). The work of Bastankhah and Porté-Agel ([5]) provides a more precise wake model by applying conservation of mass and momentum and assuming a Gaussian distribution. This is the simplest model that have such characteristics but it has been a turning point for the research in engineering models and a good reference for the studies. It is an accurate description especially for the far wake since after some downstream distance from the rotor, the velocity deficit resembles a Gaussian axisymmetric shape and it neglects viscous and pressure terms, which are relevant in the near wake.
The normalised velocity for a single turbine can be described with a self-similarity expression:

$$\frac{\Delta U}{U_\infty} = \frac{U_\infty - U}{U_\infty} = C(x)e^{-\frac{r^2}{2\sigma^2}} \quad (2.9)$$

r is the radial distance from the wake centreline and it is given by $r = \sqrt{(y-y_h)^2 + (z-z_h)^2}$.
C(x) represents the normalised velocity deficit at the center of the wake where it reaches the maximum value. Its value can be obtained solving mass and momentum conservation leading to the only acceptable value of Equation 2.10.

$$C(x) = 1 - \sqrt{1 - \frac{C_T}{8(\sigma/D)^2}} \quad (2.10)$$

Assuming a linear expansion for the wake $\frac{\sigma}{D} = k^* \frac{x}{D} + \epsilon$, Equation 2.9 can be rearranged as:

$$\frac{\Delta U}{U_\infty} = (1 - \sqrt{1 - \frac{C_T}{8(k^*x/D+\epsilon)^2}})exp(-\frac{1}{2(k^*x/D+\epsilon)^2}((\frac{z-z_h}{D})^2 + (\frac{y}{D})^2)) \quad (2.11)$$

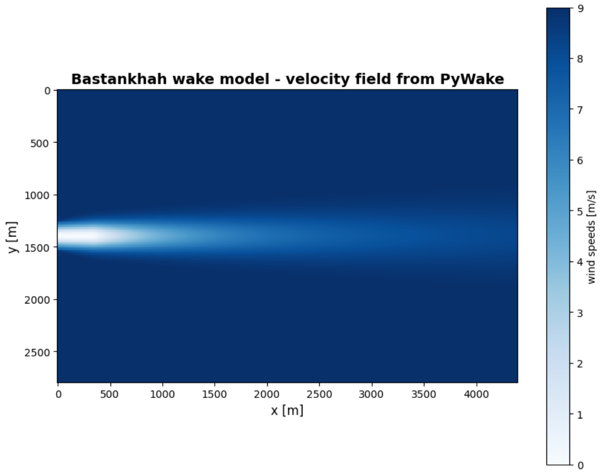

Figure 2.4: Wind velocity field generated from PyWake for Bastankhah model. The incoming wind speed is 9 m/s.

Where $k^* = \frac{\partial \sigma}{\partial x}$ is the growth rate, $\epsilon = \lim_{x \to 0} \frac{\sigma}{D} = 0.25\sqrt{\beta}$ (β is defined in 2.12), y and z are respectively spanwise and vertical coordinates and z_h is the hub height.

$$\beta = \frac{1}{2}\frac{1+\sqrt{1-C_T}}{\sqrt{1-C_T}} \tag{2.12}$$

This simple model only requires one parameter to determine the velocity in the wake: k^*. It is obtained calibrating the model with wind farm data or simulation data and it results in 0.0324555.

2.2.4. Niayifar

Niayifar and Porté-Agel ([51]) proposed a model starting from the work of [5] but reformulating the wake growth rate a function of the local streamwise turbulence intensity. This necessity comes from the unrealistic linear expansion for the wake, since it has been noticed that the wake growth rate increases when turbulence increases. Hence, the growth rate can be calculated as

$$k^* = a_1 I + a_2 \tag{2.13}$$

a_1 and a_2 are calibration parameters that are found being approximately 0.3837 and 0.003678 respectively for turbulence intensity in the range of $0.065 < I < 0.15$. Turbulence intensity is calculated immediately upwind the rotor center and it takes into consideration the effect of the nearest upwind turbines with the most significant impact. Turbulence intensity is then determined in order to evaluate the impact on downstream turbines through Crespo and Hernandez model ([19]). The total intensity is still calculated through Equation 2.6 but the added turbulence is $I_w = 0.73a^{0.8325}I_0^{0.0325(x(d)^{-0.32}}$ instead.

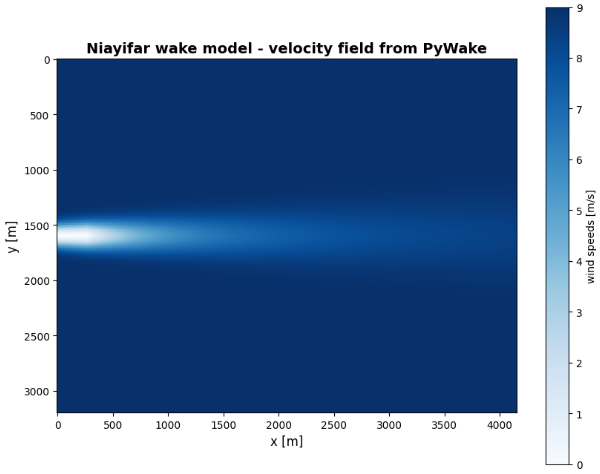

Figure 2.5: Wind velocity field generated from PyWake for Niayifar model. The incoming wind speed is 9 m/s.

2.2.5. Zong

Even if Gaussian models are based on mass and momentum conservation, this holds only for the wake produced by the single turbines. When wakes are superimposed, the total momentum is not conserved which could cause inconsistent results. Zong and Porté-Agel ([81]) propose a new model aiming to resolve such theoretical conflict.
A new wake width expression is formulated which uses the near-wake estimation x_n by ([74]) (2.15):

$$\sigma = \epsilon + k^* \ln{(1 + e^{(\frac{x-x_n}{D})})} D \tag{2.14}$$

$$x_n = \frac{1}{2} \frac{\sqrt{0.214 + 0.144m}(1 - \sqrt{0.134 + 0.124m + 0.144m})}{(1 - \sqrt{0.214 + 0.144m})\sqrt{0.134 + 0.124m + 0.144m}} \frac{D}{dr/dx} \sqrt{\frac{m+1}{2}} \tag{2.15}$$

Where $m = \frac{1}{\sqrt{1-C_T}}$ and $\epsilon = \frac{1}{\sqrt{8}} C_T$. The wake expansion rate k^* is the same as Equation 2.13.

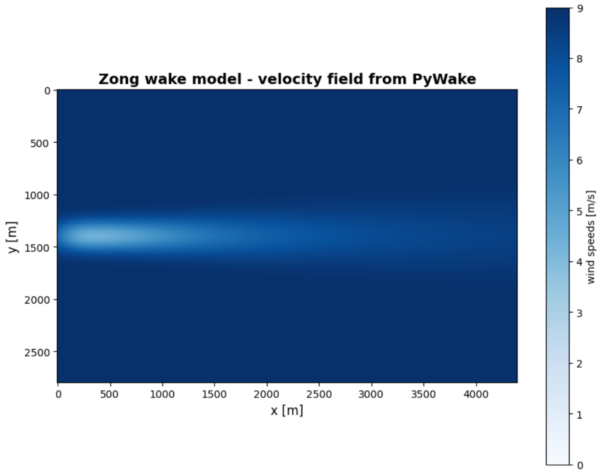

Figure 2.6: Wind velocity field generated from PyWake for Zong model. The incoming wind speed is 9 m/s.

The authors([81])found a1=0.38and a2= 4e-3 to be the best fit for the model parameters.

2.2.6. Turbo Gaussian

The present model ([55]) is based on the Gaussian deficit distribution proposed by Bastankhah and Porté-Agel ([5]) (Equations 2.9 and 2.10 still hold). The only difference is in σ/D that is not linear anymore but depends on the turbulence intensity (proposed by [42]). It is an extension of Nygaard et al. work ([51]) where a top-hat shape was assumed to describe the velocity deficit profile. The wake expansion formulation is the same as Nygaard and an equivalent espression can be retrieved:

$$\frac{\sigma}{D} = \epsilon + \frac{AI_0}{\beta}(\sqrt{(\alpha+\beta x/D)^2+1} - \sqrt{1+\alpha^2} - \ln(\frac{(\sqrt{(\alpha+\beta x/D)^2+1}+1)\alpha}{(\sqrt{1+\alpha^2}+1)(\alpha+\beta x/D)})) \tag{2.16}$$

$D\epsilon$ is the characteristic wake width at $x = 0$ where ϵ is calculated through Formula 2.17.
$\alpha = c_1 I_0$ and $\beta = \frac{c_2 I_0}{\sqrt{C_T(U_{in})}}$ where A, c_1 and c_2 are calibration parameters which are empirically fitted to 0.04, 1.5 and 0.8 respectively.

$$\epsilon = 0.25(\frac{1+\sqrt{1-C_T(u_{in})}}{2\sqrt{1-C_T(u_{in})}})^{0.5} \tag{2.17}$$

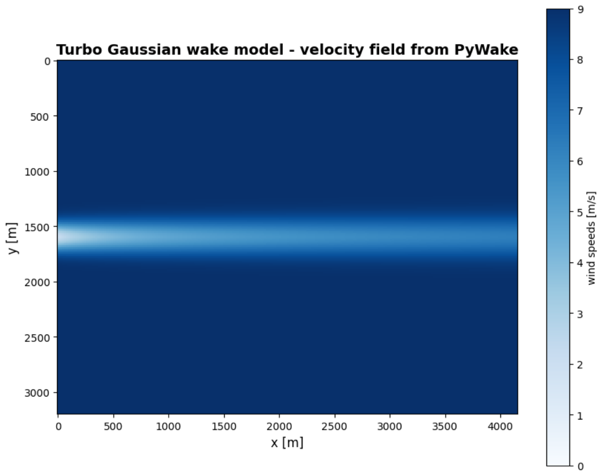

Figure 2.7: Wind velocity field generated from PyWake for Turbo Gaussian model. The incoming wind speed is 9 m/s.

2.2.7. Blondel and Cathelain (Super Gaussian)

All the models presented above are able to only describe the far wake region. Because of the different phenomena involving the two regions, it's not possible to describe uniquely the whole wake with a single distribution. Blondel and Cathelain ([11]) however found a way to fill this gap proposing an evolution of the wake deficit from top-hat to Gaussian shape using a super-Gaussian shape function. Furthermore, mass and momentum conservation laws are still valid. The super-Gaussian shape allows this transition through a parameter n that simulates a top-hat shape for high values, while for n=2 the traditional Gaussian shape is recovered. The velocity deficit is calculated as follows:

$$\frac{\Delta U}{U_\infty} = C(\tilde{x})e^{-\frac{\tilde{r}^{n(\tilde{x})}}{2\sigma^2}} \tag{2.18}$$

$$C(\tilde{x}) = 2^{2/n-1} - \sqrt{2^{4/n-2} - \frac{nC_T}{16\Gamma(2/n)\sigma^{4/n}}} \tag{2.19}$$

Wake width σ is dependent on turbulence intensity and not linear, as shown in Equation 2.20.

$$\tilde{\sigma} = (a_s I + b_s)\tilde{x} + c_s\sqrt{\beta} \tag{2.20}$$

β is the same as in 2.12.
Lastly, also n is fitted with additional parameters:

$$n = a_f e^{b_f \tilde{x}} + c_f \tag{2.21}$$

The parameters of the models that have to be calibrated are 6: a_s, b_s,c_s, a_f, b_f and c_f. This model not only can describe very well the near and far wake and the transition between the two, but having more parameters allows a more accurate calibration that results in a precise prediction of the wake flow.

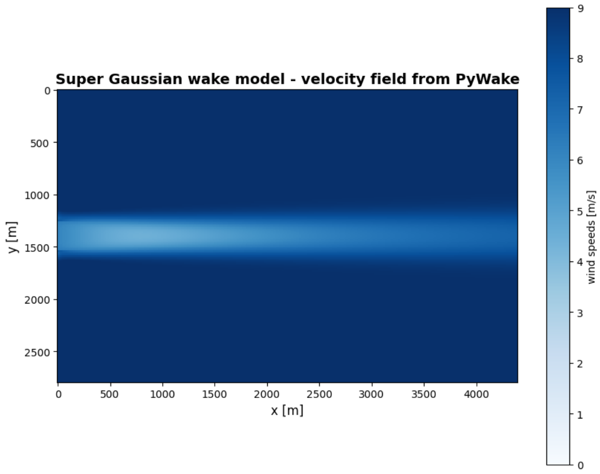

Figure 2.8: Wind velocity field generated from PyWake for Super Gaussian model. The incoming wind speed is 9 m/s.

The calibration carried out by Blondel and Cathelain end up with the following parameters for the wake expansion:
$as = 0.17$
$bs = 0.005$
$cs = 0.2$
and for the super-Gaussian order n:
$af = 3.11$
$bf = -0.68$
$cf = 2.41$

The same author Blondel then in [10] proposed a new set of calibration parameters which are dependent on turbulence intensity and thrust coefficient but are specifically dedicated to that particular study case:
$as = 0.28$
$bs = 0.01$
$cs = 0.1C_T + 0.1$
$af = -8,2635C_T^3 + 8.5939C_T^2 - 8.9691C_T + 10.7286$
$bf = 1.68exp(-25.98TI) - 1.06$
$cf = 2$

2.3. Calibration

Engineering wake models are intensively used in the wind energy industry thanks to their low computational costs and sufficient accuracy. However, their ability to describe the real nature of the wake strongly depends on the tuning of the model parameters that are strongly related to the characteristics of the site and power plant. In order to calibrate an empirical model, high fidelity data from the situation in investigation need to be provided to obtain an agreement between model predictions and experimental data. For wind field calibration usually data are collected from : Large Eddy Simulations, wind tunnel experiments, Light detection and ranging (LIDAR) measurements and data-driven high-frequency supervisory control and data acquisition (SCADA). Section 2.3.1 provides a deeper explanation of data-sets used for calibration while the main calibration procedures in literature are discussed in Section 2.3.2.

2.3.1. Experimental data for calibration

As it is for wake models, also experimental data used for tuning can affect the accuracy of the model prediction. A description of every data type will follow in decreasing order of importance:

- **Large Eddy Simulations** have been already introduced in Section 2. Because of their high accuracy, they are a very powerful tool to simulate, calibrate and validate wake models. The main difficulty in solving the flow field problem is understanding the turbulence. Turbulence is mainly composed of regions where the flow is characterized by swirling of circulating motion called eddies ([45]). Eddies can affect mass and energy transfer and they vary on the size and intensity. Large structures extract energy from the main flow and transmit it to smaller scales through energy cascade. LES resolves all turbulence scales except for those where dissipation dominates (Kolmogorov scales or small scales) that are modelled with a subgrid scale model. The wind turbine is modelled as local volume forces that extract momentum from the flow (actuator disk and actuator line).
- **LiDaR** stands for Light Detection and Ranging and it is a remote sensing technology that uses laser light to measure distances and the Doppler effect to determine the motion of air. Lidar systems emit laser pulses that interact with the moving air particles and are scattered back with a shift in the wavelength due to the Doppler effect ([80]). By analyzing the Doppler shift, the Lidar system can calculate the wind speed component parallel to the laser beam. Wind speed is not the only information that can be provided, also wind direction, temperature, humidity and pressure can be retrieved. However, lidars can have a limited number of measured points resulting in limited spatial coverage and these measurements can also suffer from poor spatial and temporal resolution.
- All wind farms have **SCADA** system as part of their equipment which can give information about meteorological conditions and wind turbine operating conditions ([71]). SCADA data usually records a wide range of data such as: wind speed, wind direction, ambient temperature, blades pitch angle and rotor speed ([70]). However, information is provided only at the turbine location while the remaining region of the wind farm flow is not measured. When it comes to predict the total power of the wind farm, information at the turbines is sufficient, while if an accurate description of the whole flow is needed it may lack of completeness.
- **Wind tunnel experiments** provide very useful data-sets but it's very difficult to recreate the real flow in the lab because assumption of similarities doesn't hold in every situation as stated in [35]. The main advantage is that particular conditions of interest can be recreated but there's a relevant difference in Reynolds numbers of the real flow and the flow in the lab. As is stated in [6], C_T and C_P depend on turbine dimensions and inevitably affect the calculations.

2.3.2. Calibration techniques

The most straightforward way to fit parameters is through an optimization algorithm. An optimization problem involves finding the best solution among a set of feasible solutions, typically defined within certain constraints. It's about maximizing or minimizing a particular objective function subject to the constraints. For a calibration process, the objective function consists on minimizing the difference between experimental data and predictions from the model. The more the error approaches zero, the more precise the calibrated parameters are. In order to have a complete set of tuned parameters, the problem must be optimized for every situation that may occur in the operational life-time of the turbine. Nevertheless, thanks to the development of AI techniques, machine learning (ML) algorithms can be trained with data sets, and if the set is wide enough the algorithm is able to associate automatically new parameters to every different circumstance.

Empirical models are widely explored in literature and their accuracy is often compared to real data from wind farms or simulations to display their potential. They are employed with the purpose of optimizing the wind energy production during operational times or to optimize the layout of the wind farm during the design stage ([29] [78]). The models are calibrated for the studied conditions accordingly, but the issue of the calibration itself is not often investigated. Zhan et al. [80] performed a minimization of the percentage error between lidar measurements and the model outputs through an heuristic method. Sood and Meyers [65] used sequential least square programming to find the optimal parameters that minimized the difference between the power and velocity field recreated from the model and extracted from Large Eddy Simulations. Other authors used heuristic methods to calibrate model parameters such as differential evolution [8] and genetic algorithm [22]. However no attention has been driven towards the definition of the optimization problem: which objective function is the most representative of the problem and which parameters boundaries can be applied universally.

2.3.3. Necessity of calibration with dynamic control

Static Induction Control involves derating individual turbines to reduce their energy extraction, thereby altering the aerodynamic wakes they generate. This method adjusts the induction coefficient by setting the turbine to extract less energy from the wind, which in turn affects the downstream wind speed and turbulence levels. The engineering models for Static Induction Control are relatively straightforward. Since the fundamental physics of wind flow and energy extraction remain unchanged, existing models can be adapted without significant modifications. In the work of Annoni et al. [4] a simple Park model (referred as Turbo NOJ by Nygaard in this work [53]) has been adopted where the optimal control configurations come from the optimal values of induction coefficients that maximises the overall power production.

Wake steering is a more dynamic and complex method. It involves intentionally yawing turbines to direct their wakes away from downstream turbines. This approach necessitates a deeper understanding of the wake dynamics and the development of new models to accurately predict the wake behavior under yawed conditions. Wake steering introduces additional aerodynamic phenomena that need to be accounted for in engineering models. These phenomena include wake deflection, increased turbulence, and changes in wake recovery rates. A yawed turbine applies a lateral force to the incoming flow generating a spanwise wake velocity that causes the wake to deflect [7]. The spanwise velocity distribution is asymmetric with respect to the wake center and has develops a kidney-shape cross-section in the far wake. Furthermore, as the rotor becomes increasingly misaligned with the incoming wind (moving away from the optimal configuration), the wake velocity deficit decreases because of reduced energy extraction. There have been attempts to model the phenomena involved and the deflection of the wake. Jiménez et al. [41] model the wake deflection using a ”top-hat” model where the wake is represented with a uniform velocity deficit. The wake is inclined at a skew angle due to the yaw of the turbine. This skew angle represents the deflection of the wake, and it is calculated based on the balance of lateral forces induced by the yawed turbine and the conservation of momentum. However, [7] observed overestimations in the wake trajectories leading to the need of more accurate modelling. Larsen et al. [44] deeloped a model extending the classic wake meandering theory. Wake/ring - vortex analogy is used to approximate the wake induced induction field generated by the counter-rotating vortices (consequence of yaw misalignment).

The most common simulating softwares *PyWake* and *FLORIS* ([50]) already include ways to describe static induction control and wake steering. Furthermore, *FLORIS* recently developed a model to include the wake mixing effect produced by the helix approach, while other active wake controls are yet to be implemented. The effect is modelled through the addition of a wake-induced mixing term which depend on the helix amplitude of the sinusoidal pitch excitation. Wake-induced mixing term can affect both the velocity deficit and wake deflection.

However, the influence of the helix approach is yet to be implemented in *PyWake* and literature is still lacking of attempts to simulate the effect with engineering models. This information can be included through the process of calibration of existing wake models. The specifics and motivations of the procedure will be explained subsequently.

2.4. Modelization on PyWake

Pywake is an open-source simulation tool based on Python [58] which allows to study the interaction of turbines within a wind farm computing the physics behind. *Pywake* has a modular architecture allowing to simulate real-world problems just setting the respective specific features. It is able to resolve a wind farm problem through engineering wind farm models which requires site’s and turbine’s information.

The outputs of the model are: calculated effective wind speed, power production and thrust coefficient of individual turbines. Engineering wind farm models are composed of models which describe how wake and blockage deficits propagate in the wind farm (PropagateDownwind and All2AllIterative) and other models including a wake deficit model, a superposition model, (optionally) a blockage deficit and a turbulence model. PropagateDownwind calculates the effective wind speed at a turbine location subtracting from the free stream wind speed the sum of the deficit created by upstream turbines. With this inflow velocity it is able to evaluate the wake created by the turbine itself in all downstream locations. It does not take into account blockage effects which are considered in All2AllIterative model. All2AllIterative proceeds iterating the calculation of effective wind speed and wind deficit until a stopping criteria is reached.

Wake deficit models

Wake deficit models, already introduced in 2.2, calculate the wind velocity downstream a single turbine modelling in this way the wind deficit. This component has to be always selected while other components are optional.

Superposition models

Superposition models take into account the interaction between different turbines's wakes calculating the effective wind speed from deficits of upstream turbines. This component is necessarily required as well when the overall wind farm needs to be simulated. The most common approaches are linear sum and squared sum models. The research in this field is still active and evolving and some wind farm models only differ for the superposition method applied.

Blockage deficit models

Blockage deficit models calculate the upstream wind speed reduction caused by a single wind turbine. The energy extraction from wind turbines induces a reduction of the wind speed right before the rotor in the so-called induction zone. Several models can be found in PyWake: Self-similar model, Vortex cylinder model, Vortex dipole model, Rathmann model and Rankine-half-body .

Rotor Average models

How the wind speed is averaged over the rotor swept area is calculated through Rotor Average Models as the name implies. Several options can be considered (the names are derived from the implemented functions in Pywake):
- Rotor Center : One single point at the center of the rotor is used to calculate the deficit
- Grid Rotor Average : Custom grid in Cartesian coordinates
- Equidistant Grid Rotor Average : Equidistant Cartesian grid
- Gaussian Quadrature Grid Rotor Average : Cartesian grid using Gaussian quadrature coordinates and weights
- Polar Grid Rotor Average : Custom grid in polar coordinates
- Circular Gaussian Integration Rotor Average : Circular Gauss integration

Turbulence models

Turbulence models are meant to calculate the added turbulence create by a single turbine and the effect it has downstream the rotor. This calculation is fundamental when an accurate representation of the flow is needed and some wake models requires it in their internal formulation. The most important models are listed below and were already mentioned in some of the wake models:
- Frandsen [25]
- Gunner Chr. Larsen (GCL) [57]
- Crespo - Hernandez [19]

Ground models

The ground and its roughness has a relevant impact on the wind inflow and on the wake. A popular technique requires adding wakes as if generated from underground mirrored wind turbines.

Deflection models

Deflection models reproduce the deflection of the wake due to phenomena such as yaw-misalignment and sheared inflow. This type of model is important whenever there is an angle mismatch between the incoming flow and the rotor, particularly relevant in active yaw control or wake steering optimization.

For those who are interested, PyWake newest version information can be retrieved from [56].

3 Methodology

In this thesis project, new dynamic control information was integrated into a wake model through calibration and parameter fitting. Therefore the methodology mainly focuses on the development of a precise wake model and robust calibration framework designed to accurately describe wake development following a single turbine. The integration of the DIPC information will be directly assessed in the dedicated chapter.

How calibration can be used to introduce external information in pre-existing engineering models:

As introduced previously, engineering wake models rely on conservation equations, which enable the accurate description of the aerodynamic phenomena associated with wakes. They differ from one another in the underlying assumptions (as detailed in 2.2), as well as in their emphasis on specific parameters that are eventually explicitly incorporated into the models to capture their respective dependency. As long as the assumptions underlying the models align with the scenario being described, they can be effectively used to approximate the flow without violating physical laws, although this may come with a trade-off in accuracy.
However, all wake models were initially developed to describe wakes under standard operational conditions without considering wind farm control. Therefore, it is reasonable to question whether their core formulations can adequately account for new control techniques. It has already been noted that only models specifically designed for yaw misalignment incorporate wind farm control effects. Given that additional phenomena are involved when the turbine is misaligned with the incoming flow, it has been necessary to incorporate these features into the initial model formulations.
When dynamic wind farm flow controls, such as dynamic induction control and the helix approach, are implemented, they induce sinusoidal variations in the resulting forces applied to the rotor. This can impact the momentum conservation, which depends on steady-state balance equations, potentially undermining its validity. However, the analysis can be conducted under steady-state conditions by capturing all features through time-averaging the effects over a suitable time range. This approach allows for modeling the overall averaged impact of the control application. Therefore, it can be concluded that existing wake models are capable of describing the (average) effects of dynamic controls on the wake. A precise formulation of the wake model for each control signal can be achieved through the process of calibration.

A calibration procedure is performed in Python with the support of *PyWake* to simulate the wind flow behaviour. Before this analysis, a suitable wake model must be identified, which will then be fitted to experimental data that characterize specific environmental and operational conditions. Figure 3.1 illustrates the flowchart of the process. The calibration is carried out through an optimization problem, which involves various sub-steps.

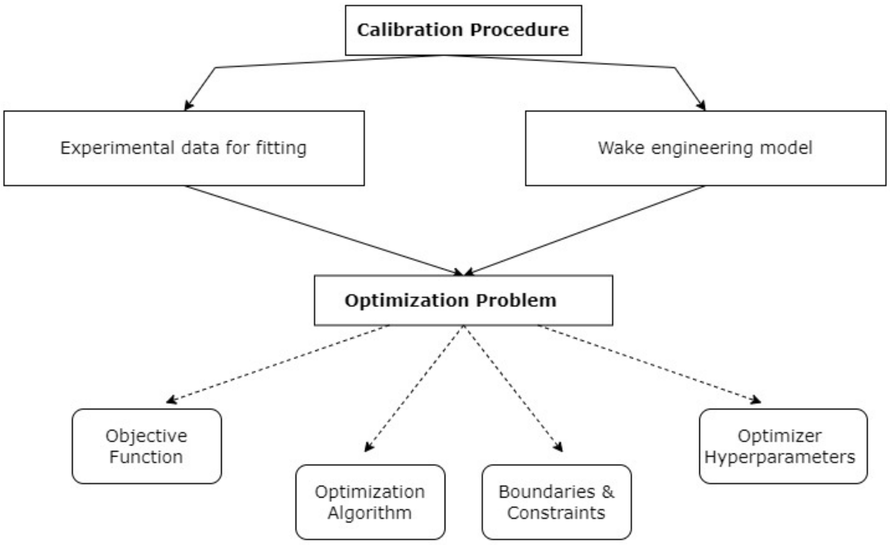

Figure 3.1: Flowchart describing the calibration procedure of engineering models though optimization.

The purpose of this analysis is twofold: firstly, it aims to identify the most effective procedure for calibrating various engineering models; secondly, it seeks to determine the best wake model. The ultimate goal is to achieve the most accurate representation of the wake based on the input experimental data. To develop a robust and universal methodology, different wake models and optimization procedures are explored within a baseline simulation environment, where no control is currently applied. This approach allows for testing the accuracy and efficiency of the methods, enabling the selection of the best configuration for use in scenarios involving dynamic control.
This chapter is structured according to the steps outlined in the flowchart shown in Figure 3.1. Section 3.1 provides the details from Large Eddy Simulations, which serve as experimental data for fitting the wake models. In Section 3.2, the wake models are adapted to the case study. Section 3.3 explores various methodologies for solving the optimization problem, aiming to identify the most suitable solver. Additionally, Section 3.4 presents a sensitivity analysis that assesses the models' responsiveness to various parameters.

3.1. Simulation environment

The calibration procedure uses Large Eddy Simulations as as experimental data for fitting. These simulations provide information about the wind velocity field within a spatial domain that includes the turbine and extends several rotor diameters downstream. The time domain is modelled through a fixed amount of time steps and the more time steps included, the more developed the flow becomes. Eventually, after a certain period from the start of the simulation or the last change in external conditions, the flow reaches a fully developed state. Calibrating the wake model for each time step requires excessive computational effort relative to the benefits it provides, making such detailed analysis unnecessary. Since the calibrated engineering model must be representative of the whole time span, simulation data are time-averaged over the entire spatial domain for the time range the flow has fully developed. The moment the wake develops completely is not fixed and it depends on the environment set for the simulation. In order to find this value, different time frames have been compared until no difference in the wake shape is detected.
The behaviour of a single turbine is considered with the purpose of studying as accurately as possible the parameters that describe the wake. Therefore, the influence of the wake on other turbines is not taken into consideration but the focus is rather on the propagation of the wake itself after the turbine. Therefore, no superposition models are applied in this analysis and the incoming wind's turbulence intensity is reduced to the ambient turbulence. The choice of using data from LES is necessarily related to the single turbine investigation. SCADA data ,while they are widely used to easily retrieve conditions in wind farms, are not informative when a single turbine is used. In order to describe the whole wake accurately, information about the flow is needed for every spatial point in the investigated domain and

only LES can provide that. This analysis can then be applied to the overall farm with appropriate experimental data.
Tables 3.1 provides a detailed overview of the conditions under which LES was conducted for the baseline case. The turbine used in this analysis is the IEA 22 MW reference for Task 37 [79], whose parameters are summarized in Table 3.2. This turbine serves as a standard benchmark within the field. A further investigation with different simulation data will be analyzed in Chapter 4.2 and 5.1 and the different outputs will then be compared. It is worth emphasizing that this result is universal: the use of different LES does not affect the validity of the considerations and choices made in the methodology, but only numerical results of the calibration.

Table 3.1: Baseline Large Eddy Simulation Parameters.

Parameter	Value
Simulation time duration	1795 s
Simulation time @ fully developed conditions	1300 s
Domain size x-y plane	2800 x 4400
Inflow hub height wind speed	9 m/s
Turbulence intensity	0
Atmospheric Boundary Layer Conditions	Steady, Uniform and Laminar flow

Table 3.2: Tested Wind Turbine parameters.

Parameter	Value
Turbine	IEA 22 MW (Task 37 reference)
Hub height	170 m
Rotor diameter	283.21 m
Rated power	22 MW (@ 11 m/s)
Number of blades	3

The simulated flow is steady, uniform and laminar. This means that no roughness and no effect of the ground is taken into consideration and there is no ambient turbulence because of the absence of mixing between the fluid particles layers. Turbulence intensity is therefore minimal or negligible and velocity fluctuations are small. Laminar flow condition is consistent for all the further analysis in this research.

Modelization of the Turbine through OpenFast

The turbine and its response to inflow conditions are modeled through OpenFAST [21], an advanced aero-hydro-servo-elastic simulator for analyzing the coupled dynamics of wind turbines. OpenFAST integrates aerodynamic, hydrodynamic, structural, and control system dynamics into a comprehensive modeling framework. Using the Blade Element Momentum (BEM) theory, OpenFAST calculates aerodynamic forces on the turbine blades, accounting for complex interactions between the blades and the wind flow. This approach provides detailed turbine response characteristics under various wind conditions, enabling accurate performance prediction and load analysis.
Information about the turbine is fundamental for the subsequent analysis, as PyWake models its behavior using characteristics such as the power curve and thrust coefficient curve. To ensure coherent results, the turbine has been modeled in the same way as it was for the LES. It is recommended to always model the turbine consistently across different simulations to avoid conflicts. The rotor has been modeled as rigid, meaning there are no degrees of freedom in either the flapwise direction (perpendicular to the plane of rotation) or the edgewise direction (within the plane of rotation). This simplifies the computation while still maintaining accuracy. Additionally, the tower has been set to remain still in both the fore-aft and side-to-side directions. The only degree of freedom is the rotation of the generator, which is crucial for implementing control strategies. Without any degrees of freedom, the generator's rotational speed would be fixed, preventing it from responding to varying wind conditions or control inputs. This would not accurately represent a real wind turbine, where the generator speed varies and is controlled to optimize power output and manage loads. The control strategy includes generator torque

control and pitch control after the rated wind speed is reached. The generator torque control uses a PID controller to regulate torque and maintain optimal rotor speed. Pitch control is activated at wind speeds above the rated value, adjusting blade pitch to keep rotor speed within safe limits. Figures 3.2 and 3.3 are generated from OpenFast and represent the power curve and thrust coefficient.

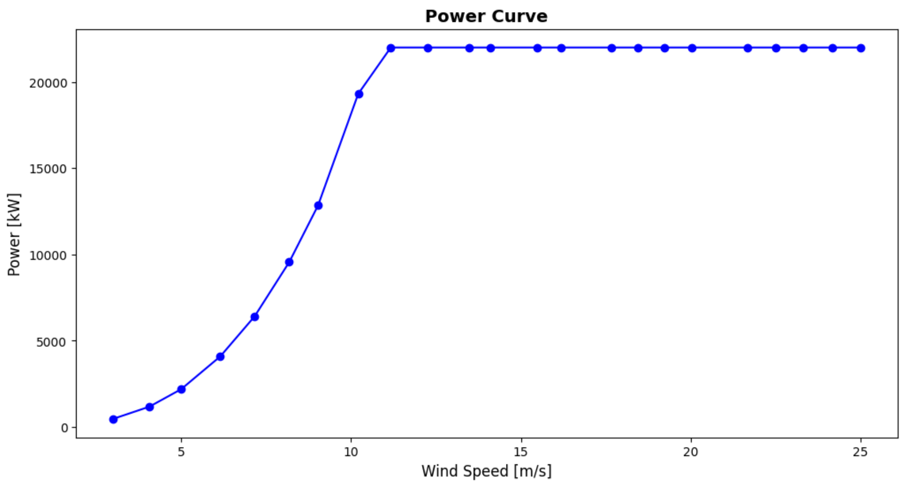

Figure 3.2: Turbine IEA 22MW rotor performance: Power Curve [kW]

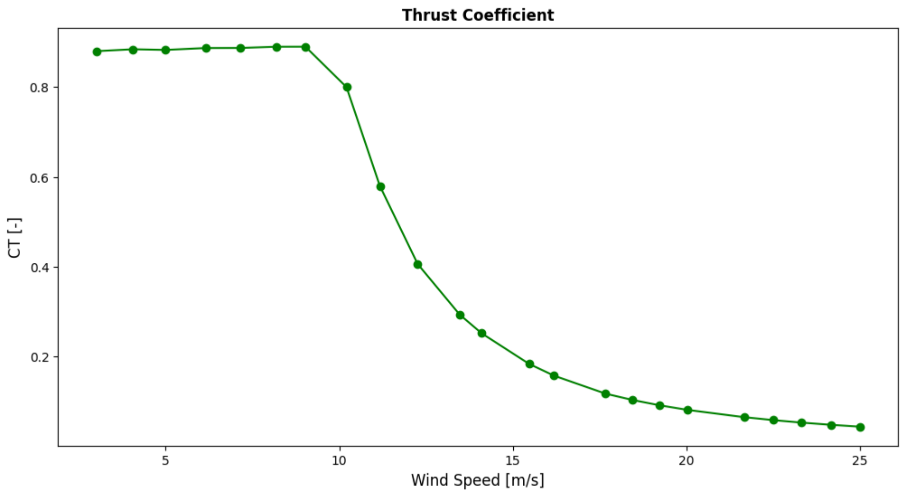

Figure 3.3: Turbine IEA 22MW rotor performance: Thrust coefficient Curve [-].

For further details on OpenFast modeling, please refer to Appendix B.

3.2. Wake Models from Pywake

For the purposes of this analysis, not all engineering wake models discussed in 2.2 will be examined. Only the following Gaussian models will be considered: Bastankhah (2.2.3) and Blondel and Cathelain (Super Gaussian) (2.2.7). The Super Gaussian model has two versions, with the most recent (2023) specifically formulated for the environment in which it was calibrated ([10]). As a result, the 2020 version of the model will be used in this analysis.
The model proposed by Niels Otto Jensen (2.2.1) and Nygaard's adaptation (2.2.2) both consider a top hat shape that describes the wake very poorly. Regardless their important influence in the research field, Gaussian profiles are known to be more suitable to describe the real behaviour of the wake and therefore only those will be tested. Niayifar model (2.2.4) can be brought back to the Bastankhah formulation for fixed turbulence intensities (consequence of the presence of only one turbine and absence of

simulations with different intensities). Zong model differs from Niayifar model only for a more adequate superposition technique. However, for a single turbine analysis this difference is not noticeable. Turbo Gaussian (2.2.6) model would be an interesting comparison, however it is formulated for conditions where the turbulence intensity is present which is not the situation in this analysis.
The aim of this analysis is to calibrate the parameters within each model and, with a fully tuned representation of the wake, determine which model is the most accurate. However, there's a preliminary consideration to do before applying every model. Some of the models are defined to take into account different inputs that depends on the wind inflow conditions and the turbine itself such as turbulence intensity and thrust coefficient. This leads to the most general description of the model suitable for a wide range of applications, but in this study it is applied to the same turbine and turbulence intensity. If this is the case, the model results in being overparametrized and the parameters not unique. If the parameters describing the model are not unique, a poor comparison may be when different calibration procedures or different inputs are used. Taking this into account, all the models will be listed as follows with the appropriate modifications:

Bastankhah Model

No changes were made to the original formulation.

$$\frac{\Delta U}{U_\infty} = (1 - \sqrt{1 - \frac{C_T}{8(k^* x/D + \epsilon)^2}}) exp(-\frac{1}{2(k^* x/D + \epsilon)^2}((\frac{z - z_h}{D})^2 + (\frac{y}{D})^2)) \tag{3.1}$$

Super Gaussian Model

As in Niayifar and Zong, when only a single turbine is considered, the turbulence intensity just upstream of the rotor corresponds to the ambient turbulence intensity. Therefore, due to the expression $a_s I_0 + b_s$, there is an over-parameterization since I_0 is constant. A more general approach would combine these contributions into a single parameter $ks = a_s I_0 + b_s$. This is the general formulation; however, under laminar conditions, where the turbulence intensity is zero, it simplifies to the single parameter b_s.

$$\frac{\Delta U}{U_\infty} = C(\tilde{x}) e^{-\frac{\tilde{r}^{n(\tilde{x})}}{2\sigma^2}} \tag{3.2}$$

$$C(\tilde{x}) = 2^{2/n-1} - \sqrt{2^{4/n-2} - \frac{nC_T}{16\Gamma(2/n)\sigma^{4/n}}} \tag{3.3}$$

$$\tilde{\sigma} = b_s \tilde{x} + c_s \sqrt{\beta} \tag{3.4}$$

$$n = a_f e^{b_f \tilde{x}} + c_f \tag{3.5}$$

As already mentioned in Section 2.4, PyWake offers an interactive environment where engineering models which describe various phenomena could interact. Table 3.3 includes the engineering models employed in the analysis.

Table 3.3: Engineering Models in PyWake

Engineering Wind Farm Model	All2AllIterative
Superposition Model	None
Blockage Deficit Model	Rathmann
Rotor Average Model	Rotor Center
Turbulence Model	GCL
Ground Model	Mirror
Deflection Model	None

The Rathmann model, as implemented in Pywake, has been selected as the blockage model. This decision is based on the observations in [14]. While vortex dipole and self-similar models are unsuitable

for describing the near flow, and the vortex cylinder model effectively captures the entire induction zone, the latter is computationally slower. Ole Sten Rathmann developed a model that approximates the vortex cylinder solution with a speed comparable to the vortex dipole method, combining both suitability and computational efficiency.
It has to be noted that blockage effect is not the main focus of this thesis, therefore blockage models have not all been tested and compared, only the selected model has been used to generate results. Excluding the blockage effect would misrepresent the wake model's true impact.
As turbulence model, GCL model formulated by Gunner Chr. Larsen et al. [57] has been employed. The model includes parameters to adjust for turbulence intensity, which affects how turbulence is spread in the wake. This helps in simulating how turbulent eddies interact with the turbine and how they evolve over distance. Deflection model is not implemented whenever yaw misalignment is not simulated which is the case of this analysis.

3.3. Problem formulation

The solution is formulated as an optimization problem, where the variables are adjusted to enable the wake model to closely approximate the field simulated by LES. The outputs of LES are velocity vectors on specific planes such as xy plane (at the hub level, the horizontal plane parallel to the ground), xz plane (vertical plane perpendicular to the ground which contains the evolution of the wake downstream the rotor) and yz plane (vertical snapshot of the core of the wake at certain distances from the rotor). At this point the three-dimensional nature of the wake raises a new question : which plane(s) should be considered the most representative in order to describe the overall behaviour? All the engineering models are axisymmetric which means that there is no difference between xy and xz plane, but this ideal condition is not present in reality and in the simulations. In order to obtain tuned parameters which take into consideration all the three dimensions, it would be ideal carrying out the procedure of calibration for both planes xy and xz and then averaging the final results. However, this is valid only if the averaged solution still respects the constraints. It's been observed that this criteria is not always satisfied for every simulation tested, therefore it has been discarded and only one plane is taken into consideration instead. To decide which plane best represents the whole wake, the calibration procedure has been performed for both configurations and their mean absolute error evaluated (mean absolute error is described in Formula 3.10). Subsequently, the calibrated parameters which best fit one plane are used to describe the wake on the other plane and the value of the error of this approximation is evaluated once more. The plane's calibration which produces the lowest impact on the other plane solution is the one that is going to be used for the overall analysis. Table 3.4 shows the different combinations and the respective errors.

Table 3.4: The results of the Super Gaussian model calibration along the XY and XZ planes using LES are presented. The error (MAE) [m/s], which represents the final value of the cost function in the optimization problem, indicates how closely the calibrated model matches the input LES data. Lower error values correspond to more accurate solutions. Four combinations of 2D planes are shown, with the first column representing the planes used for calibration and the second column showing the planes where the cost function was evaluated.

Plane used for calibration	Plane used for error evaluation	Error [m/s]
(x-y)	(x-y)	0.2275
(x-z)	(x-z)	0.2347
(x-y)	(x-z)	0.2349
(x-z)	(x-y)	0.2291

Along plane xy the wake can be described better than plane xz but it is the last two rows that give most valuable insight. If parameters calibrated along the xy plane are applied also for xz, the difference in the error in xz planes for cost function evaluation (0.2349-0.2347) is lower than in xy plane (0.2291-0.2275). This means that calibration in xy plane affects less the performance in the other plane than it would be the other way around. From now on only the xy plane is considered for all the calculations.

Now the optimization problem can finally be explored. Every element of the optimization procedure will be discussed and motivated based on the results obtained for every wake deficit model selected.

3.3.1. Objective function

The objective function is the first and one of the most important aspects to be determined in an optimization process. There's no unique objective function (OF) for this purpose and it mainly depends on the desired results and accuracy levels. Zhan et al. [80] propose an objective function only taking into account the velocity field (Equation 3.6), while [8] minimizes the error in the power production (Equation 3.7).

$$OF = \langle \frac{|U_{model} - U_{realdata}|}{U_{realdata}} \rangle \tag{3.6}$$

$$OF = \langle \frac{|P_{model} - P_{realdata}|}{P_{realdata}} \rangle \tag{3.7}$$

$\langle \cdot \rangle$ represents the arithmetic mean operation.
A combination of these two solutions is proposed by Sood and Meyers [65] in which velocity and power relative errors are added with weighting parameters as can be seen in 3.8.

$$OF = w_u \langle \frac{|U_{model} - U_{realdata}|}{U_{realdata}} \rangle + w_p \langle \frac{|P_{model} - P_{realdata}|}{P_{realdata}} \rangle \tag{3.8}$$

Both the power produced and the velocity fields can serve as metrics for the optimization. The key difference between using velocity and power lies in the spatial domain under investigation. Analyzing power becomes relevant when observing the interaction of multiple wakes, whether in a cluster of turbines or across an entire wind park. Since the goal of this analysis is to accurately represent the entire wake, only the wind field can provide relevant information for every point in the flow.

In a calibration process, the cost function must quantify the discrepancy between the model approximation and real data. Minimizing this function ensures the model closely matches the target condition. Since errors between simulation data and model output can be represented in various ways, the most common methods will be analyzed, and their strengths and weaknesses discussed. Root Mean Square Error (RMSE) and Mean Absolute Error (MAE), as defined in Equations 3.9 and 3.10, are standard metrics used to evaluate the performance of predictive models [18] .

$$RMSE = \sqrt{\frac{1}{N}\sum_{i=1}^{N}(U_{model} - U_{realdata})^2} \tag{3.9}$$

RMSE quantifies the average magnitude of errors between predicted and actual values, effectively measuring how spread out these errors are. The squaring operation gives more weight to larger errors, meaning outliers or significant errors have a greater impact on the RMSE value. The summation refers to the spatial domain considered, with the difference evaluated and minimized for every point in the domain, and N represents the total number of spatial grid points.

$$MAE = \frac{1}{N}\sum_{i=1}^{N}|U_{model} - U_{realdata}| \tag{3.10}$$

On the other hand, MAE assesses the average difference between predicted and actual values. While [76] argues that RMSE is ambiguous and not a reliable indicator, [18] found that RMSE can be powerful if the error has a normal distribution. Therefore, it is important to understand how the error distribution varies, considering it differs for each engineering model due to the different modeling of the wake deficit. Figure 3.4 shows the distribution of errors when Super Gaussian wake model is applied. The error is evaluated as the difference between wind speed fields from LES and the wake model calibrated. As can be noticed, it can not be considered as normal distribution and the errors are mainly small. A RMSE evaluation is therefore less suitable to describe the problem but it can still give powerful insight about the accuracy of the solution.

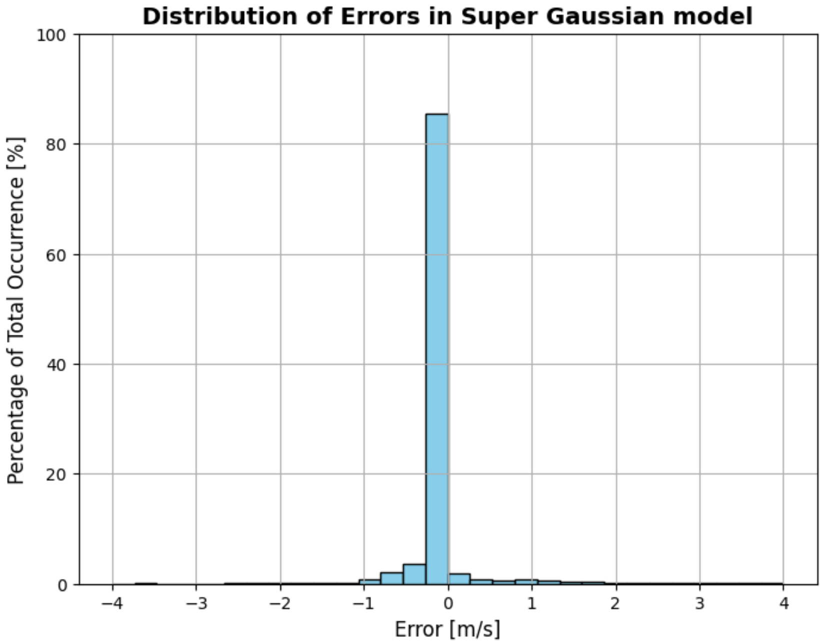

Figure 3.4: Distribution of errors resulting from approximating LES wind speed field using the calibrated Super Gaussian wake model. Errors are quantified by their percentage occurrence over the total. The peak in occurrence indicates that the errors in the velocity field produced by these approximations are predominantly small and do not follow a normal distribution.

Tables 3.6 and 3.5 collect results from the optimization problem solved with a Differential Evolution algorithm using the two different objective functions for every wake model.

Table 3.5: Results with MAE

Wake Model	Error [m/s]	Calibrated parameter(s)
Bastankhah	0.2804	0.0163
Super Gaussian	0.2275	bs = 0.0223 cs = 0.137 bf = -0.327 cf = 2.689

Table 3.6: Results with RMSE

Wake Model	Error [m/s]	Calibrated parameter(s)	Error if with MAE [m/s]
Bastankhah	0.999	k=0.0179	0.2821
Super Gaussian	0.837	bs = 0.0222 cs = 0.127 bf = -0.326 cf = 3.069	0.2284

A more extensive discussion about the engineering models can be found in Section 4.1, here the attention should focus on the different results using the two objective functions. Since different functions yield different results, comparing the errors directly is unreasonable. To obtain comparable results, parameters calibrated from the RMSE are introduced into the respective wake model, and the MAE is then calculated using the calibrated model, as shown in the last column of Table 3.6. It is worth noticing that RMSE (and then traduced in terms of MAE) seems having larger values compared to MAE. This information does not provide any insight into accuracy because the latter is directly optimized for that specific function, whereas the former is not. The expression in terms of absolute error is solely for the purpose of comparison. Comparing Mean Absolute Errors in 3.5 and 3.6, it can be noticed that the difference is noticeable only after the third decimal number. Although MAE is identified as the more suitable function, this observation demonstrates the robustness of the problem formulation. It shows that similar optimal solutions are obtained even when using different decision criteria, with the optimal parameters varying accordingly due to the differences in residuals.

3.3.2. Optimization Algorithm

Another fundamental aspect to take into consideration in an optimization problem is the algorithm that will perform the optimum search. There are many optimization algorithms in literature, and their performance depends on the problem itself (objective function, boundaries and decision variables). Because of the complex form of the velocity field, the problem is most of the time non linear, non convex and it may be non differentiable. Because of that, stochastic and heuristic direct search approaches are preferred over gradient-based algorithms.
Direct search generally refers to methods that do not rely on derivatives or gradient information, while stochastic methods introduce randomness to explore the solution space more effectively and handle uncertainty. The most popular and accurate are: differential evolution, particle swarm optimization, simulated annealing, evolution strategies and genetic algorithm. Furthermore, all the mentioned optimization algorithms are defined as global methods and they are particularly useful when the problem may have multiple local minima. These algorithms systematically explore the entire feasible region to identify the best overall solution, even if it involves navigating through various local optima. A more detailed analysis of the single methods will follow:

- In **Simulated Annealing**, the annealing of metal is resembled [68]. The objective function is associated to the energy of the metal that needs to be minimized to obtain a crystal-like structure. If the metal is cooled down too fast it will end up with a meta-stable structure which is only locally optimal and it does not correspond to the minimum energy configuration. Therefore, a basic simulated annealing method will simulate a slow cooling. As every heuristic method, it can be formulated though an initialization, iteration and stopping stage.
  Initialization: Initial point, initial temperature and cooling factor α are selected. k=0 (iteration step).
  Iteration: A random point x_n is generated in the neighborhood of x(k) and the objective function is calculated. $\sigma = f(x_n) - f(x(k))$. If $\sigma < 0$ (a reduction of the objective function is observed) then the current solution is updated ($x(k+1) \leftarrow x_n$). Otherwise, the iteration continues until a solution that has a lower objective function is found. However, in some situations an increase in the objective function is allowed. When $r < exp(-\sigma/T)$ the solution can be updated anyways (r random number between 0 and 1). There's a strong dependence on the temperature, when it's high, more up-hill moves are allowed and this permits to escape from local minima. After a fixed amount of iteration the temperature decreases $T(k+1) = \alpha T(k)$.
  Stop: Stopping criterion is satisfied.
- **Genetic Algorithms** try to find an optimal solution by mimicking evolution in biology ([77]). The objective function corresponds to the fitness of individual solutions. Different solutions are modified to maximize their fitness through cross-over and mutation. Genetic algorithm uses encoded solution as binary strings. The sequential steps are formulated as follows:
  Initialization: An initial population is created as a set of binary strings and their fitness is evaluated.
  Iteration: New generations are created from original strings selected according to their relative fitness and merged together in the so-called stage of crossover. Mutation is also applied, mutating the genetic information of a string, preserving in this way genetic diversity which avoid local minima.
  Stop: Maximum number of generation is reached.
- **Differential evolution** (DE) is a population-based multi-directional search algorithm, which belongs to the class of evolutionary algorithms. Here's a step-by-step description of the Differential Evolution algorithm proposed by [67] :
  Initialization: An initial population is initialized randomly in the search space. Every solution has a uniform probability distribution.
  Iteration: Mutations and crossovers of population vectors are performed until a solution that minimizes the objective function is found. DE performs mutation by adding the weighted difference between two population vectors to another vector. The elements of the mutant vector are then combined with parameters of a predefined target vector (cross-over), bringing to the so-called trial

vector. The crossover operation helps balancing exploration and exploitation of the search space. If the trial vector has a lower objective function value than the target vector, the target vector is replaced by the trial vector in the population, yielding a different generation. Every population vector has to serve once as the target vector.
Stop: Termination criterion is met.

- **Evolution Strategies** (ES) [34] belongs with Genetic Algorithm and Differential Evolution to the evolutionary algorithms class.
  Initialization: An initial population of candidate solutions is created. Every solution is represented by a vector of parameters.
  Iteration: For each population vector, a mutant solution is created by adding a perturbation to the current solution. The objective function is then evaluated for both the initial and mutant population vectors. Depending on the performance in the objective function, next generation is chosen. This process is also called survival of the fittest. Perturbation techniques is eventually changed depending on the success of the mutations. If the mutations lead to improvements in the objective function, the strategy parameters are adjusted to encourage similar mutations in the next iteration.
  Stop: Termination criterion is met.
- **Particle Swarm Optimization** (PSO) is a stochastic optimization algorithm inspired by animal's social behavior ([75]). There's a cooperative way to find food where each member change the pattern of the research based on its or other members' experience. In PSO, potential solutions to the optimization problem are presented as particles. Each particle has a velocity and position assigned in the search space. The position represents a candidate solution. It is assumed every particle has the ability to remember the best position it ever reached.
  Initialization: An initial population is created randomly with an initial position and velocity.
  Iteration: Velocity and position are updated based on the current velocity,position, personal best and global best aiming at reducing the objective function value. The position is constantly changing in the multi-dimensional search space until a balance is reached.
  Stop: Termination criterion is met.

In particular, Differential Evolution, Simulated Annealing and Genetic Algorithm have been performed. For Bastakhah model also Grid Search has been implemented as a comparison tool. However, this last method, despite its accuracy for high enough numbers of grid points, is computationally inconvenient because of the amount of time it requires to find the solution since every possible combination is tested. The best performance is the result of a trade-off between the accuracy of the method and its computation time. The optimization is performed through pre-built optimization functions in Python provided in the libraries *scipy* and *scikit-opt*. Every algorithm requires other information for the optimum search but this is the focus of Section 3.3.3. Figure 3.5 presents the calibration results for the Bastankhah and Super Gaussian models using various solving algorithms with the MAE objective function. The corresponding computation times are illustrated in Figure 3.6. Detailed numerical values are provided in Tables 3.7 and 3.8.

Table 3.7: Errors (MAE) [m/s] with Different Solving Algorithms

Wake Model	Differential Evolution	Simulated Annealing	Genetic Algorithm	Grid Search
Bastankhah	0.28040	0.28040	0.28042	0.28041
Super Gaussian	0.2275	0.2276	0.2281	-

Table 3.8: Computation Time with Different Solving Algorithms

Wake Model	Differential Evolution	Simulated Annealing	Genetic Algorithm	Grid Search
Bastankhah	18.84 s	27.99 s	86.25 s	87.67 s
Super Gaussian	559.55 s	847.75 s	602.97 s	-

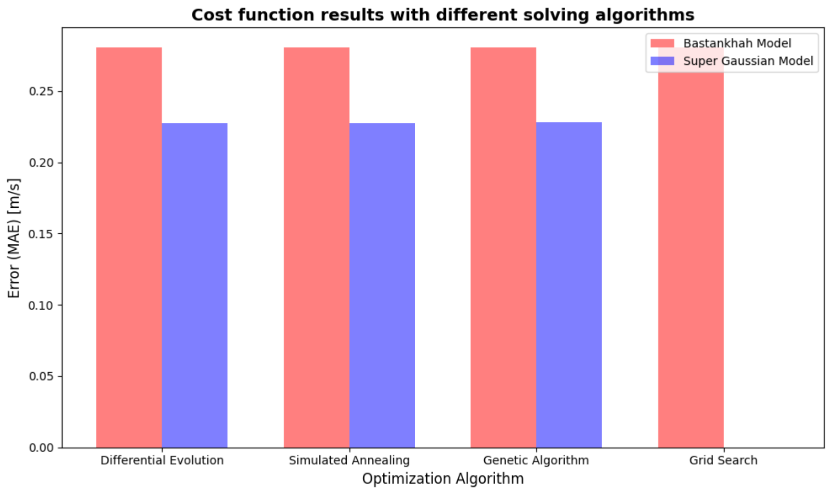

Figure 3.5: MAE cost function values of the calibration procedure with different solving algorithms for Bastankhah (red bar) and Super Gaussian (blue bar) wake models. Grid search was not conducted for the Super Gaussian model, and this is indicated as missing data.

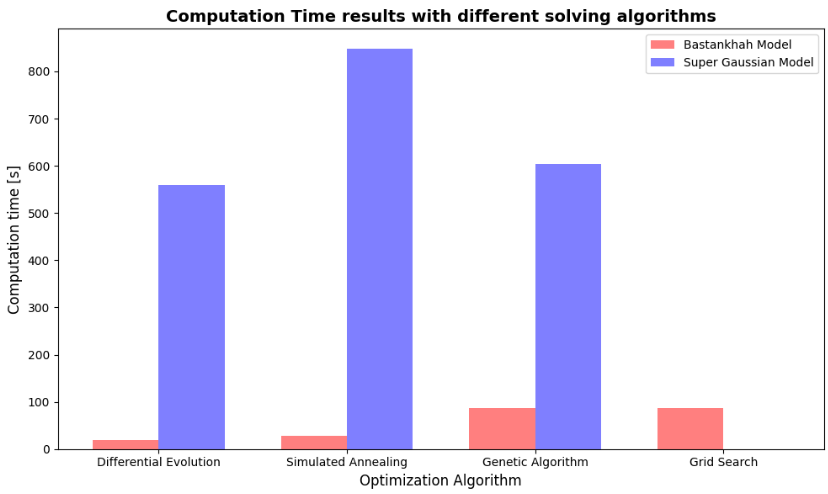

Figure 3.6: Computation time [s] employed in the calibration procedure with different solving algorithms for Bastankhah (red bar) and Super Gaussian (blue bar) wake models. Grid search was not conducted for the Super Gaussian model, and this is indicated as missing data.

The first noticeable consequence of the analysis is the lower error produced by the Super Gaussian model. Because of its characteristics, it is able to describe the wake in the most accurate way. The ideal outcome would be reaching zero error but unfortunately it is not possible due to the intrinsic limitation of using empirical formulas. However, the model becomes more complicated and it is easily noticeable by the increasing computation time. This result still holds when different objective functions are tested as shown previously in Tables 3.5 and 3.6. Secondly, the performance of the optimization algorithms can be evaluated. Differential evolution and simulated annealing outperform genetic algorithm and grid search even though the difference is not largely noticeable. Despite simulated annealing achieves good results, it is penalised by its higher computation time leading differential evolution to being the preferred method, which will be used for the rest of the analysis.

Because of the different solving techniques behind every algorithm and the way new generations are created (for heuristic methods), the optimal set of parameters can be found in different regions with consequently different values of the cost function. However, as Table 3.9 shows, the calibrated parameters are close to each other, meaning that most probably the global optimum region has been identified. These outputs show that valid results can be achieved with minimal impact on accuracy, regardless of the chosen option.

Table 3.9: Calibrated Parameters with Different Solving Algorithms

Wake Model	Differential Evolution	Simulated Annealing	Genetic Algorithm	Grid Search
Bastankhah	k=0.016275	k=0.016276	k=0.01642	k=0.016273
Super Gaussian	bs=0.02233 cs=0.1368 bf=-0.3274 cf=2.689	bs=0.02237 cs=0.1383 bf=-0.3073 cf=2.572	bs= 0.02279 cs=0.1402 bf=-0.3584 cf= 2.644	-

As previously mentioned, grid search is only implemented for Bastankhah wake model. When implementing grid search, each problem parameter can vary across multiple discrete values arranged in a grid of points, and every combination is tested. Since grid search also explores regions less likely to contain the optimum, it requires significant computational effort. However, it provides a clear understanding of how the cost function behaves and identifies potential optimal solutions. Figure 3.7 shows the distribution of the error depending on the parameter k.

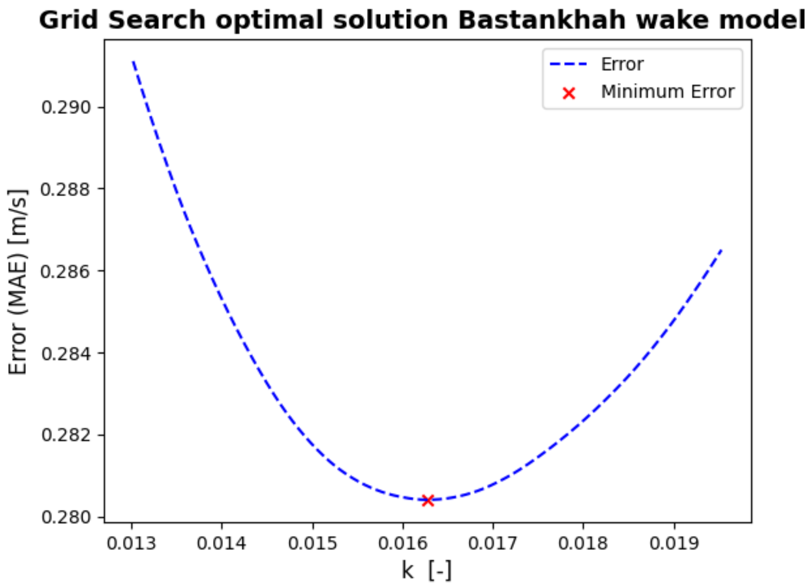

Figure 3.7: Cost function evaluation though Grid Search algorithm for Bastankhah wake model. The cost function corresponds to the value in m/s of the MAE. The blue dotted line represents the value of the cost function varying the parameter *k*, while the red cross shows the optimal value of k which corresponds to the minimum of the curve.

As it can be noticed, the optimum is found at the minimum of the curve. When there's only one parameter, such as for Bastankhah model, identifying the optimum is much easier also because of the single combination that gives the minimum. The more parameters there are and the more difficult the analysis can become. When there is an interplay of different parameters, it is possible that different combinations bring different results even in search regions far from each other. This is a problem called multiple local optima (which will be explored more deeply in Chapter 3.3.3) and it is an intrinsic issue in some optimization problems. It is impossible to get rid of it, but the solution can be refined acting on the algorithm specifications, boundaries and constraints. Next section focuses completely on that.

3.3.3. Optimization settings

Optimization settings play a crucial role in heuristic algorithms, determining their efficiency and effectiveness in finding optimal or near-optimal solutions to complex problems. These settings, including boundaries, max iterations, recombination, mutation, population size, and tolerance, are essential parameters that influence the behavior and performance of heuristic algorithms. Properly tuned optimization settings can significantly enhance the efficiency of the algorithms by guiding the search process towards promising regions of the solution space.

Boundaries and Constraints

Selection of boundaries is an essential aspect in an optimization problem and usually it is addressed together with the determination of constraints. However, in literature there's no information regarding this for any of the engineering model, thus further details depend strictly on every single problem and parameter used in the model. Constraints are important to include in order to obtain feasible solutions that don't neglect the physics behind the problem. It is worth remembering that every wake model has its foundations in mass and momentum conservation theories, consequently physics perspective must always be respected.
On the other hand, since the parameters that need to be calibrated are an artefact derived from empirical fitting, it is more difficult to select adequate boundaries for each one. In addition, model parameters can widely change depending on external conditions they want to represent (set by simulation data). Too strict or incorrect boundaries can restrict the solution or direct it to the wrong search space. It is possible not to include them but having the correct range help redirecting the solver's computational effort to guaranteeing a more accurate solution.
In order to overcome this problem, the optimization is performed over a wide range for the parameters' boundaries and then a technique of local refinement is performed to improve the solution. Local refinement can be mainly performed in two ways around the initial optimum: local search and monte carlo method. Least squares algorithm has been used as local search method since it can handle non linear problems formulated as difference between two signals. Local search algorithm can be applied in this region because it is restricted near the optimum and a continuous and smooth behaviour of the function is assumed. This is not valid in the overall search space for which heuristic methods are designated. Monte carlo method is an equally popular option to be used as local refinement. For each parameter, a probability distribution that characterize their variability is defined. A normal distribution has been selected and random samples are generated from the probability distribution in a range of 20% from the old optimum. The number of samples should be sufficient to adequately explore the variability of the input space. For each sample of input parameters, the solution is evaluated and the minimum is picked among the samples. A new refined option is formulated which is more accurate than the first raw solution. Even if monte carlo method is the most accurate, it has to evaluate the objective function iteratively for a very large number of combinations and it requires a lot of computational effort. A local search methodology is found to be the most suitable for the purpose of this research and it will be used from now on.

Algorithm hyperparameters

Selecting appropriate population sizes and mutation rates can prevent premature convergence and facilitate exploration of diverse solutions. The choice of optimization parameters directly impacts the algorithm effectiveness in finding high-quality solutions. By adjusting parameters such as recombination rates and tolerance levels, it is possible to fine-tune the balance between exploration and exploitation, leading to better convergence towards optimal solutions. Strong implications can also be found in convergence, determining how quickly and reliably satisfactory solutions are approached. Setting appropriate maximum iterations and tolerance levels helps prevent excessive computation while ensuring convergence to acceptable solutions within reasonable timeframes.
A well-configured framework contribute to the robustness of heuristic algorithms, enabling them to perform consistently across different problem instances and scenarios. Sensitivity analysis and parameter tuning can help identify optimal settings that are robust to variations in problem complexity and characteristics. Determining the right set of optimizer parameters is not straightforward since there's a strong correlation between the values and sharpening them can increase the computation time excessively. Different set of parameters have been tested and the final results can be found in Table 3.10.

Finally also the seed can be tuned. The seed initializes the random number generator and determines the sequence of random numbers generated during the execution of the algorithm. Setting a predetermined value for the seed is crucial at all times, ensuring that the sequence of random numbers generated is deterministic and reproducible across different runs of the algorithm. If different seeds result in the same solution, the solution is considered stable.

Table 3.10: Best set of hyperparameters for every engineering model

Parameter	Bastankhah	Super Gaussian
Maximum number of iterations	100	150
Population size	50	150
Tolerance	1E-06	1E-06
Mutation rate	1	1.5
Recombination rate	0.7	0.7
Seed	42	42

Ideally the best configuration is reached when enhancing the metrics (which most of the time means increasing) the convergence is reached at the same point. In practice, as already mentioned, it can increase the computation time excessively bringing the analysis to being too demanding. Metrics in Table 3.10 reflect this compromise.

However, although tuning the hyperparameters helps mitigate the aforementioned problem of local minima, it cannot be completely eliminated, as it is an intrinsic aspect of every optimization problem. To explore the prevalence and distribution of local minima, multiple optimizations will be performed by varying the random seed for each run. Changing the seed causes the optimizer to generate different initial populations and search paths each time, leading to a more comprehensive exploration of the solution space.
By comparing the results from these runs, the study will demonstrate how frequently and where the optimization process gets trapped in local minima. This approach highlight the local minima problem and emphasizes the need to effectively address these challenges in optimization tasks.

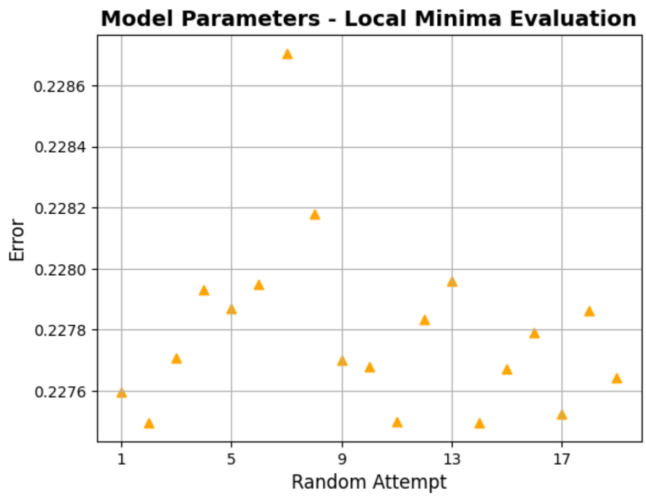

Figure 3.8: Final value of the cost function in terms of MAE [m/s] for several randomized runs of the calibration procedure defined as "Random Attempts".

Figure 3.8 shows the value of the cost function for several optimization runs with different random seeds. The value of the cost function varies largely as a consequence of the exploration around different regions. In Figure 3.9, the change in the parameters can be seen for the same conditions. Every other variable in the optimization (such as maximum iterations number, population size, mutation and generation rates) has been kept the same. If nothing is changed except the randomization of candidate generation and different solutions are found in different regions, the problem can be solely attributed to local minima. Unfortunately it can not be solved, but finely tuning optimizer parameters for every different problem helps reducing the phenomenon. However, running multiple tests with different seeds not only highlights the problem but also proposes a solution. If the final set of optimized parameters, associated with the lowest cost function, falls within a region where values are densely concentrated, the probability of achieving an accurate solution for the analysis increases. This can be observed in Figure 3.9 where the final set of optimal parameters is represented by the grey dashed line.

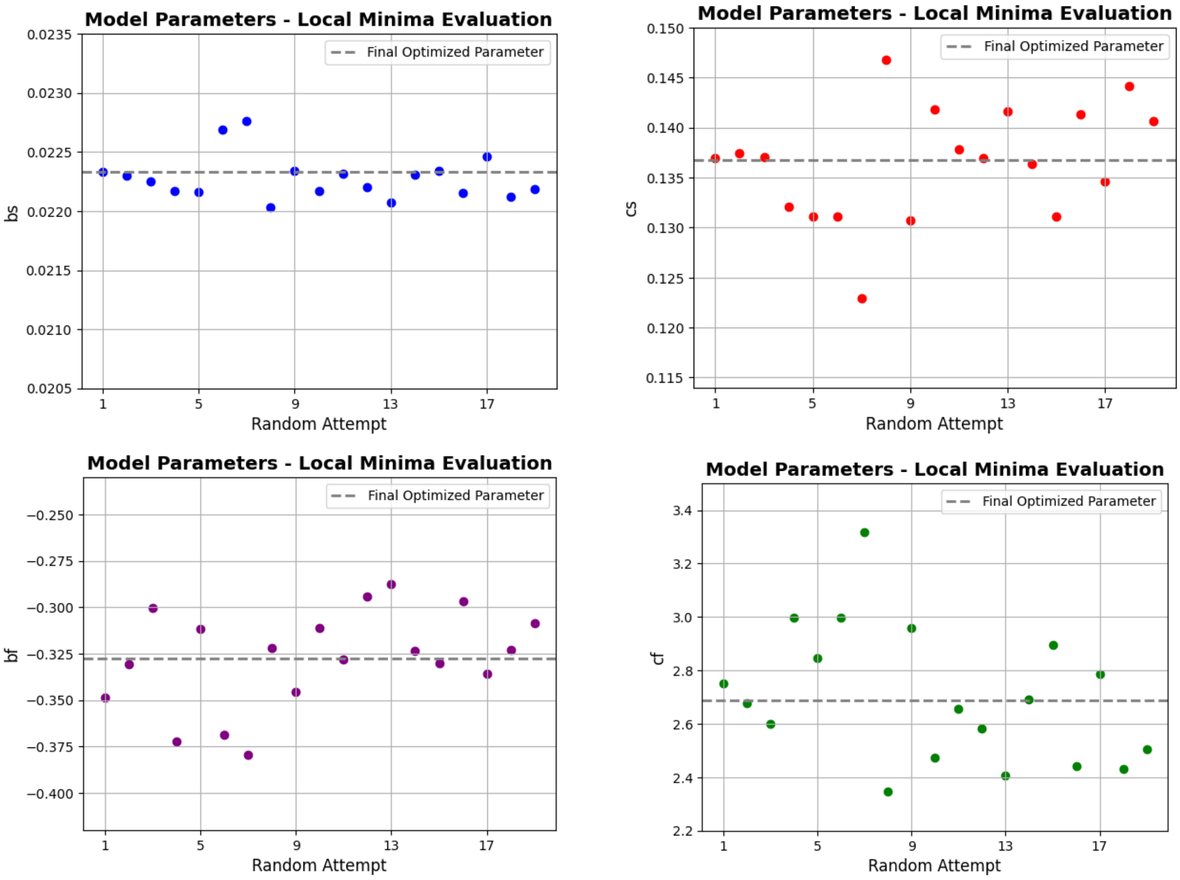

Figure 3.9: Super Gaussian model parameters distribution for several randomized runs of the calibration procedure. The optimal value of each parameter is represented by the grey dotted line.

Final Optimization Problem formulation

Here the final choices are summarized and the problem is finally formulated comprehensively. The objective function consists in the Mean Absolute Error between the velocity field predicted by the wake model in PyWake and LES. The boundaries are initially set to a broad range and then locally fine-tuned. For further analysis and to speed the process of calculation, fictitious boundaries are calculated as 20% from the refined solution. Constraints depend strictly on the engineering model employed and the problem is solved with Differential Evolution.

Bastankhah Model:

$$U_{\text{model}} = U_\infty \left(1 + \left(1 - \sqrt{1 - \frac{C_T}{8\left(k^* \frac{x}{D} + \epsilon\right)^2}}\right) \times \exp\left(-\frac{1}{2\left(k^* \frac{x}{D} + \epsilon\right)^2} \left(\left(\frac{z - z_h}{D}\right)^2 + \left(\frac{y}{D}\right)^2\right)\right)\right)$$

$$\text{Objective Function} = \frac{1}{N}\sum_{i=1}^{N} |U_{\text{model}} - U_{\text{real data}}|$$

Constraints: $k > 0$

Boundaries: $0 < k < 2$

Super Gaussian Model:

$$U_{\text{model}} = U_\infty (1 - 2^{2/n-1} + \sqrt{2^{4/n-2} - \frac{nC_T}{16\Gamma(2/n)(b_s\tilde{x} + c_s\sqrt{\beta})^{4/n}}}) e^{-\frac{\tilde{r}^{n(\tilde{x})}}{2(b_s\tilde{x}+c_s\sqrt{\beta})^2}})$$

$$n = a_f e^{b_f \tilde{x}} + c_f$$

$$\text{Objective Function} = \frac{1}{N}\sum_{i=1}^{N} |U_{\text{model}} - U_{\text{real data}}|$$

Constraints:

$$\sigma > 0$$

$$n > 2$$

Boundaries:

$$0 < b_s < 2$$

$$-2 < c_s < 2$$

$$-2 < b_f < 2$$

$$-2 < c_f < 4$$

3.4. Post processing

The output calibrated parameters are post-processed through a sensitivity analysis. In the context of parameter calibration, sensitivity analysis allows to identify which parameters have the most significant impact on model outcomes and it connects output uncertainties with inputs uncertainties. By focusing calibration efforts on the most influential parameters, resources can be allocated more efficiently, leading to better-informed decision-making processes. This process is executed alongside each previous analysis. In the boundaries selection it can give powerful insight by restricting the range of the dominating parameters prioritizing their accuracy. However, there are other reasons for this analysis: it enhances model simplification by modifying model inputs which have no influence on the output and creates more understanding of the relationships between input and output variables. There are several methods to perform sensitivity analysis and depending on the problem characteristics some are more valid than others. The most popular solving methods are:

- **One-at-a-time** (OAT): It is the simplest approach and it changes one factor at a time to measure each effect on the output [16] [48].
- **Derivative-based methods**: Derivative-based methods can perform locally or globally. Local methods execute partial derivatives of the output with respect to each input singularly while Global methods is performed by averaging local derivatives (at selected points within the full range of uncertainty) using Monte Carlo or Quasi Monte Carlo sampling methods [15].
- **Regression analysis**: A linear regression is fitted to the model response and standardized regression coefficients are used as a measure of sensitivity. The regression is strictly required to be linear otherwise the standardized coefficients lose their sense [61].
- **Variance-based methods**: Input and output uncertainties are defined as probability distributions. The output variance is then decomposed in the influences of input variables and combinations of variables. The sensitivity of the output depending on one variable is calculated by the fraction of the variance connected to that input. Variance-based methods allow full exploration of the input space, accounting for interactions, and nonlinear responses [64].

The studied problem requires attention towards non linearity and interdependence of input parameters. Despite the simplicity of changing one factor at a time (OAT and local derivative-based methods), this approach does not account for simultaneous variations of input variables [20], while regression techniques are more suitable when the model response is linear. Variance-based measures, therefore, offer the most suitable solution for the problem at hand, preferred over global derivative-based methods because they do not require derivative evaluation.

Variance-based Sensitivity Analysis

Variance-based sensitivity analysis is often called Sobol' method because of the contribution of Sobol' research in the field ([64]). However, Sobol' solution is not the only way of performing variance-based sensitivity testing but other methods such as FAST (Fourier amplitude sensitivity testing) can be used. The sensitivity of each input is then defined as a numerical value called sensitivity index. Depending on the degree of parameter interactions, a respective order corresponds to sensitivity indices:

1. First order indices: measures the contribution to the output variance by single inputs alone.
2. Second order indices: measures the contribution to the output variance by the interaction of two model inputs.
3. Total order indices: Firstly introduced by [37], it measures the contribution to the output variance caused by a model input including the correlation with the other input parameters. Therefore first and higher orders are all taken into account.

Given a model in the form $Y = f(X_1, X_2, ..., X_k)$, the first order sensitivity index for the parameter X_i is ([59]):

$$S_i = \frac{V_{Xi}(E_{X-i}(Y|X_i))}{V(Y)} \tag{3.11}$$

X_i is the i-th factor and $X-i$ is the matrix of all factors but X_i. In this whole analysis "E(.)" represents the mean value while "V(.)" represents the variance of their argument. $V_{Xi}(E_{X-i}(Y|X_i))$ is the expected

reduction in variance if X_i could be fixed .
The total effect index T_i is calculated through Formula 3.12 and it takes into account first and higher order effects (interactions).

$$T_i = \frac{E_{X-i}(V_{Xi}(Y|X_{X-i}))}{V(Y)} = 1 - \frac{V_{X-i}(E_{Xi}(Y|X-i))}{V(Y)} \tag{3.12}$$

$V_{X-i}(E_{Xi}(Y|X-i))$ is the contribution off all factors but X_i and in $E_{X-i}(V_{Xi}(Y|X_{X-i}))$ all terms which consider X_i are included. For independent factors it always holds:

$$1 = \sum_i S_i + \sum_i \sum_{j>i} S_{ij} + \sum_i \sum_{j>i} \sum_{k>j} S_{ijk} + ... \tag{3.13}$$

Parameters like S_{ij}, S_{ijk} are the so-called interaction terms.
Sobol sensitivity indices are ratios between partial variance to total variance and can vary between 0 and 1. This is because from the relation in Formula 3.13 since no index can be negative, then none can exceed one. As it is stated by [30], the sum of S_j over all inputs j cannot exceed 1 and equals 1 whenever all the interaction terms are zero. However, the sum of T_j over all j can never be less than 1 and equals one only if all the interaction terms are zero.

4
Results Baseline

A comprehensive calibration procedure has been developed, providing a solid framework to ensure accurate and reliable results. This chapter highlights the outcomes of applying this calibration framework to the wake models.
First, the calibration results for the baseline simulation at 9 m/s, as introduced in 3.1, are presented. The impact of calibration on the flow field for both the Gaussian and Super-Gaussian models is examined, definitively confirming the superiority of the latter (Section 4.1). The analysis is then extended to wind speeds other than the initial 9 m/s in Section 4.2 to assess how varying inflow conditions affect the results. This approach ensures a comprehensive understanding of how different wind speeds influence the performance and accuracy of the wake models.

4.1. Final wake model at 9 m/s

This section includes the results in terms of velocity fields of the engineering model calibrated. The closer to the simulation data is, the most accurate the model is able to describe the selected situation. Figures 4.1 shows the wind velocity field from LES while 4.2 the results of the models. Each engineering model investigated describes the wake in a different way resulting in different shapes. This allows to investigate different features of the models and compare them. It can be finally noticed the effect of the calibration on the representation of the wake. Comparing Figure 4.2 with the description from literature (2.2), it is possible to notice the upgrade gained with the parameter tuning.

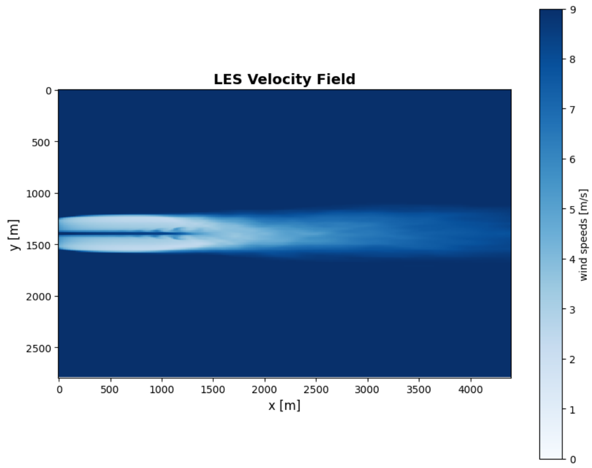

Figure 4.1: Wind velocity field from LES in [m/s] across the xy plane intersecting the rotor. The wake is highlighted by the lighter region, indicating a significant reduction in wind speed. The range of wind speeds varies from 0 to 9 m/s which is the incoming wind.

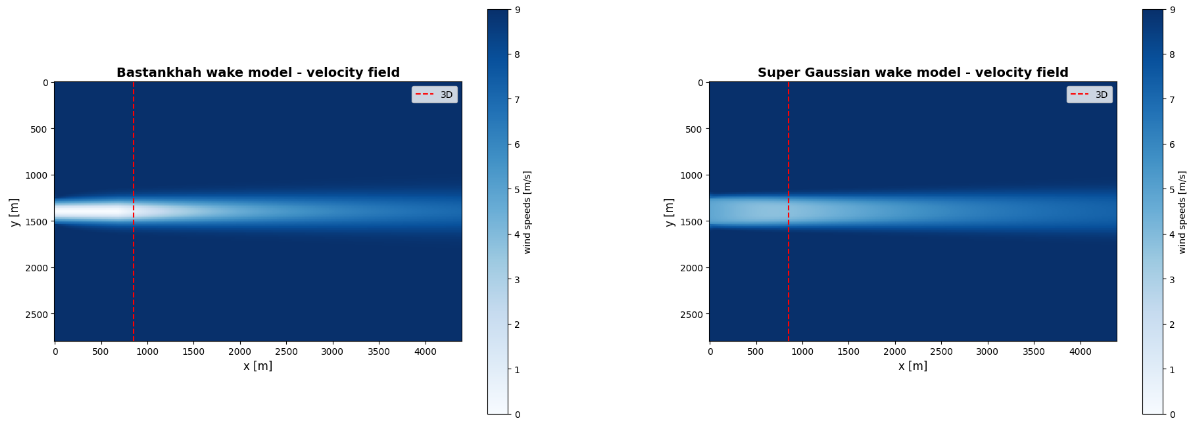

Figure 4.2: Wind velocity field in [m/s] described by Bastankhah and Super Gaussian wake models after calibration. The red dotted line is located at a distance of 3 diameters after the rotor and represents the transition from the near wake towards the far wake region. The range of wind speeds varies from 0 to 9 m/s which is the incoming wind.

Dark blue areas are characterized by free-stream flow which continues undisturbed, while the effect of the rotor decreases the intensity sometimes up to reset it.
Section 3.3.2 already points out that the Super Gaussian model reaches the lowest errors, making it the most suitable for applications. The same conclusion can be detected at the same time from the Figure above (4.2).
Bastankhah models accurately only the far wake, while Super Gaussian is built to refine also the near wake. This comes directly from the formulation of the model itself. Most of the models in literature only shape accurately the far wake because the effect of the shading over downstream turbines is usually over this range. However, even if such a compromise is accepted, it is not the most attractive assumption for this analysis. Since the aim of the present research is describing the wake as accurately as possible in its whole, an accurate description is required. Moreover, the analysis is intended to be used with new dynamic controls applied. These new techniques completely interfere with the wake evolution and because of their early stage in the investigation, a high level of precision is required. The transition from near to far wake is highlighted by the dashed vertical line at the distance of three diameters after the rotor.
Figure 4.3 shows the difference in wind speed field representation between LES and the Bastankhah model output, both before and after calibration using Equation 4.1. The deficit provides insight into how closely the model approximates the data, with zero error representing a perfect match. It is evident that parameter tuning significantly reduces the discrepancy between the model and the data.

$$deficit = U_{model} - U_{realdata} \tag{4.1}$$

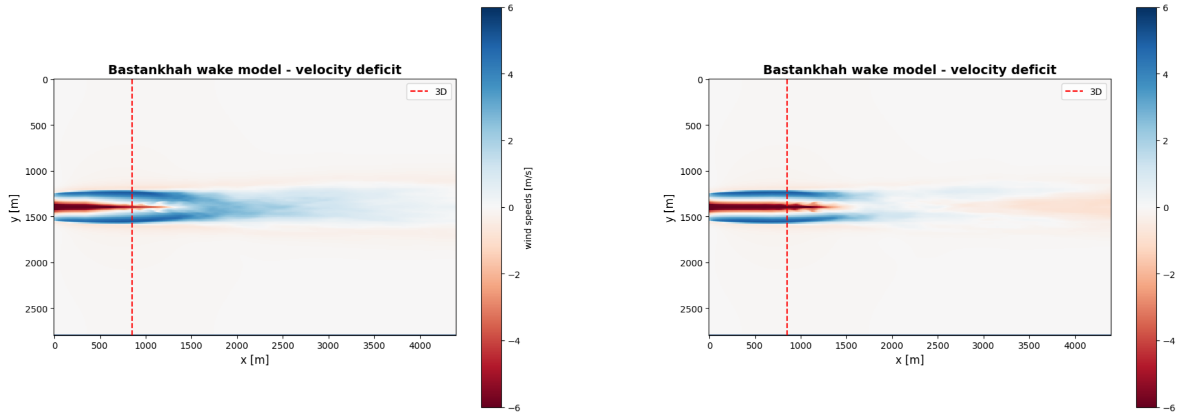

(a) Model parameter k defined in literature (deficit evaluated before the calibration process).

(b) Model parameter k defined through the calibration process and equal to k=0.016275.

Figure 4.3: Wind velocity deficit evaluated for Bastankhah wake model before and after calibration. The red dotted line is located at a distance of 3 diameters after the rotor and represents the transition from the near wake towards the far wake region. The range of wind speeds represented varies from -6 to 6 m/s with the desired result at 0 m/s.

Here it is evident the influence of Bastankhah model in the far wake only. Far from the rotor, the model approximates accurately the wake, as the quasi-zero deficit shows.

Blondel and Cathelan calibrated their model (Super Gaussian) under turbulence conditions with intensities in a range from 5% to 10.7% which is quite far from the laminar simulations used for this calibration. This results in a set of parameters which can not describe zero-turbulence conditions because are not inside the problem feasible area anymore. Performing the calibration is therefore necessary for an adequate representation and the deficit can not be represented for non calibrated parameters. Figure 4.4 shows the deficit after calibration is performed. Super Gaussian is able to represent the near wake region much more accurately than Bastankhah normal Gaussian distribution as the lower values of the velocity deficit show. In the far wake the two models tend to coincide because the Super Gaussian model approaches a Gaussian distribution as it extends further downstream.

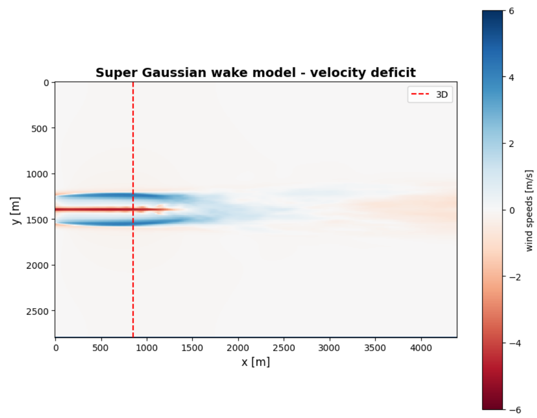

Figure 4.4: Wind velocity deficit evaluated for Super Gaussian wake model after calibration. The red dotted line is located at a distance of 3 diameters after the rotor. The range of wind speeds represented varies from -6 to 6 m/s with the desired result at 0 m/s.

Section 3.3.2 already pointed out that Super Gaussian model could describe the wake more accurately because of its lower value of MAE from the LES wind speed field in input. However, now this result is further strengthened by this visual representation. It is at this point clear that Super Gaussian outperforms Bastankhah model. This is also attributed to its greater number of parameters, allowing for finer adjustments. The increased number of parameters enables a more detailed investigation as they can influence the distribution in multiple dimensions.

From now on, the analysis will focus exclusively on the Super Gaussian model with the optimal configuration of the optimization procedure previously specified.

After identifying the calibrated parameters that best represent the wake shape, a sensitivity analysis is conducted to determine which parameters have the greatest influence on the final representation. Additionally, the analysis examines whether overparameterization is present, indicating the need for further model simplification. To perform this analysis, a library from Python called *SALib* ([39],[36]) is been used where a Sobol' method has been considered The boundaries of this analysis are the same previously defined for each parameter which is the feasible range at a 20% distance from the optimal solution. A sensitivity analysis gives relevant information only when two ore more metrics are compared to each other. This is the reason why Bastankhah model has not been considered. Figure 4.5 shows the result of the sensitivity analysis. First- and Total-order sensitivity indices are evaluated and the numerical results can be found in Table 4.1.

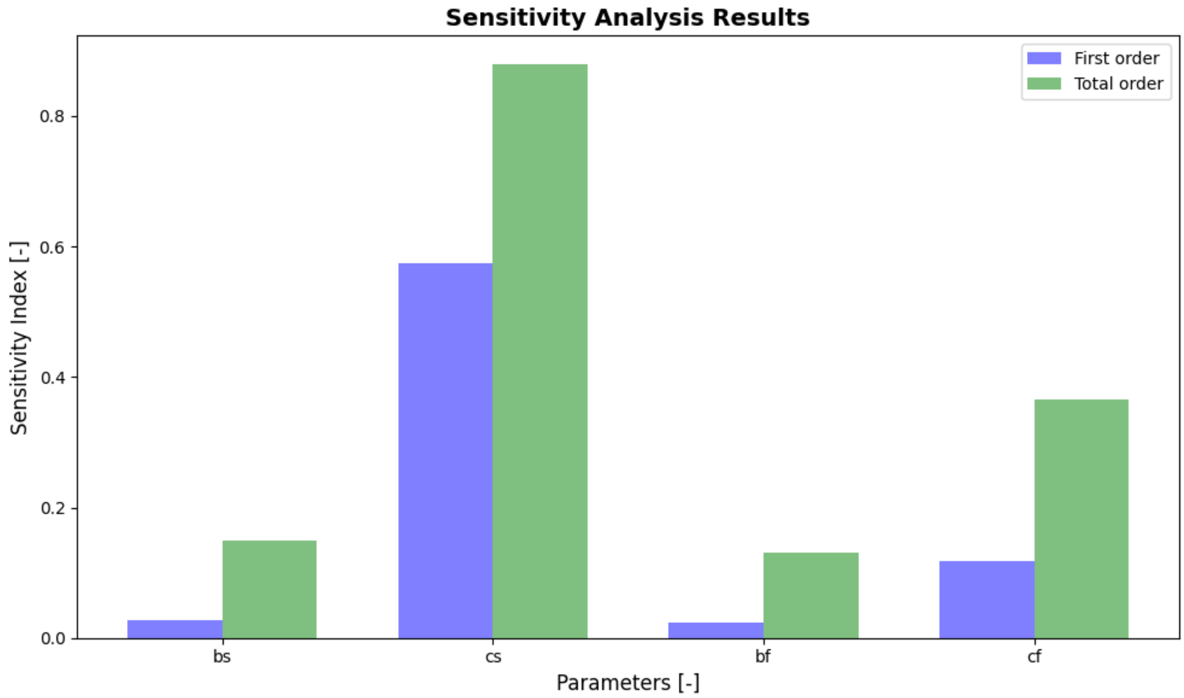

Figure 4.5: Variance-based sensitivity analysis for Super Gaussian model parameters: first-order and total-order. The first-order and total-order sensitivity indices are non-dimensional numbers ranging from 0 to 1. Higher total-order indices compared to first-order indices indicate a strong interaction between model parameters.

Table 4.1: Variance-based sensitivity analysis results in terms of sensitivity indices for Super Gaussian model parameters - first and total order.

	bs	**cs**	**bf**	**cf**
First-order SI	0.026	0.574	0.023	0.118
Total-order SI	0.148	0.879	0.131	0.365

The first noticeable result is that total-order sensitivity indices are largely bigger than first order. This is because total order considers not only direct effects of single input parameters but also interactions and in the studied case interactions play an important role.
The sensitivity indices for each parameter are substantial enough to be relevant, meaning that each parameter influences the final result to some extent, with some being more impactful than others. This suggests that there is no overparameterization in the current formulation.

The parameter cs has the highest influence in both first-order and total-order evaluations, followed by cf, bf, and bs. Therefore, for further analysis, special attention should be given to the most influential parameters, as even minor variations can lead to significant deviations in the results.
Sensitivity indices are always positive numbers between 0 and 1. Values outside that range are a consequence of ill-conditioned problems or ill-conditioned sensitivity analysis. Sobol sensitivity is implemented generating a large number of samples and the higher the number and the more accurate the analysis is. Increasing its value can also solve the problem of indices outside [0,1] range.

Figures 4.6 represents the result of the first order sensitivity analysis for Super Gaussian model. Every model parameter has been varied individually in its range while the other parameters have been kept constant at their optimal value. In this way no dependency on other inputs' influence is considered and the sensitivity analysis is restricted to the first order. The variation of every parameter value from its optimal position in the desired range is obtained generating equidistant coordinates. The whole region within the boundaries (20% range) is not fully explored as a consequence of constraints not respected (represented in the following graphs by the grey area). The unfeasible region gives another important insight: a uniform range of 20% from the optimal solution can not be considered as a correct boundary range as the minimum acceptable value is the optimal value itself. The minimum error represented by a red cross derives from the optimization procedure performed in Section 3.3 with the final metrics selected.

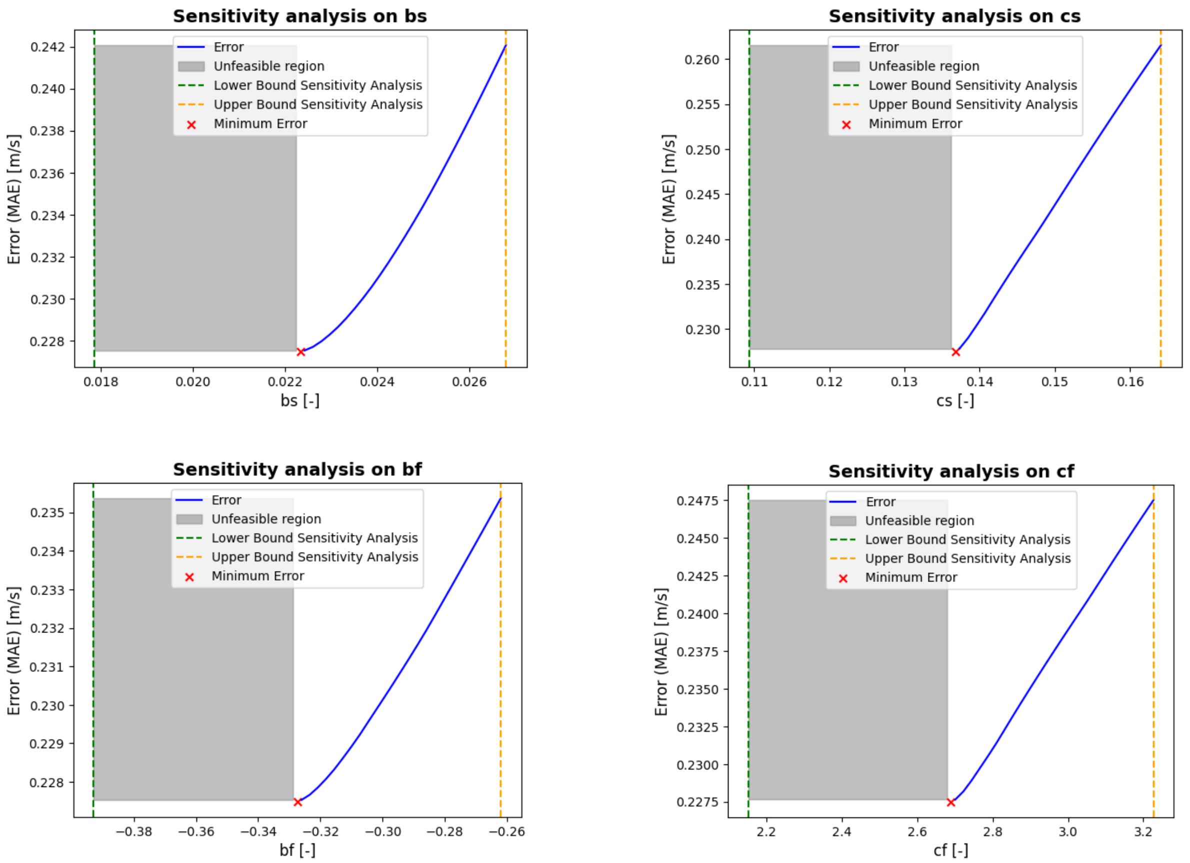

Figure 4.6: First-order sensitivity analysis of the Super Gaussian model parameters. The green and yellow vertical dashed lines delineate the range of values within 20% of the optimal solution. Grey areas represent unfeasible regions where solutions cannot be found due to unmet constraints. The error represented by the blue line is the value of the cost function (MAE) in m/s, while the optimal solution is identified by the red cross. The different sensitivity of the parameters over the cost function is observed though the different ranges of the cost function variation along y-axis.

4.2. Exploring different inflow wind speeds

A calibration procedure and a final calibrated model have been proposed. However, as previously mentioned, the solution is highly dependent on the input information. The next section addresses this issue by expanding the analysis to include various inflow wind speeds. This approach aims to establish a universal representation of the environment, identifying a range of conditions (wind speeds) within which the calibrated model remains valid. Additionally, the results will evaluate how well a single calibrated model can be used to describe all turbines within a wind farm. This is crucial because downstream turbines, affected by the wake of upwind turbines, experience reduced incoming wind speeds. If the calibration proves effective within a specified range of wind speeds, it can be applied to all turbines in wind farms operating under those conditions.

All the previous considerations have been carried out comparing the wake model to a single simulation from LES where the inflow wind speed was equal to 9 m/s. However, parameters may be wind speed dependent so it is fundamental analyzing different wind speeds to allocate the right values to the parameters for every condition. This section focuses on analysing this aspect, giving a better understanding about the sensitivity of parameters on input conditions. Only the inflow wind speed has been changed while all the other conditions have been kept the same as summarized in Table 4.2. It has been decided to take into account only wind speeds below rated which is at 11 m/s. The reason for this is twofold: at one side, this reduced analysis is sufficient to give an overall idea of parameters' behavior and additional time to produce and evaluate LES is avoided. On the other side, wake effects are significantly reduced above rated. Since the main purpose of this work is studying the wake itself, the selected range of winds speeds is assumed to give insightful information.

Table 4.2: Baseline LES and Turbine Parameters - Different Wind Speeds

Parameter	Value
Turbine	IEA 22 MW (Task 37 reference)
Hub height	170 m
Rotor diameter	283.21 m
Rated power	22 MW (@ 11 m/s)
Number of blades	3
Simulation time duration	1900 s
Domain size x-y plane	2280 x 4400
Inflow hub height wind speed	[4, 5, 6, 7, 8, 9, 10, 11] m/s
Turbulence intensity	0
Atmospheric Boundary Layer Conditions	Steady, Uniform and Laminar flow

LES have been reproduced again for every wind speed. Since the flow is laminar, there is no ambient turbulence involved and the wind speed is the only external parameter that could affect the calibration of parameters. Simulation time is 1900 s but the moment where the flow starts developing is not fixed and depends on the wind speed analyzed. Slower wind speeds cause a slower formation of the wake, therefore it requires more time to reach fully developed conditions. For every tested wind speed, the velocity output information from LES has been averaged over time after developed conditions have been reached. For the sake of completeness, the starting averaging time for every wind speed has been included in Table 4.3. It can be deducted that the time over which the simulation is averaged changes between the different wind speeds. However, since the flow has reached fully developed conditions, the flow shape is stable and the different time range does not influence the subsequent calculations.

Table 4.3: Starting time for time-averaging LES wind speed fields for all the conditions tested.

Wind speed	Starting time for averaging
4 m/s	1600 s
5 m/s	1600 s
6 m/s	1500 s
7 m/s	1500 s
8 m/s	1330 s
9 m/s	1330 s
10 m/s	1170 s
11 m/s	1170 s

Methodology described in Chapter 3 has been used: Differential evolution is performed to optimize the parameters of Super Gaussian model along the xy plane, with particular attention towards optimization settings as maximum number of iterations that may need to be changed to ensure convergence in every condition. Figure 4.7 reflects the results of the calibration for all the different inflow wind speeds and all the model parameters, where Figure 4.8 focuses more in particular on the parameters singularly. A comprehensive representation of the wind velocity fields before and after calibration can be retrieved in Appendix A.1 for all the wind speeds tested.

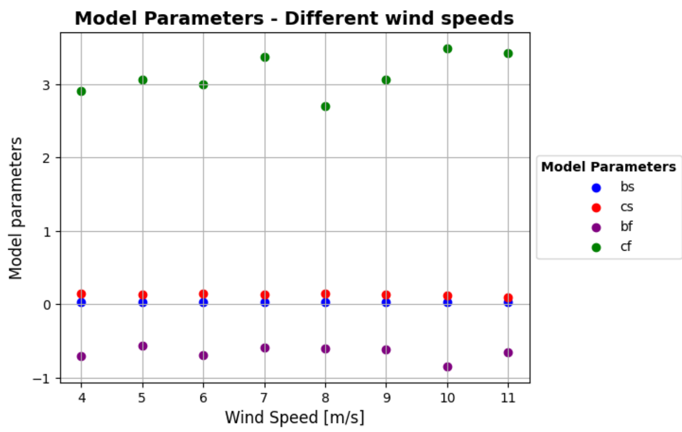

Figure 4.7: Model parameters values after the calibration with different incoming wind speeds in the range (4,11) m/s.

Table 4.4: Super Gaussian calibrated parameters for every wind speed.

Wind speed [m/s]	bs	cs	bf	cf
4 m/s	0.0311	0.145	-0.711	2.913
5 m/s	0.0302	0.134	-0.565	3.059
6 m/s	0.0295	0.143	-0.695	3.00
7 m/s	0.0280	0.129	-0.589	3.370
8 m/s	0.0303	0.146	-0.597	2.699
9 m/s	0.0278	0.139	-0.612	3.062
10 m/s	0.0242	0.121	-0.847	3.491
11 m/s	0.0242	0.0901	-0.659	3.423

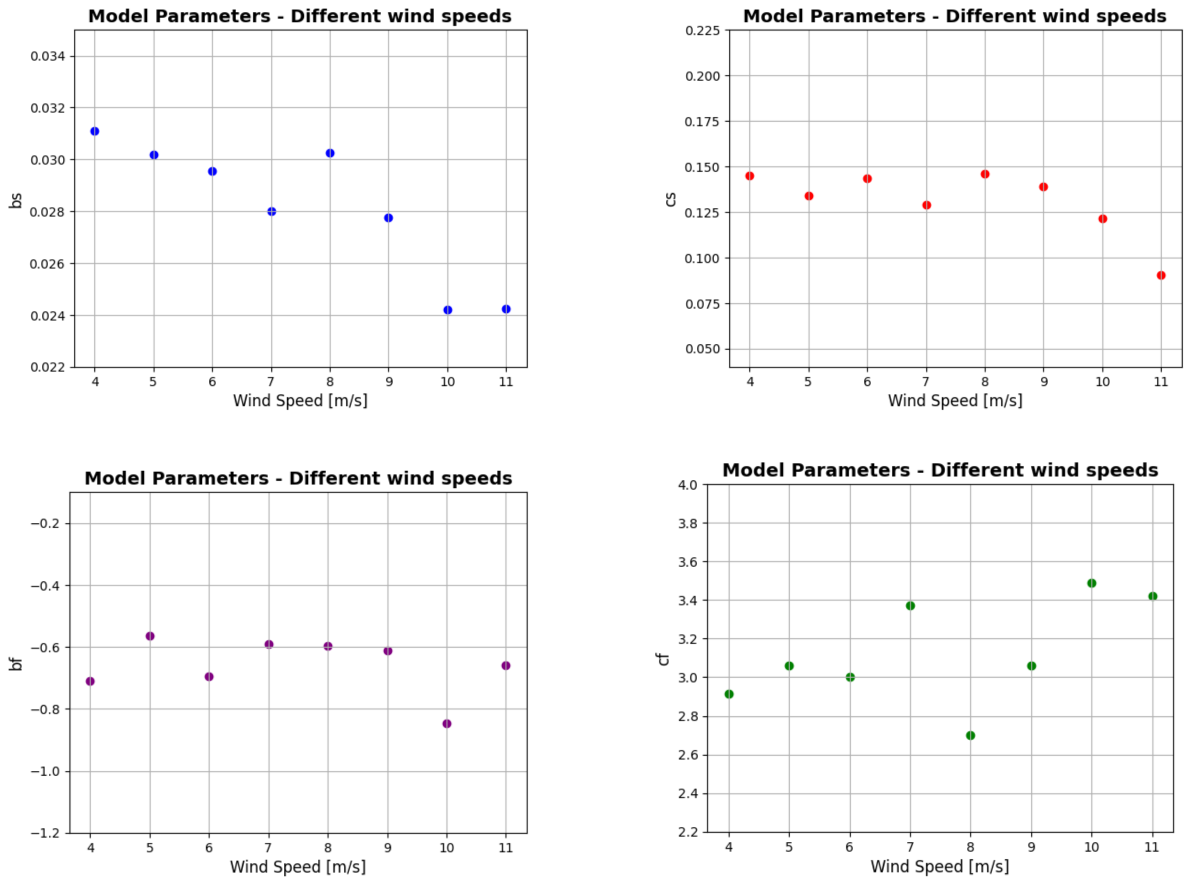

Figure 4.8: Model parameters behaviour with different incoming wind speeds in the range (4,11) m/s. The behaviours are displayed singularly for clarity.

All the numerical values are contained in Table 4.4 for a more accurate evaluation.
From Figure 4.7 cf seems to be the only parameter experiencing meaningful variations, but there is a different entity of variation along the y axes for the other parameters, therefore it is important having a deeper look at every single parameter singularly (Figure 4.8). The parameter cf changes in a wider range, followed by cs, bf and bs. There is no established trend, supported also by the fact that there is a strong inter-correlation between the parameters as showed in the sensitivity analysis (Figure 4.5). However, bs and cs change considerably for wind speeds of 10 m/s and 11 m/s, while they remained mostly constant at lower speeds. This can be attributed to the change in the thrust coefficient (CT), which decreases as shown in the CT curve (Figure 3.3). In wind turbine operation, CT measures the fraction of the wind's kinetic energy captured by the turbine. A lower CT indicates that the turbine is capturing less energy from the wind, directly impacting the wake characteristics: there is a less significant reduction in wind speed and pressure drop, resulting in a narrower wake. Since bs and cs are model parameters involved in calculating the wake width (σ), they decrease accordingly. This behavior of the wake width is illustrated in Figure 4.9, where it remains relatively consistent for similar CT values (with minor differences due to variations in the flow from LES) and consistently reduces as CT decreases.

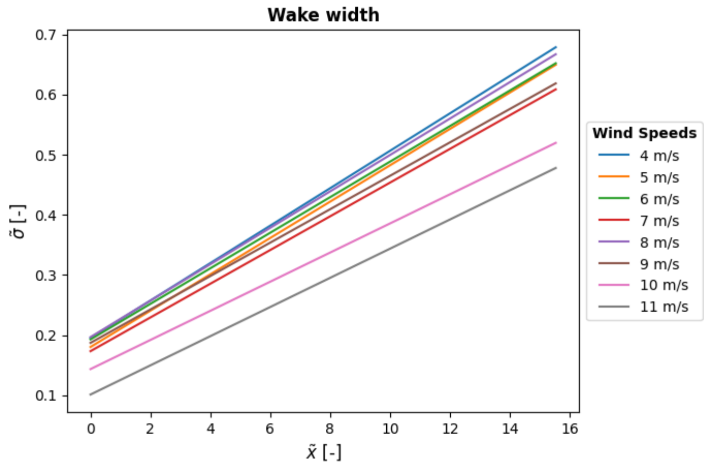

Figure 4.9: Wake characteristic width for different wind speeds. The $\tilde{\cdot}$ notation denotes normalization with respect to the rotor diameter. Specifically, $\tilde{x}$ represents the distance downstream of the turbine rotor, expressed in terms of rotor diameters.

It might seem that the parameters exhibit significant variation, suggesting a dependence on wind speed. However, it is possible that the strong interplay between the parameters, coupled with their different response to changes, results in a negligible impact on the wake representation. Figure 4.10 represents the relative error calculated by using the parameters calibrated for 4 m/s to approximate also the other wind speeds. Except for 10 m/s and 11 m/s, in every other condition, the error of doing such approximation is below 3%. A wind speed of 4 m/s is just used as a comparison, any other option can be used as well. The higher values can be easily explained by the reduction of CT which is a consequence of the fact that from rated wind speed (the process even starts slightly before) the turbine behaviour changes. From partial load region (before rated wind speed) to full load region (after rated wind speed) the purpose of the turbine imposed by control settings is different and turbine's blades are pitched to keep the generated power constant at the rated value.
The error is calculated as the difference between the cost function (formulated as MAE) of the correct calibration and cost function of the approximation. Relative errors of 3% can be considered negligible and it can finally be stated that the parameters are not indeed wind speed dependent in the partial load region, therefore a unique set of parameters can be used in such conditions still guaranteeing an accurate employment of the wake model.

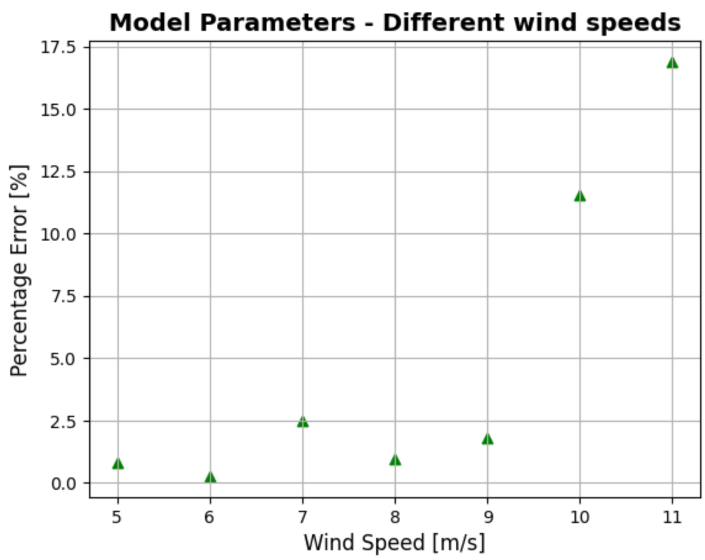

Figure 4.10: Relative error [%] produced by using 4 m/s calibrated parameters as approximation for the other wind speeds.

Sensitivity analysis is then performed for every parameters and results can be found in Figure 4.11 and 4.12. The sensitivity index of a particular parameter remains relatively stable, especially for the total-order evaluation, which accounts for all interactions and thus holds greater significance, except at 10 m/s and 11 m/s. This indicates that, despite variations in the solution due to differing calibrated parameters, their proportional influence on output error remains largely consistent. These findings suggest that the calibration process is robust and comprehensive, requiring no specific adjustments. Additionally, this stability highlights that although parameters are highly responsive to inflow conditions, the overall outcome shows comparatively lower sensitivity.

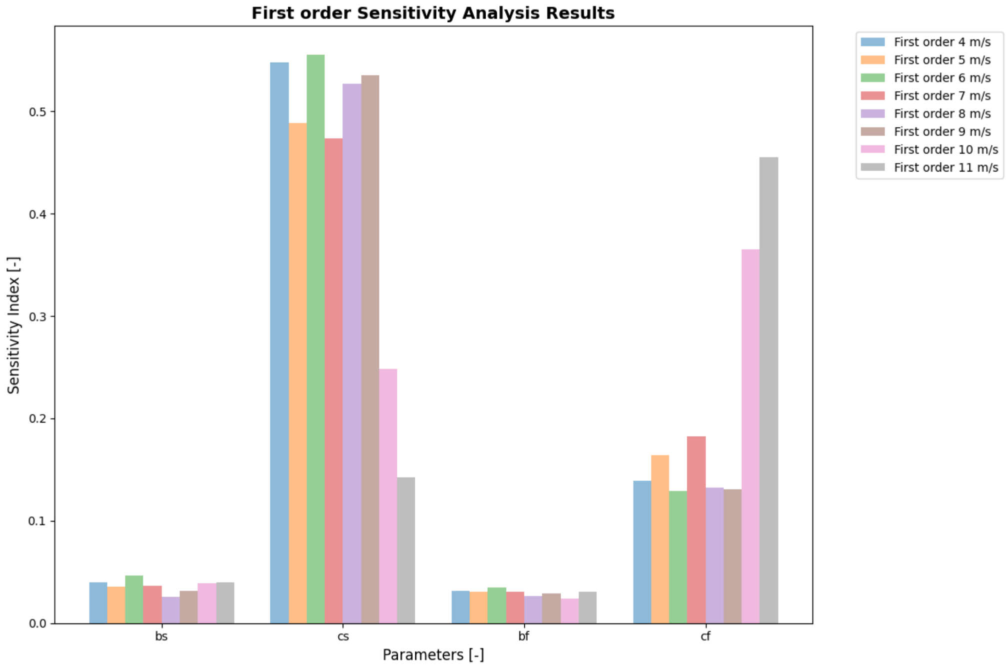

Figure 4.11: Sensitivity analysis results for model parameters at different wind speeds - First Order Sobol Indices.

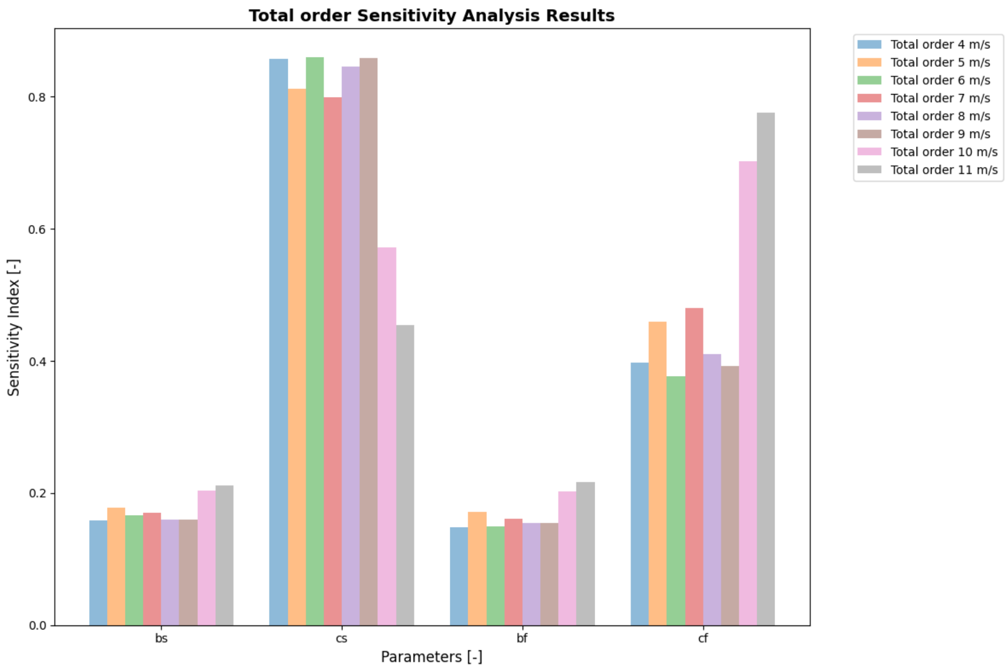

Figure 4.12: Sensitivity analysis results for model parameters at different wind speeds - Total Order Sobol Indices.

5
Results Helix

In this research, the primary objective was to calibrate engineering wake models, specifically focusing on comparing the Gaussian and Super-Gaussian wake models. The initial step involved developing a robust calibration method to identify the most accurate wake model and the most effective calibration technique. To achieve this, various optimization algorithms and problem formulations with different objective functions were explored. The experimental data for calibration was obtained from large eddy simulations (LES) over the xy plane. Upon comparing the Gaussian and Super-Gaussian models, it was determined that the Super-Gaussian model provided superior accuracy. This finding was significant as it highlighted the model's ability to better capture the intricacies of wake behavior, thus making it a more reliable tool for engineering applications. Following the initial calibration, a sensitivity analysis was conducted on the parameters of the Super-Gaussian model. This analysis aimed to identify which parameters had the most substantial impact on the model's accuracy. Understanding the sensitivity of these parameters is crucial because it allows for more focused calibration efforts, improving the model's precision and reliability. The sensitivity analysis revealed that certain parameters were indeed more influential, providing valuable insights for refining the model further.

In possess of a resilient resolution model and having explored the main characteristics and challenges, it is possible to expand the analysis to a wider range of cases. In this chapter the main question of the thesis will be investigated: *Which is the relation between model parameters and control input settings*.

5.1. Helix Approach Calibration for a single turbine

In wind farm operational optimization, Dynamic Induction Control (DIC) and Dynamic Individual Pitch Control (DIPC) are the most sophisticated techniques proposed to optimize turbine performance and enhance overall energy production. While both DIC and DIPC offer significant benefits, the latter is often preferred because it directly addresses one of the major challenges in wind turbine operation: mechanical loads. High mechanical loads can lead to increased wear and tear, higher maintenance costs, and reduced turbine lifespan. DIPC mitigates these issues by controlling blade pitch to balance loads and reduce stress.
For its larger potential in wind farm applications, Individual Pitch Control (IPC) has been chosen for further analysis. Various scenarios have been studied by changing the pitch angle of the turbine blades and study the effects on the wake and on the model which describes it. This study aims to identify trends in model parameters across various pitch angles, with the goal of generating a dataset that covers a much broader range of angles than those directly tested. With this dataset, it becomes possible to optimize the wind farm operation by incorporating the contributions of individual pitch control directly in the wake deficit model.

5.1.1. Simulation environment testing different pitch angles

The calibration procedure used earlier has been applied again for this analysis. The environmental conditions and turbine configuration are identical to those in Chapter 3, with the exception that DIPC is now implemented. LES, with the characteristics outlined in Table 5.1, have been used as experimental data for the calibration. The information specifically related to the applied control is in Table 5.2.

Table 5.1: Helix approach - Turbine and LES Parameters.

Parameter	Value
Turbine	IEA 22 MW (Task 37 reference)
Hub height	170 m
Rotor diameter	283.21 m
Rated power	22 MW (@ 11 m/s)
Number of blades	3
Simulation time duration	3000 s
Simulation time @ fully developed conditions	1100 s
Domain size	2800 x 4400
Inflow hub height wind speed	9 m/s
Turbulence intensity	0
Atmospheric Boundary Layer Conditions	Steady, Uniform and Laminar flow

Table 5.2: Helix approach - Control related Parameters.

Parameter	Value
Strouhal Number	0.2825
Pitch Angle Amplitude	[0.5, 1, 1.5, 2, 2.5, 3, 4, 4.5, 5]
Phase Offset	90° - Counterclockwise motion

The control input is a low-frequency periodic signal for the pitch angle, divided into tilt and yaw components which differ only for a phase offset ϕ as showed in Formulas 5.1 and 5.2 ([26], [69]). A counterclockwise (CCW) helix is obtained for a phase offset of $\phi = \pi/2$. Individual blade pitch is used to generate directional moments on the rotor by dynamically varying tilt and yaw angles such that the resulting wake is manipulated in both vertical and horizontal motion, producing an helical shape.

$$\beta_{tilt} = \beta sin(w_e t) \tag{5.1}$$

$$\beta_{yaw} = \beta sin(w_e t + \phi) \tag{5.2}$$

Like any periodic signal, it is characterized by a specific amplitude (β) and frequency (f_e from $w_e = 2\pi f_e$). It is very common to represent the frequency though a dimensionless number called Strouhal Number (St). For the actuation, tilt and yaw signals needs to be transformed to three blade pitch actuation signals in the rotating coordinate system. This is implemented though a Multi-Blade Coordinate transformation (more insight about the coordinate transformation can be found in [9]).

$$St = \frac{f_e D}{U_\infty} \tag{5.3}$$

D the rotor diameter and U_∞ the inflow velocity.
In this analysis, U_∞ is set to 9 m/s. As discussed in Chapter 4.2, for wind speeds below the rated value, calibration can be performed at a single velocity and generalized across the entire range. Consequently, this analysis is valid for all wind speeds up to 11 m/s.

Nine different conditions were analyzed, varying the pitch angle amplitude up to 5°, while keeping the signal frequency fixed at the corresponding Strouhal number of 0.2825. The optimal signal amplitude and frequency have not yet been identified in literature. For Dynamic Induction Control (DIC), an optimal Strouhal number of 0.25 was found ([27]), and this value has been used for several evaluations of the helix approach, assuming similar optimal conditions ([26], [69], [38]). However, [72] and [49] state that for the helix approach, the optimal excitation frequency is higher compared to DIC, and the value used in this analysis is derived from [72].

Since the procedure is carried over steady state conditions, simulations must be time averaged whenever fully developed conditions are reached as done previously. However, this time the procedure is slightly different due to the dynamic aspect in control inputs. The simulation must be time averaged over multiples of helix revolutions to capture the full information of the signal applied. The maximum number of revolutions in the time range of fully developed conditions has been used. Figure 5.1 shows the averaged velocity field from LES under different pitch angle amplitudes. The representation with the full set of pitch amplitudes tested is shown in the appendix A.3. The region extending 5 rotor diameters behind the turbine has been highlighted as a reference, as this is a typical distance between turbines in a wind farm. This makes the effects of the DIPC and its potential impact on downstream turbines more evident. It can be observed that increasing the amplitude shortens the wake and alters its shape. The same behavior can be observed from the velocity field described by the Super Gaussian model after calibration in Figure A.4.

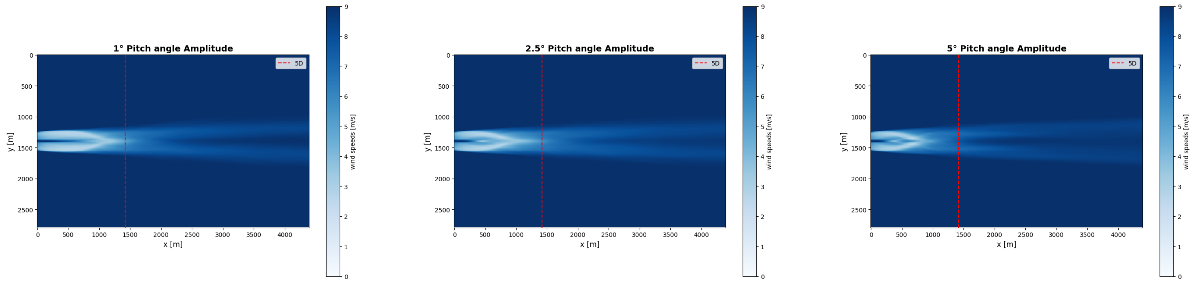

(a) LES pitch angle amplitude=1° **(b)** LES pitch angle amplitude=2.5° **(c)** LES pitch angle amplitude=5°

Figure 5.1: Wake representation from LES for different pitch angle amplitudes of DIPC. The red dotted line indicates a distance of 5 rotor diameters from the turbine rotor, which is a typical spacing between adjacent turbines in wind farms.

Calibration of parameters is performed using data from all nine discrete pitch angle amplitudes. However, this alone is insufficient for replicating the flow fields generated by Large Eddy Simulations. The control strategy involves generating different resultant forces at the rotor level through varied individual blade pitching. This approach affects the turbine's operational configuration, deviating from the simpler single turbine control. Consequently, both the thrust coefficient and power coefficient are varied, which in turn affects the power output. This information must be included in the analysis. In PyWake it is possible to define the turbine using its power curve and thrust coefficient curve, both of which have been extracted by OpenFast. Without this, the only information on individual pitch control would derive from parameters calibrated with various LES flow fields, which only describe the conditions downstream of the turbine, not the configuration at the rotor level. For each different pitch angle amplitude considered, the turbine's power curve and CT curve were reconstructed, resulting in a total of nine distinct turbine configurations. In Figure 5.2 the changes in CT and power values across different pitch angle amplitudes for 9 m/s can be observed. The reduction in power is straightforward: as the blade moves further from its optimal configuration, less power is generated. Similarly, the thrust coefficient also decreases as it deviates from its optimal value. More insights about the OpenFast model can be found in B.2.

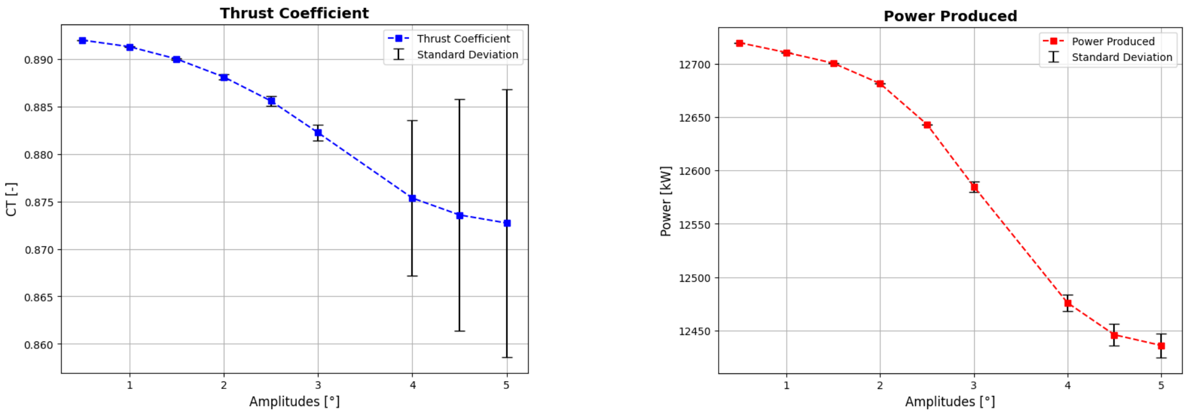

(a) CT Curve

(b) Power Curve

Figure 5.2: Degradation of CT and Power with the application of Individual Pitch Control (values generated with input wind speed of 9 m/s). Mean values and range of oscillation.

5.1.2. Calibration and Curve fitting over different pitch angles

The results of the calibration for different pitch angle amplitudes in terms of wind fields are shown in the appendix (A.2). Since the velocity field strongly changes, it is required to tune optimizer's hyperparameters every time in order to guarantee a global solution.
Due to practical constraints, only the selected set of simulations were used for the calibration. However, the individual pitch control can select the optimal pitch configuration over a continuous range of values. Consequently, a fitting procedure was performed for each model parameter, enabling a wider range of values and describing how they vary with the amplitude. Since the goal is to keep the model as simple as possible, the parameters are fitted using simple polynomial functions. While higher-degree polynomials provide more accurate fits, a second-degree polynomial has been considered sufficiently precise.

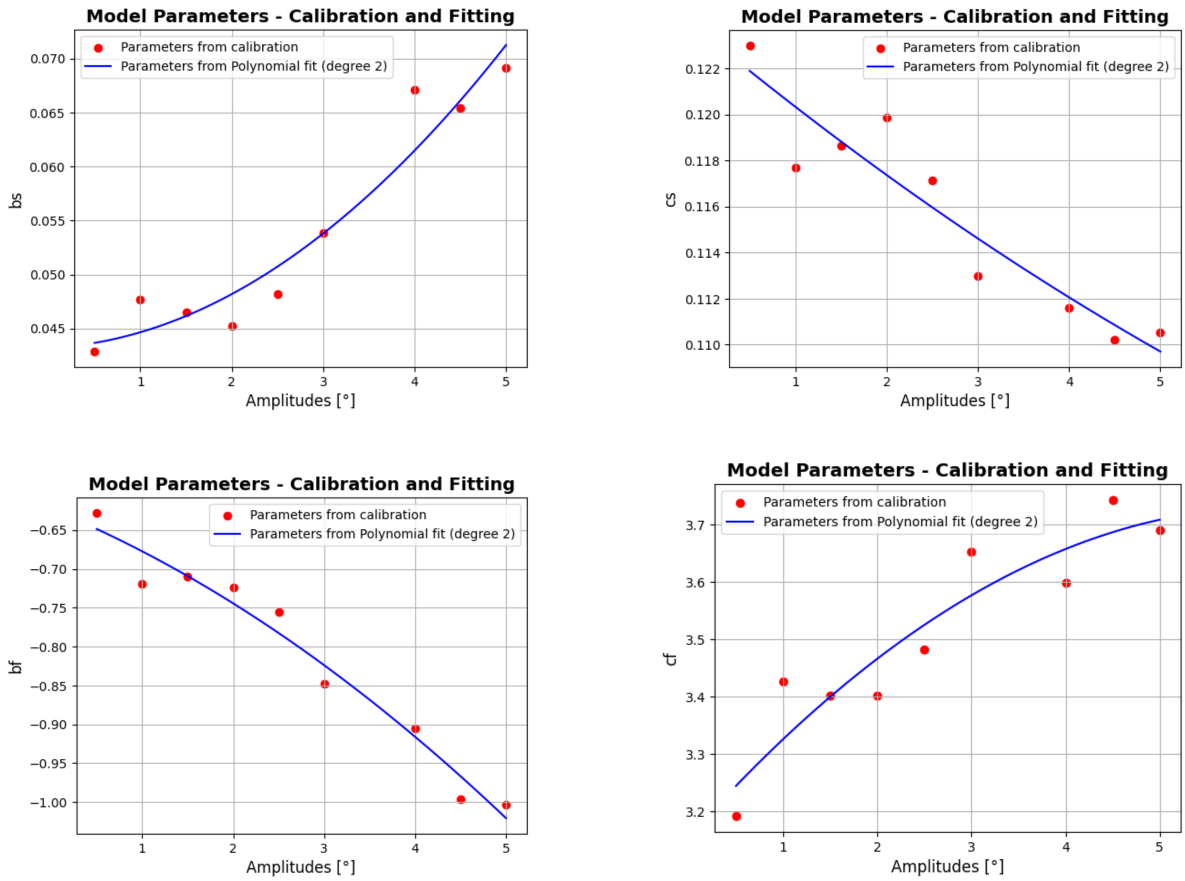

Figure 5.3: Super Gaussian calibrated parameters for different pitch angle amplitude (red dots) and polynomial second-grade fit (blue line).

Figure 5.3 shows the results of the calibration and their polynomial interpolation. It can be observed a different trend for each parameter. The relationship between the parameters and the wake dynamics is complex and nonlinear, due to the intricate nature of the wake model and the frequent inclusion of numerous terms in the equations. However, certain values in the formulas hold physical significance and can be explained more easily such as $\tilde{\sigma}$ and the super Gaussian coefficient n.

$$\tilde{\sigma} = b_s \tilde{x} + c_s \sqrt{\beta} \tag{5.4}$$

$$n = a_f e^{b_f \tilde{x}} + c_f \tag{5.5}$$

The term $\tilde{\sigma}$ represents the characteristic wake width, which increases linearly downward from the rotor (the tilde symbol denotes a normalization by the turbine diameter). The rate of this expansion is determined by the parameter bs, while the offset is influenced by cs and varies with the thrust coefficient (beta is a function of the thrust coefficient). Increasing the pitch angle amplitude typically reduces the thrust coefficient (CT) (subfigure 5.2a). This happens because the turbine deviates from its optimal angle of attack for energy extraction, resulting in less effective utilization of the wind's kinetic energy. As the thrust coefficient decreases with higher pitch angle amplitudes, β does the same and the parameter bs in the wake width formula tends to increase. This means the rate at which the wake width expands downstream becomes steeper. Concurrently, the offset parameter cs, which accounts for the starting point or baseline of the wake width, tends to decrease. This indicates that the wake starts narrower at the turbine (or rotor plane) due to the reduced thrust coefficient. The combined effect of increasing bs and decreasing cs leads to an overall increase in the wake width $\tilde{\sigma}$ downstream from the turbine. This means that despite the decrease in thrust coefficient and less efficient energy extraction, the wake

spreads out more extensively as it moves downstream.
In some cases, a wider wake could potentially lead to better wake mixing because it may allow for more uniform distribution of momentum and kinetic energy within the wake over a larger area. This could theoretically reduce the velocity deficit downstream, allowing downstream turbines to operate more efficiently.

In the super Gaussian wake model, the coefficient n describes how the super Gaussian order varies with downstream distance. Increasing the pitch angle enhances mixing in the wake. bf in the super Gaussian model represents the rate at which the wake profile transitions with downstream distance. With enhanced mixing, the gradients and variations in the wake profile along $\tilde{x}$ become smoother. This smoother transition explains the decrease of bf in Figure 5.3. cf represents the baseline or offset of the wake profile. It increases with increasing pitch angle amplitudes adjusting to the variation in the wake shape, reflecting the baseline value of n. Overall the value of n increases with the amplitude: the enhanced mixing tends to deviate the wake profile from a Gaussian distribution (which is obtained when n=2).

The behaviour of $\tilde{\sigma}$ and n is illustrated below for a select set of amplitudes to enhance clarity:

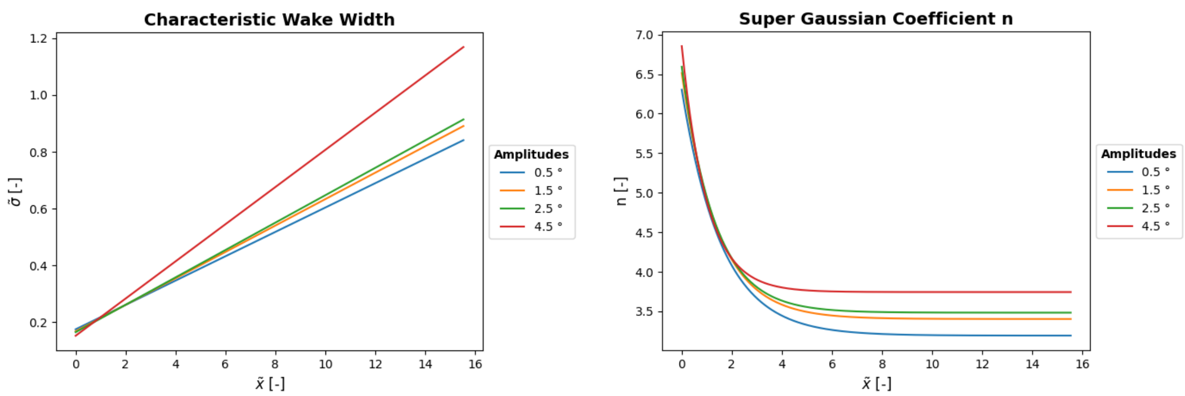

(a) Characteristic Wake Width

(b) SuperGaussian coefficient

Figure 5.4: Characteristic Wake Width and SuperGaussian coefficient for pitch angle amplitudes=[0.5°,1.5°,2.5°,4.5°].

Now, attention can be directed towards fitting the trend. Initially, it's crucial to ensure that the polynomial fit adheres to the physical constraints imposed by the optimization and respects the boundaries. Additionally, the new distribution should accurately depict the problem at hand. Given that the optimized values should already represent the optimal configuration, there may be slight deviations in the fit. It could better describe the wake (resulting in a lower cost function) or perform worse. In the former scenario, this could be due to the optimizer encountering local minima, thus failing to identify the global optimum while the fit succeeds. In the latter case, it's important to assess whether the approximation error significantly worsens, indicating that the fit no longer accurately represents the selected conditions. Figure 5.6 illustrates that, with the exception of the first two tested amplitudes where the fitting performs worse, it generally improves performance. Therefore, the fitting is considered valid.

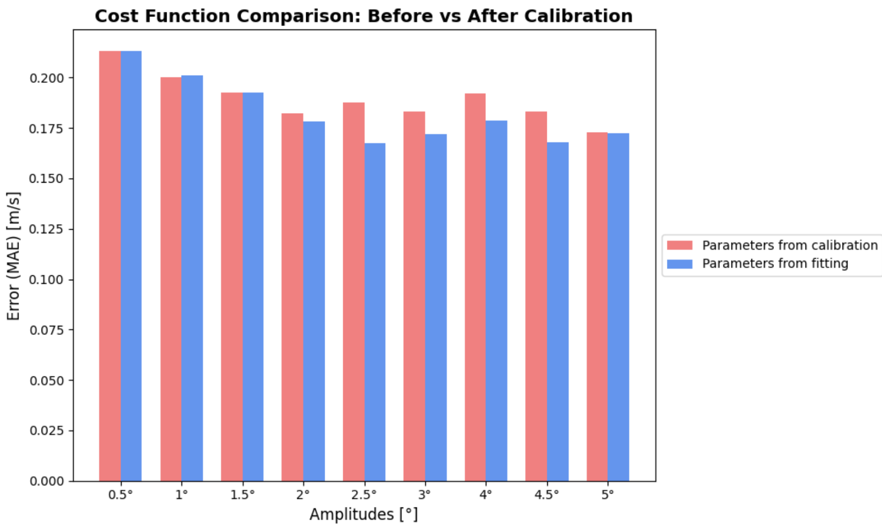

Figure 5.5: Cost function evaluation (MAE) with model parameters immediately after calibration and after polynomial fitting.

The final problem formulation including the information of DIPC can be finally presented as follows, where x is the pitch angle amplitude of the control signal:

Super Gaussian Model:

$$U_{\text{model}} = U_\infty(1 + 2^{2/n-1} - \sqrt{2^{4/n-2} - \frac{nC_T}{16\Gamma(2/n)(b_s\tilde{x} + c_s\sqrt{\beta})^{4/n}}})e^{-\frac{\tilde{r}^{n(\tilde{x})}}{2(b_s\tilde{x}+c_s\sqrt{\beta})^2}})$$

$$n = a_f e^{b_f\tilde{x}} + c_f$$

$$b_s = b_{s,1}x^2 + b_{s,2}x + b_{s,3}$$

$$c_s = c_{s,1}x^2 + c_{s,2}x + c_{s,3}$$

$$b_f = b_{f,1}x^2 + b_{f,2}x + b_{f,3}$$

$$c_f = c_{f,1}x^2 + c_{f,2}x + c_{f,2}$$

$$b_{s,1} = 0.00104 b_{s,2} = 0.00042 b_{s,3} = 0.04319$$
$$c_{s,1} = 0.0001 c_{s,2} = -0.0033 c_{s,3} = 0.123$$
$$b_{f,1} = -0.0063 b_{f,2} = -0.048 b_{f,3} = -0.623$$
$$c_{f,1} = -0.015 c_{f,2} = 0.184 c_{f,3} = 3.15$$

5.1.3. Curve fitting verification

The recently obtained fit will be validated for a different wind speed to demonstrate its universal applicability across all wind speeds below rated conditions. As mentioned in Section 4.2, the calibration process can be simplified to a single procedure for wind speeds below rated conditions. However, this has only been confirmed for baseline simulations without the helix approach. Therefore, it is crucial to validate this under conditions where DIPC is implemented. To this end, the calibration procedure has been repeated for an LES wind speed field with a 7 m/s incoming wind speed. The helix control approach has been applied to the rotor at the same frequency corresponding to a Strouhal number of

0.2825, with an amplitude of 3°. For the purpose of this verification, only a single additional data set from LES has been utilized. However, additional data can be incorporated to achieve a more comprehensive verification. Figure 5.6 shows the results of the calibrated parameters with 3° amplitude of the helix signal. Both 9 m/s and 7 m/s incoming wind speeds are used for the comparison.

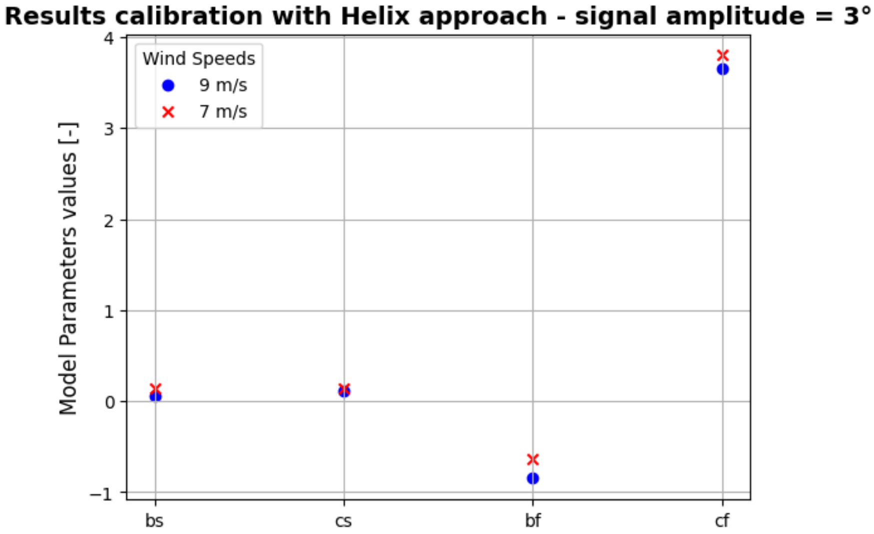

Figure 5.6: Result of the calibration process in terms of model parameters with a 3° amplitude helix control signal applied for incoming wind speeds of 7 m/s and 9 m/s. Blue dots correspond to 9 m/s wind speed while red crosses to 7 m/s.

The discrepancy in the parameter values is minimal, thus confirming the aforementioned statement. The expanded model retrieved in Section 5.1.2 is considered valid in the whole range of wind speeds before rated conditions.

5.2. Helix approach Application in a wind farm

The next phase of the research aims to demonstrate the practical benefits of using helix control with the calibrated parameters in a realistic setting: a real wind farm. This analysis will evaluate the advantages of applying helix control under different wind directions, considering the varying degrees of wind superposition and interaction that occur in such environments. The objective is to validate the enhanced Super-Gaussian model by proving its efficacy in optimizing wake dynamics and improving overall wind farm performance. By examining different wind directions, this study will account for the complex interactions that occur in real-world conditions, providing critical insights into the practical applications of helix control and its potential to enhance wind farm efficiency and output.
To achieve this, the analysis will optimize the helix configuration for each turbine in the wind farm to maximize power production. This process will consider the unique characteristics of each turbine, its position within the farm, and prevailing wind conditions. Helix control, although currently theoretical and not yet applied in real-world settings, holds significant promise for improving wind farm efficiency. By systematically adjusting the helix angles and evaluating the resulting power output, the study will identify optimal configurations that lead to the highest power production. This approach not only highlights the potential of helix control, but also provides a practical simulation of its performance in a real wind farm setting.

5.2.1. Wind Farm Simulation

To delve deeper into the optimization of wind farm configurations, this chapter will focus on the Lillgrund Wind Farm as a case study ([73]). The Lillgrund Wind Farm, located 10 km off the coast near Malmö, Sweden, is an ideal site for this analysis due to its compact layout, which makes wake effects a significant issue. This characteristic is particularly relevant for our study, as it amplifies the potential benefits of helix control in mitigating wake losses.
The wind farm comprises 48 Siemens SWT-2.3-93 turbines, each with a capacity of 2.3 MW. These

turbines are arranged in a grid pattern, which is designed to optimize space usage and maximize power production. The distance between the turbines is approximately 3.3 rotor diameters within rows, which are distant 4.3 rotor diameters between each other as showed in Figure 5.7. Each turbine is identified by the number of the row and the letter of the respective position.

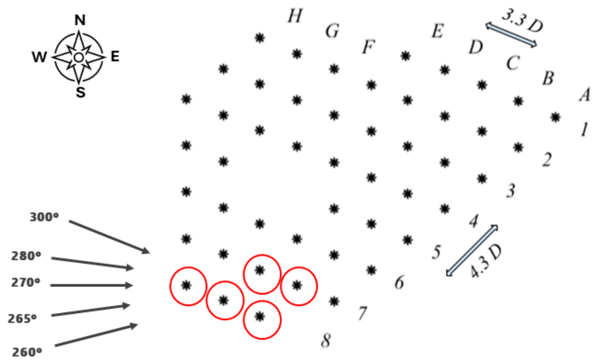

Figure 5.7: Layout of the Lillgrund Wind Farm in Sweden (adapted from [62]). Wind directions are evaluated from North (0°) and represent the tested wind directions. The turbines under consideration are marked by the red circle. The distance between turbine rows is 3.3D and 4.4D.

Due to computational time constraints, only the section of the wind farm highlighted in the figure above will be simulated, rather than the entire farm. This region has been selected because it is located on the border, ensuring it is not influenced by upstream wakes and therefore it can be isolated for the present analysis. Furthermore, according to the [31] where seven months data records have been retrieved (wind rose in Figure 5.8), the winds predominantly come from west, making this area ideal for the study.

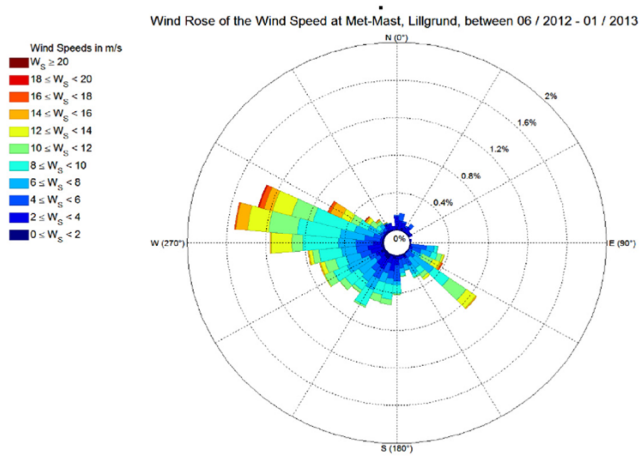

Figure 5.8: Wind rose Lillgrund wind farm recorded at met mast location (61 m) from 06/2012 to 01/2013

For the five wind turbines analyzed, an optimization problem is solved to determine the optimal helix angle amplitudes for each turbine in order to obtain the overall maximum power production. The wake evolution is modeled using the Super Gaussian model, with model parameters adjusted based on the optimal helix amplitudes. The amplitude range is between 0 and 5, and the relationship with model parameters is established through fitting performed in Chapter 5.1.2. The problem is again non-linear and non-convex due to the nature of the Super Gaussian model. Consequently, only heuristic methods are suitable for finding a solution. The optimization process is implemented in Python using genetic algorithm from the *scikit-opt* library.

The interaction and superposition of wakes depend on the wind direction. When turbines align with the wind, the wake effect is strongest, significantly reducing power for shaded turbines. Partial wake impacts have less severe consequences. The Helix Approach is expected to be most effective in fully aligned conditions, where mitigating wind speed reduction is crucial. However, it can also boost power production in other configurations. To explore different scenarios, the optimization is conducted for various wind directions, primarily from the west. The wind directions used are shown in Figure 5.7 and are measured from the north. The primary focus should be on the upstream turbines, as their impact influences the performance of those downstream. Nevertheless, the configuration of the downstream turbines is also taken into account in the optimization process. This consideration is due to potential overlaps in certain directions and to demonstrate that when the wake effect does not require optimization (i.e., there are no turbines behind), the optimal configuration involves no control to maximize power production.

Wind direction= 270°:

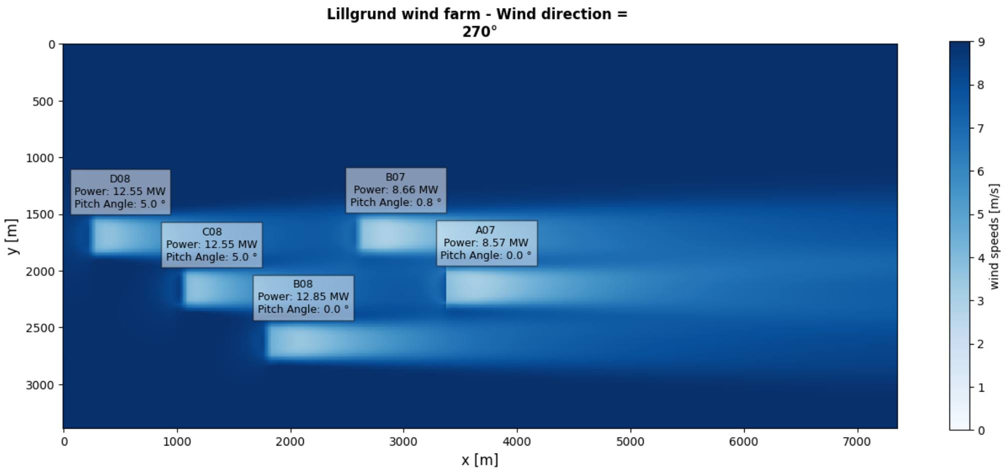

Figure 5.9: Lillgrund wind farm helix angle optimization results for a wind direction of 270°: The final power output and the optimal pitch angle amplitude are provided for each turbine.

When the wind blows from the west at 270°, turbines B07 and A07 are fully shadowed by the wake produced by turbines D08 and C08. The contribution of turbine B08 is almost negligible. Turbines D08 and C08 have optimal pitch angles set to 5°, which maximizes the rate of mixing and minimizes their impact on the other turbines. While this reduces the power output of D08 and C08, the benefit of increased power production in B07 and A07 makes it worthwhile. B07 and A07 generate more power and their configuration requires minimal control since their wake effect does not impact any other turbines.

Wind direction= 260°:

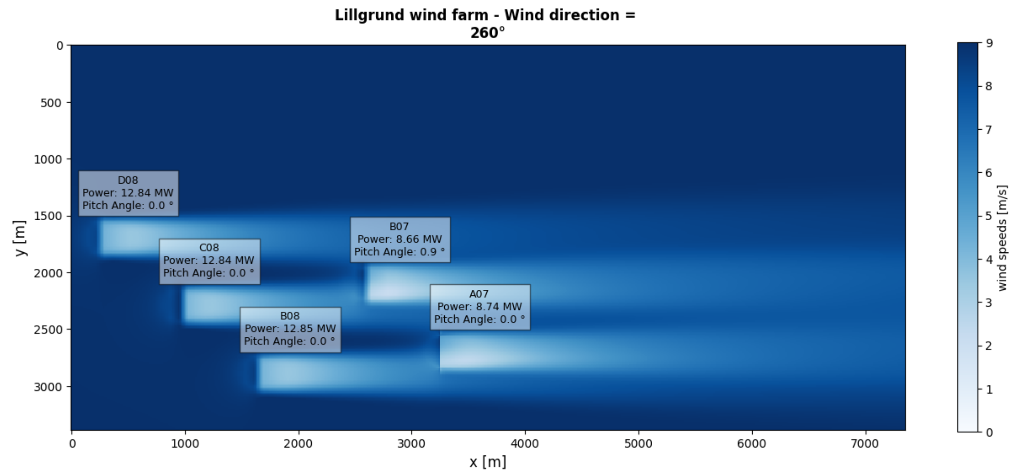

Figure 5.10: Lillgrund wind farm helix angle optimization results for a wind direction of 260°: The final power output and the optimal pitch angle amplitude are provided for each turbine.

In this configuration, the wake from the first row of turbines partially affects the second row. While at 270°, B07 and A07 are impacted by the wake from D08 and C08, in this scenario, the primary influence comes from C08 and B08, respectively. Despite the shorter distance, the shading is only partial. Here, helix control does not enhance the performance of the downstream turbines because its optimal configuration requires negligible pitch angle values.

Wind direction= 265°:

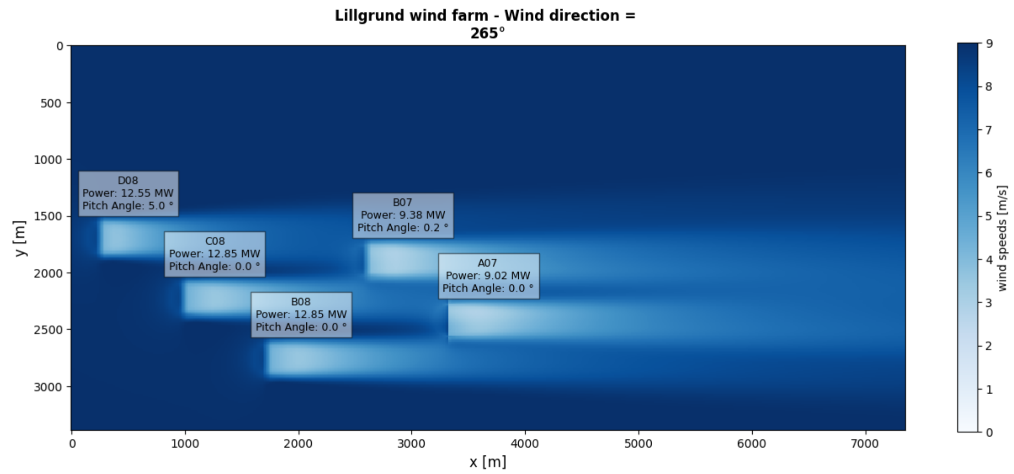

Figure 5.11: Lillgrund wind farm helix angle optimization results for a wind direction of 265°: The final power output and the optimal pitch angle amplitude are provided for each turbine.

The turbines in the second row are now almost completely shaded again. This time, however, they are affected by the presence of both nearby upstream turbines, not just one. This results in a combination of upstream turbines working to minimize their impact on the affected turbines by enhancing mixing. However the benefits of using the helix approach are still minimal and its effect is comparable to no control. That is why D08 and C08 seem having different configurations for similar relative distance with their closer downstream turbine. This effect is more evident when the no control case is compared in next chapter. B07 and A07 again minimize their individual pitch control since it is not needed. B08 barely influences A07.

Wind direction= 280°:

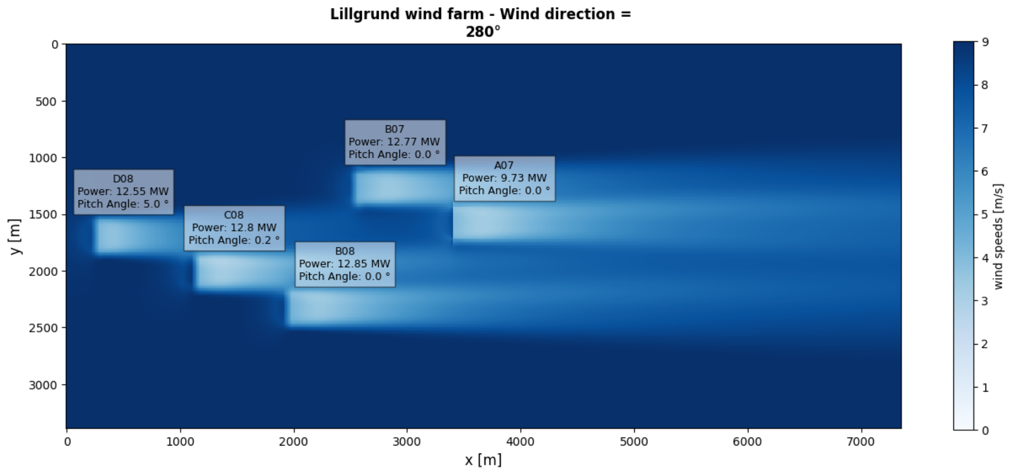

Figure 5.12: Lillgrund wind farm helix angle optimization results for a wind direction of 280°: The final power output and the optimal pitch angle amplitude are provided for each turbine.

As the wind shifts northward, turbines in rows 7 and 8 begin to affect each other. A07 is now completely within the wake of the preceding turbine, even though the distance from D08 has increased and the wake has started to recover. The result is higher power production compared to the other cases where the turbines were completely inside the wake but with closer distances.

Wind direction= 300°:

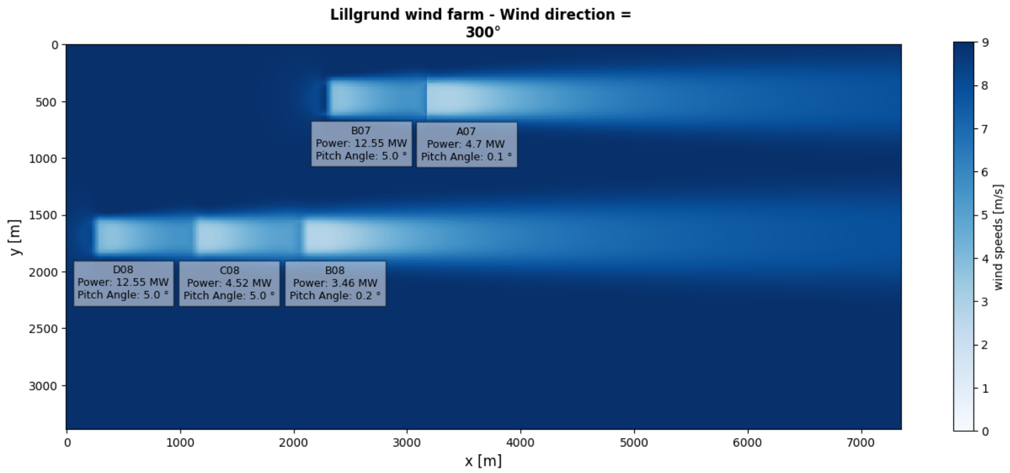

Figure 5.13: Lillgrund wind farm helix angle optimization results for a wind direction of 300°: The final power output and the optimal pitch angle amplitude are provided for each turbine.

When the wind direction is 300° from north, the wind farm layout is in its worst configuration. The minimum distance between rotors is experienced which is 3.3D. The wake has just transitioned from near to far wake and the wind deficit produced is still very impactful. Here is where the helix approach exploits its full potential. Turbines which wake impact other turbines are forced to the configuration that produces the maximum rate of mixing behind, which is for a pitch amplitude of 5°. The power produces is significantly lower compared to other configurations where the turbines were more spaced.

5.2.2. Improvements Wind Farm Optimization with Helix Approach

In this section, a detailed analysis of the power production in the wind farm is presented, comparing the performance of the conventional "greedy control" method (referred to as "No Control") with the "helix control" approach. The greedy control strategy, which optimizes each turbine's output individually, often leads to suboptimal overall performance due to wake effects on downstream turbines. In contrast, the helix control method strategically adjusts turbine operations to enhance wake mixing, thereby improving the power output of downstream turbines. In the following comparison, it is observed that the power output of the first turbines decreases as they no longer operate at their optimal configuration. However, the turbines affected by the wake of these leading turbines benefit significantly from the induced wake mixing, resulting in an overall enhancement in performance (depicted in Figure 5.14). The helix pitch angles of every turbine are the results of the optimization just performed in 5.2.1, where each amplitude is the best value that maximizes the overall performance. Figure 5.15 shows the power production with and without helix control applied. It can be observed the effect on single turbines and on the overall configuration for the different wind direction considered.

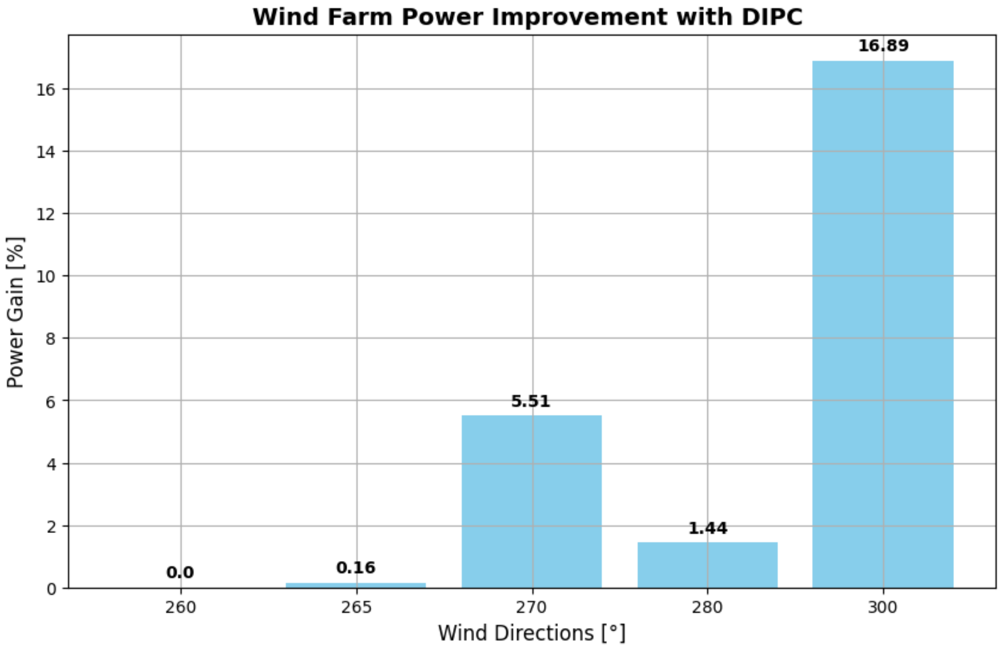

Figure 5.14: Overall percentage wind farm power gain [%] using DIPC instead of simple "greedy control" for different wind directions tested.

As mentioned before, the helix approach expresses its full potential when turbines are arranged all in a row, which is the case for 300° with an increase of 16.89% in the power production. Also for wind directions of 270° and 280° some turbines are completely shaded and the improvement is straightforward. The biggest the distance between the turbines and the lowest the effect of the helix control is because of the natural recovery of the wind flow. This is the reason why for 270° the effect on the second row of turbines is around 25% while for 280° is around 15%. For 260° the optimal configuration is with no control and for 265° the use of control is almost imperceptible.

These results show the effectiveness of DIPC application, only formulated theoretically, in a real wind farm simulation. Moreover, they highlight the importance of well-informed engineering models for executing online control and advancing this emerging field of research.

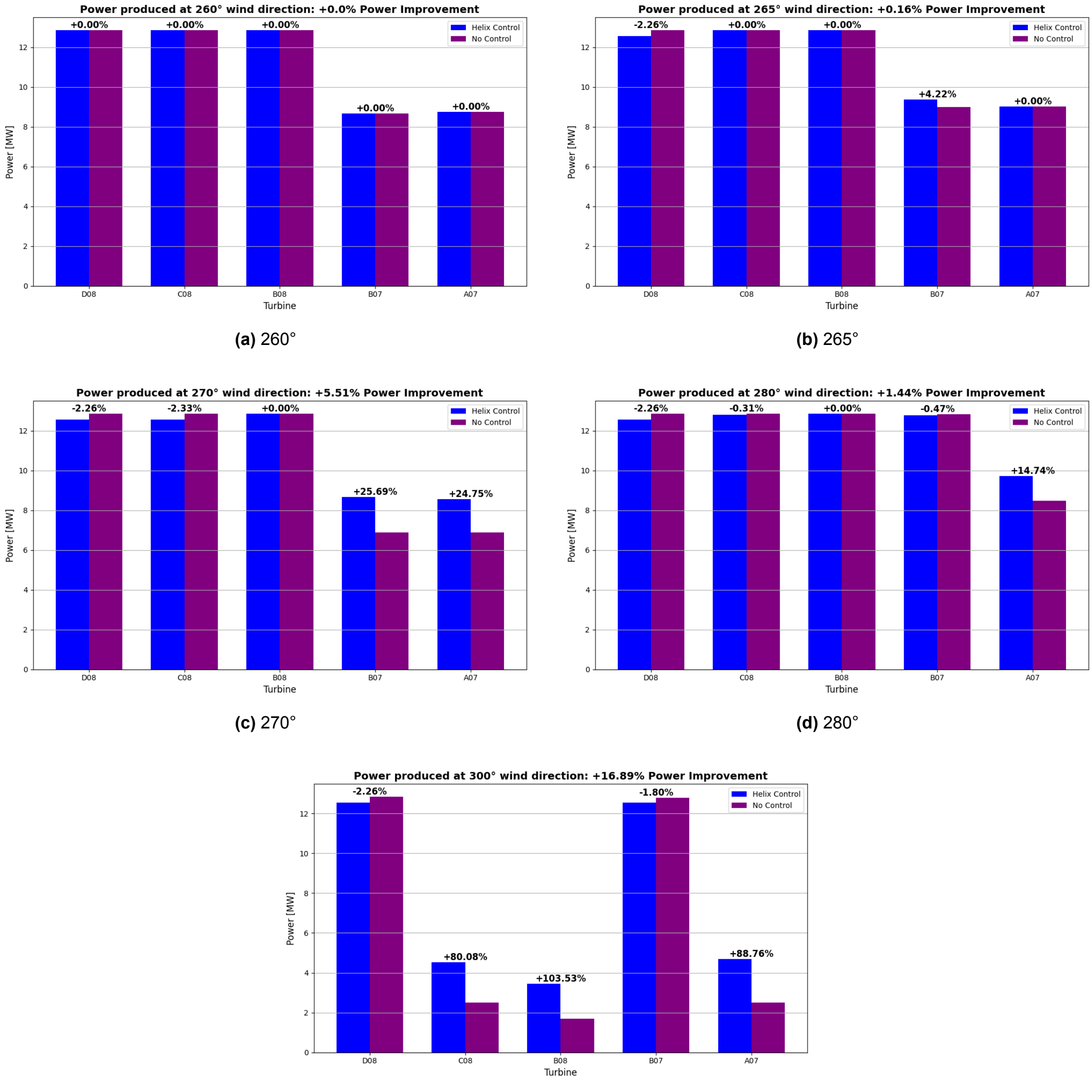

Figure 5.15: Power produced by single turbines comparison with (purple) and without (blue) helix control for different wind directions. The single turbine's power change is relative to the condition with no control applied. The overall power improvement is stated in the title.

6 Conclusions and Further Work

6.1. Conclusions

The objective of this master thesis was to introduce the information of the helix approach into an engineering wake model to expand existing wake model formulations, facilitate the calibration process and provide a structure of an observer for real-time applications. Wake models represent the flow field created downstream of a turbine (commonly known as the wake) with varying levels of accuracy depending on the specific model used. These models already encompass a wide range of environmental and operational conditions, enabling the description of almost every application scenario. However, novel control techniques are currently being investigated by researchers, and this information is yet to be integrated into any engineering model. Engineering wake models are crucial for the future application of new control strategies. To dynamically optimize the configuration of turbines within a wind farm, it is essential to have accurate information about their wakes and how these wakes affect neighboring turbines. This information can be easily extracted from wake models.
The proposed framework aims to incorporate the helix approach into the engineering wake model through the model's parameters and their calibration process.

First of all, the best wake model is chosen between the Bastankhah (Gaussian) and Super Gaussian model. Despite the simplicity of a purely Gaussian description, the model is not able to describe accurately the wake in the immediately below region of the rotor. The super Gaussian model evolves from a top-hat shape to a Gaussian shape, resembling the Gaussian model far away from the rotor, but increasing the accuracy in the near wake were the wake profile appear to be more flattened. This has been proven by calculating the mean absolute error between the wind velocity field extracted from LES and the wind velocity field generated by the respective models. The error produced by the Gaussian model is 0.28, while with Super Gaussian a value of 0.23 is reached (18% lower).

Secondly, a robust calibration procedure has been identified through a trade off between accuracy and computation time. The two wake models have been calibrated through an optimization problem aiming at minimizing the mean absolute error between the velocity fields from real data and from the respective models. Large Eddy Simulations have been used as the reference wind field that should be reproduced by the wake model because of their completeness in representing the overall wake effect compared to the others data sets. Different heuristic optimization algorithms have been tested: Differential Evolution, Simulated Annealing and Genetic Algorithm. Genetic Algorithm resulted in being the less accurate while Simulated Annealing despite its high accuracy requires more time to converge to the optimal solution. Differential Evolution turned out to be the best because of its ability to combine accuracy and speed of convergence.

The accuracy of the calibration process is very sensitive and the optimizer hyper-parameters must be tuned adequately in order to assure the discovery of the global optimum. **The stability of the solution is found as a trade-off between the hyper-parameters**, challenging the most common problem of optimization: the existence local minima. The more the wake model is complicated (often supported by a larger number of model parameters) and the more the search space must be investigated. For the Super Gaussian model this is achieved increasing the population size of the Differential Evolution algorithm prioritizing the identification of the region were the optimum resides rather than an accurate search around a presumed optimum.

Testing how sensitive the analysis is depending on inflow conditions allows the determination of the range of application of a certain set of calibrated parameters. The calibration process has been carried out for different inflow wind speeds below rated conditions. The error in using a generic set of parameters calibrated for a specific wind speed to describe also the other wind speeds has been proven to be negligible. This analysis allows to extend the range of application of one single calibration for all the wind speeds in the partial load region of the power curve (if nothing else in the environment conditions is changed).

Finally the information of the wind farm flow control is introduced in the analysis. **The helix approach has been investigated by calibrating the Super Gaussian model for different pitch angle amplitudes with a fixed frequency of the control signal.** The new discovery consists in a trend the model parameters have depending on the signal amplitude that can be described by a polynomial function of second order. If each model parameter is included in the original Super Gaussian model though this dependence on the pitch angle's amplitude, the final model has a new set of parameters which still requires calibration but reduces this need to a single procedure instead of one every different amplitude.

The newly extended model, incorporating helix approach information, was tested to optimize online wind farm performance for different wind directions. The benefits of the helix approach were demonstrated by comparing its performance to normal "greedy control," where the turbines operate to maximize their own singular performance. This comparison showed the helix approach's advantage in reducing wake losses and improving overall wind farm efficiency especially when turbines are arranged in a row. The power can increase up to 17% in a cluster of five turbines if the upstream ones have the helix control applied.

6.2. Limitations and Further Work

The current study has some limitations that must be addressed to improve the robustness and applicability of the wake model. Firstly, the calibration process needs to incorporate more realistic inflow conditions, including varying turbulence intensities and atmospheric stability classes. This would ensure that the model performs accurately under diverse environmental conditions typically encountered in real-world scenarios.
Another improvement resides in the adequacy of the blockage and turbulence models used. Enhancing these models to more accurately reflect the physical phenomena occurring in wind farms would likely improve the overall performance and reliability of the wake predictions. Since aerodynamic properties are influenced by environmental conditions, the blockage and turbulence models may vary under different inflow scenarios. Therefore, it is essential to carefully examine and evaluate each situation to ensure accurate modeling.
Additionally, the dependency of the helix approach on the Strouhal number should be further investigated, as the frequency is a crucial parameter in the helix signal that can significantly influence the wake shape. This exploration could lead to the development of a three-dimensional function that describes the relationship between model parameters and both the amplitude and frequency of the helix signal. The resulting expanded wake model would comprehensively account for all potential scenarios arising from the application of the helix approach.
The current study's application is limited to a specific set of wind farm configurations for a single wind farm. Extending the analysis to a wider range of wind farms with varying layouts, turbine types, and operational strategies is essential for validating the model's generalizability and effectiveness across different scenarios.

6.3. Recommendations

To advance the integration and optimization of the helix approach in engineering wake models, several recommendations are proposed. Firstly, parallelizing the optimization problems could significantly decrease the computation time required for calibration, making the process more efficient and feasible for large-scale applications.

Secondly, for effective model calibration, it is essential to model the turbine in a manner consistent with experimental data by incorporating detailed power and thrust coefficient curves into PyWake. This alignment will ensure that the wake model accurately represents the actual performance characteristics of the turbines.
Conducting highly accurate calibrations when the helix approach is active is crucial. Ensuring precision in the calibration process will enhance the reliability of the model, as the parameters are highly sensitive and even slight changes can lead to significant variations in the fitting curve and the final extended model. Therefore, a meticulous fine-tuning process of the optimizer's hyperparameters is essential and necessary.
Finally, it is recommended to formulate a completely new engineering model that directly incorporates the aerodynamics resulting from the control signal applied to the rotor. This approach would provide a more integrated and holistic representation of wake dynamics, enhancing the model's ability to optimize wind farm performance. Subsequently, the analysis can be extended to non-steady-state conditions to dynamically describe wake formation over time.

References

[1] S J Andersen et al. “Comparison of Engineering Wake Models with CFD Simulations”. In: *Journal of Physics: Conference Series* 524.1 (June 2014), p. 012161. DOI: 10.1088/1742-6596/524/1/012161. URL: https://dx.doi.org/10.1088/1742-6596/524/1/012161.

[2] Leif Erik Andersson et al. *Wind farm control - Part I: A review on control system concepts and structures*. July 2021. DOI: 10.1049/rpg2.12160.

[3] Jennifer Annoni et al. “Evaluating wake models for wind farm control”. In: *2014 American Control Conference*. 2014, pp. 2517–2523. DOI: 10.1109/ACC.2014.6858970.

[4] Jennifer Annoni et al. “Evaluating wake models for wind farm control”. In: *2014 American Control Conference*. 2014, pp. 2517–2523. DOI: 10.1109/ACC.2014.6858970.

[5] Majid Bastankhah and Fernando Porté-Agel. “A new analytical model for wind-turbine wakes”. In: *Renewable Energy* 70 (2014). Special issue on aerodynamics of offshore wind energy systems and wakes, pp. 116–123. ISSN: 0960-1481. DOI: https://doi.org/10.1016/j.renene.2014.01.002. URL: https://www.sciencedirect.com/science/article/pii/S0960148114000317.

[6] Majid Bastankhah and Fernando Porté-Agel. “A New Miniature Wind Turbine for Wind Tunnel Experiments. Part I: Design and Performance”. In: *Energies* 10.7 (2017). DOI: 10.3390/en10070908. URL: https://www.mdpi.com/1996-1073/10/7/908.

[7] Majid Bastankhah and Fernando Porté-Agel. “Experimental and theoretical study of wind turbine wakes in yawed conditions”. In: *Journal of Fluid Mechanics* 806 (2016), pp. 506–541.

[8] Maarten T. van Beek, Axelle Viré, and Søren J. Andersen. “Sensitivity and Uncertainty of the FLORIS Model Applied on the Lillgrund Wind Farm”. In: *Energies* 14.5 (2021). DOI: 10.3390/en14051293. URL: https://www.mdpi.com/1996-1073/14/5/1293.

[9] Gunjit Bir. “Multi-blade coordinate transformation and its application to wind turbine analysis”. In: *46th AIAA aerospace sciences meeting and exhibit*. 2008, p. 1300.

[10] F. Blondel. “Brief communication: A momentum-conserving superposition method applied to the super-Gaussian wind turbine wake model”. In: *Wind Energy Science* 8.2 (2023), pp. 141–147. DOI: 10.5194/wes-8-141-2023. URL: https://wes.copernicus.org/articles/8/141/2023/.

[11] F. Blondel and M. Cathelain. “An alternative form of the super-Gaussian wind turbine wake model”. In: *Wind Energy Science* 5.3 (2020), pp. 1225–1236. DOI: 10.5194/wes-5-1225-2020. URL: https://wes.copernicus.org/articles/5/1225/2020/.

[12] Sjoerd Boersma et al. “A tutorial on control-oriented modeling and control of wind farms”. In: *2017 American control conference (ACC)*. IEEE. 2017, pp. 1–18.

[13] Ervin A Bossanyi. “Individual blade pitch control for load reduction”. In: *Wind Energy: An International Journal for Progress and Applications in Wind Power Conversion Technology* 6.2 (2003), pp. 119–128.

[14] Emmanuel Branlard et al. “Wind farm blockage effects: comparison of different engineering models”. In: *Journal of Physics: Conference Series* 1618.6 (Sept. 2020), p. 062036. DOI: 10.1088/1742-6596/1618/6/062036. URL: https://dx.doi.org/10.1088/1742-6596/1618/6/062036.

[15] Dan G Cacuci, Mihaela Ionescu-Bujor, and Ionel Michael Navon. *Sensitivity and uncertainty analysis, volume II: applications to large-scale systems*. CRC press, 2005.

[16] J Elliott Campbell et al. “Photosynthetic control of atmospheric carbonyl sulfide during the growing season”. In: *Science* 322.5904 (2008), pp. 1085–1088.

[17] Fernando Carbajo Fuertes, Corey D. Markfort, and Fernando Porté-Agel. “Wind Turbine Wake Characterization with Nacelle-Mounted Wind Lidars for Analytical Wake Model Validation”. In: *Remote Sensing* 10.5 (2018). ISSN: 2072-4292. DOI: 10.3390/rs10050668. URL: https://www.mdpi.com/2072-4292/10/5/668.

[18] Tianfeng Chai, Roland R Draxler, et al. “Root mean square error (RMSE) or mean absolute error (MAE)”. In: *Geoscientific model development discussions* 7.1 (2014), pp. 1525–1534.

[19] Antonio Crespo, J Herna, et al. “Turbulence characteristics in wind-turbine wakes”. In: *Journal of wind engineering and industrial aerodynamics* 61.1 (1996), pp. 71–85.

[20] Veronica Czitrom. “One-factor-at-a-time versus designed experiments”. In: *The American Statistician* 53.2 (1999), pp. 126–131.

[21] OpenFAST Documentation. “Release v3. 1.0”. In: *National Renewable Energy Laboratory. Code published at. https://github. com/OpenFAST/openfast. https://openfast. readthedocs. io/en/master* (2022).

[22] Bart M Doekemeijer, Jan-Willem Van Wingerden, and Paul A Fleming. “A tutorial on the synthesis and validation of a closed-loop wind farm controller using a steady-state surrogate model”. In: *2019 American Control Conference (ACC)*. 2019, pp. 2825–2836. DOI: 10.23919/ACC.2019.8815126.

[23] Hongyang Dong, Jingjie Xie, and Xiaowei Zhao. *Wind farm control technologies: From classical control to reinforcement learning*. July 2022. DOI: 10.1088/2516-1083/ac6cc1.

[24] T. Duc et al. “Local turbulence parameterization improves the Jensen wake model and its implementation for power optimization of an operating wind farm”. In: *Wind Energy Science* 4.2 (2019), pp. 287–302. DOI: 10.5194/wes-4-287-2019. URL: https://wes.copernicus.org/articles/4/287/2019/.

[25] Sten Frandsen. “Turbulence and turbulence-generated structural loading in wind turbine clusters”. In: (2007).

[26] Joeri A Frederik et al. “The helix approach: Using dynamic individual pitch control to enhance wake mixing in wind farms”. In: *Wind Energy* 23.8 (2020), pp. 1739–1751.

[27] Joeri Alexis Frederik et al. “Periodic dynamic induction control of wind farms: proving the potential in simulations and wind tunnel experiments”. In: *Wind Energy Science* 5.1 (2020), pp. 245–257.

[28] Siemens Gamesa. *Siemens Gamesa Wake Adapt*. [Accessed: 20-Jul-2024]. 2019. URL: https://www.siemensgamesa.com/en-int/newsroom/2019/11/191126-siemens-gamesa-wake-adapt-en.

[29] Pieter Gebraad et al. “Maximization of the annual energy production of wind power plants by optimization of layout and yaw-based wake control”. In: *Wind Energy* 20.1 (2017), pp. 97–107.

[30] Graham Glen and Kristin Isaacs. “Estimating Sobol sensitivity indices using correlations”. In: *Environmental Modelling Software* 37 (2012), pp. 157–166. ISSN: 1364-8152. DOI: https://doi.org/10.1016/j.envsoft.2012.03.014. URL: https://www.sciencedirect.com/science/article/pii/S1364815212001065.

[31] Tuhfe Göçmen and Gregor Giebel. “Estimation of turbulence intensity using rotor effective wind speed in Lillgrund and Horns Rev-I offshore wind farms”. In: *Renewable energy* 99 (2016), pp. 524–532.

[32] Jay P. Goit and Johan Meyers. “Optimal control of energy extraction in wind-farm boundary layers”. In: *Journal of Fluid Mechanics* 768 (2015), pp. 5–50. DOI: 10.1017/jfm.2015.70.

[33] John F. Hall et al. “Wind energy conversion with a variable-ratio gearbox: design and analysis”. In: *Renewable Energy* 36.3 (2011), pp. 1075–1080. ISSN: 0960-1481. DOI: https://doi.org/10.1016/j.renene.2010.08.037. URL: https://www.sciencedirect.com/science/article/pii/S0960148110004088.

[34] Nikolaus Hansen, Dirk V. Arnold, and Anne Auger. “Evolution Strategies”. In: *Springer Handbook of Computational Intelligence*. Ed. by Janusz Kacprzyk and Witold Pedrycz. Berlin, Heidelberg: Springer Berlin Heidelberg, 2015, pp. 871–898. DOI: 10.1007/978-3-662-43505-2_44. URL: https://doi.org/10.1007/978-3-662-43505-2_44.

[35] Amr Hegazy et al. “LiDAR and SCADA data processing for interacting wind turbine wakes with comparison to analytical wake models”. In: *Renewable Energy* 181 (2022), pp. 457–471. ISSN: 0960-1481. DOI: https://doi.org/10.1016/j.renene.2021.09.019. URL: https://www.sciencedirect.com/science/article/pii/S0960148121013173.

[36] Jon Herman and Will Usher. "SALib: An open-source Python library for Sensitivity Analysis". In: *The Journal of Open Source Software* 2.9 (Jan. 2017). DOI: 10.21105/joss.00097. URL: https://doi.org/10.21105/joss.00097.

[37] Toshimitsu Homma and Andrea Saltelli. "Importance measures in global sensitivity analysis of nonlinear models". In: *Reliability Engineering & System Safety* 52.1 (1996), pp. 1–17.

[38] LJ Huang et al. "Enhancing Wake Mixing in Wind Farms by Multi-Sine Signals in the Helix Approach". In: *2023 American Control Conference (ACC)*. IEEE. 2023, pp. 824–830.

[39] Takuya Iwanaga, William Usher, and Jonathan Herman. "Toward SALib 2.0: Advancing the accessibility and interpretability of global sensitivity analyses". In: *Socio-Environmental Systems Modelling* 4 (May 2022), p. 18155. DOI: 10.18174/sesmo.18155. URL: https://sesmo.org/article/view/18155.

[40] N O Jensen. *A Note on wind generator interaction*. Denmark, 1983.

[41] Ángel Jiménez, Antonio Crespo, and Emilio Migoya. "Application of a LES technique to characterize the wake deflection of a wind turbine in yaw". In: *Wind energy* 13.6 (2010), pp. 559–572.

[42] I Katic, Jørgen Højstrup, Niels Otto Jensen, et al. "A simple model for cluster efficiency". In: *European wind energy association conference and exhibition*. Vol. 1. A. Raguzzi Rome, Italy. 1986, pp. 407–410.

[43] Hyungyu Kim et al. "Wind Turbine Wake Characterization for Improvement of the Ainslie Eddy Viscosity Wake Model". In: *Energies* 11.10 (2018). ISSN: 1996-1073. DOI: 10.3390/en11102823. URL: https://www.mdpi.com/1996-1073/11/10/2823.

[44] Gunner C Larsen et al. "Yaw induced wake deflection-a full-scale validation study". In: *Journal of Physics: Conference Series*. Vol. 1618. 6. IOP Publishing. 2020, p. 062047.

[45] D. Mehta et al. "Large Eddy Simulation of wind farm aerodynamics: A review". In: *Journal of Wind Engineering and Industrial Aerodynamics* 133 (2014), pp. 1–17. ISSN: 0167-6105. DOI: https://doi.org/10.1016/j.jweia.2014.07.002. URL: https://www.sciencedirect.com/science/article/pii/S0167610514001391.

[46] Johan Meyers et al. *Wind farm flow control: Prospects and challenges*. Nov. 2022. DOI: 10.5194/wes-7-2271-2022.

[47] W. Munters and J. Meyers. "Towards practical dynamic induction control of wind farms: analysis of optimally controlled wind-farm boundary layers and sinusoidal induction control of first-row turbines". In: *Wind Energy Science* 3.1 (2018), pp. 409–425. DOI: 10.5194/wes-3-409-2018. URL: https://wes.copernicus.org/articles/3/409/2018/.

[48] James M Murphy et al. "Quantification of modelling uncertainties in a large ensemble of climate change simulations". In: *Nature* 430.7001 (2004), pp. 768–772.

[49] C Muscari et al. "Physics informed DMD for periodic dynamic induction control of wind farms". In: *Journal of Physics: Conference Series*. Vol. 2265. 2. IOP Publishing. 2022, p. 022057.

[50] National Renewable Energy Laboratory (NREL). *FLORIS*. Version 2.0.1. 2020. URL: https://github.com/NREL/floris.

[51] Amin Niayifar and Fernando Porté-Agel. "Analytical Modeling of Wind Farms: A New Approach for Power Prediction". In: *Energies* 9.9 (2016). ISSN: 1996-1073. DOI: 10.3390/en9090741. URL: https://www.mdpi.com/1996-1073/9/9/741.

[52] Jackson G. Njiri and Dirk Söffker. "State-of-the-art in wind turbine control: Trends and challenges". In: *Renewable and Sustainable Energy Reviews* 60 (2016), pp. 377–393. ISSN: 1364-0321. DOI: https://doi.org/10.1016/j.rser.2016.01.110. URL: https://www.sciencedirect.com/science/article/pii/S1364032116001404.

[53] Nicolai Gayle Nygaard et al. "Modelling cluster wakes and wind farm blockage". In: *Journal of Physics: Conference Series* 1618.6 (Sept. 2020), p. 062072. DOI: 10.1088/1742-6596/1618/6/062072. URL: https://dx.doi.org/10.1088/1742-6596/1618/6/062072.

[54] Lucy Y. Pao and Kathryn E. Johnson. "A tutorial on the dynamics and control of wind turbines and wind farms". In: *2009 American Control Conference*. 2009, pp. 2076–2089. DOI: 10.1109/ACC.2009.5160195.

[55] J G Pedersen et al. “Turbulence Optimized Park model with Gaussian wake profile”. In: *Journal of Physics: Conference Series* 2265.2 (May 2022), p. 022063. DOI: 10.1088/1742-6596/2265/2/022063. URL: https://dx.doi.org/10.1088/1742-6596/2265/2/022063.

[56] Mads M. Pedersen et al. *PyWake 2.5.0: An open-source wind farm simulation tool*. Version 2.5.0. Feb. 2023. URL: https://gitlab.windenergy.dtu.dk/TOPFARM/PyWake.

[57] JTG Pierik et al. “European wind turbine standards II (EWTS-II)”. In: *1999 European Wind Energy Conference*. Routledge. 2014, pp. 568–571.

[58] Python Software Foundation. *Python Programming Language*. Version 3.10.0, Accessed: 2024-08-10. 2024. URL: https://www.python.org/.

[59] Andrea Saltelli et al. “Variance based sensitivity analysis of model output. Design and estimator for the total sensitivity index”. In: *Computer Physics Communications* 181.2 (2010), pp. 259–270. ISSN: 0010-4655. DOI: https://doi.org/10.1016/j.cpc.2009.09.018. URL: https://www.sciencedirect.com/science/article/pii/S0010465509003087.

[60] Benjamin Sanderse, SP Van der Pijl, and Barry Koren. “Review of computational fluid dynamics for wind turbine wake aerodynamics”. In: *Wind energy* 14.7 (2011), pp. 799–819.

[61] Hilary L Seal. “Studies in the History of Probability and Statistics. XV The historical development of the Gauss linear model”. In: *Biometrika* 54.1-2 (1967), pp. 1–24.

[62] Alessandro Sebastiani et al. “Data analysis and simulation of the Lillgrund wind farm”. In: *Wind Energy* 24.6 (2021), pp. 634–648.

[63] Rabia Shakoor et al. “Wake effect modeling: A review of wind farm layout optimization using Jensen׳s model”. In: *Renewable and Sustainable Energy Reviews* 58 (2016), pp. 1048–1059. ISSN: 1364-0321. DOI: https://doi.org/10.1016/j.rser.2015.12.229. URL: https://www.sciencedirect.com/science/article/pii/S1364032115016123.

[64] IM Soboĺ. “Sensitivity estimates for nonlinear mathematical models”. In: *Math. Model. Comput. Exp.* 1 (1993), p. 407.

[65] Ishaan Sood and Johan Meyers. “Tuning of an engineering wind farm model using measurements from Large Eddy Simulations”. In: *Journal of Physics: Conference Series* 2265.2 (May 2022), p. 022045. DOI: 10.1088/1742-6596/2265/2/022045. URL: https://dx.doi.org/10.1088/1742-6596/2265/2/022045.

[66] Maarten Steinbuch et al. “Optimal control of wind power plants”. In: *Journal of Wind Engineering and Industrial Aerodynamics* 27.1 (1988), pp. 237–246.

[67] Rainer Storn and Kenneth Price. *Differential Evolution-A Simple and Efficient Heuristic for Global Optimization over Continuous Spaces*. 1997.

[68] B Suman and P Kumar. “A survey of simulated annealing as a tool for single and multiobjective optimization”. In: *Journal of the Operational Research Society* 57.10 (2006), pp. 1143–1160. DOI: 10.1057/palgrave.jors.2602068. URL: https://doi.org/10.1057/palgrave.jors.2602068.

[69] Emanuel Taschner et al. “On the performance of the helix wind farm control approach in the conventionally neutral atmospheric boundary layer”. In: *Journal of Physics: Conference Series*. Vol. 2505. 1. IOP Publishing. 2023, p. 012006.

[70] Jannis Tautz-Weinert and Simon J. Watson. “Using SCADA data for wind turbine condition monitoring – a review”. In: *IET Renewable Power Generation* 11.4 (2017), pp. 382–394. DOI: https://doi.org/10.1049/iet-rpg.2016.0248. eprint: https://ietresearch.onlinelibrary.wiley.com/doi/pdf/10.1049/iet-rpg.2016.0248. URL: https://ietresearch.onlinelibrary.wiley.com/doi/abs/10.1049/iet-rpg.2016.0248.

[71] Jian Teng and Corey D. Markfort. “A Calibration Procedure for an Analytical Wake Model Using Wind Farm Operational Data”. In: *Energies* 13.14 (2020). URL: https://www.mdpi.com/1996-1073/13/14/3537.

[72] Daan Van der Hoek et al. “Maximizing wind farm power output with the helix approach: Experimental validation and wake analysis using tomographic particle image velocimetry”. In: *Wind Energy* 27.5 (2024), pp. 463–482.

[73] Vattenfall. *Lillgrund Wind Farm*. Accessed: 2024-06-23. 2024. URL: https://powerplants.vattenfall.com/en/lillgrund/#/.

[74] P. E. J. Vermeulen. “An experimental analysis of wind turbine wakes”. In: *3rd International Symposium on Wind Energy Systems*. Jan. 1980, pp. 431–450.

[75] Dongshu Wang, Dapei Tan, and Lei Liu. “Particle swarm optimization algorithm: an overview”. In: *Soft Computing* 22 (2 Jan. 2018), pp. 387–408. ISSN: 14337479. DOI: 10.1007/s00500-016-2474-6.

[76] Cort J. Willmott, Kenji Matsuura, and Scott M. Robeson. “Ambiguities inherent in sums-of-squares-based error statistics”. In: *Atmospheric Environment* 43.3 (2009), pp. 749–752. ISSN: 1352-2310. DOI: https://doi.org/10.1016/j.atmosenv.2008.10.005. URL: https://www.sciencedirect.com/science/article/pii/S1352231008009564.

[77] Pushpendra Kumar Yadav and NL Prajapati. “An overview of genetic algorithm and modeling”. In: *International Journal of Scientific and Research Publications* 2.9 (2012), pp. 1–4.

[78] Puyi Yang and Hamidreza Najafi. “The effect of using different wake models on wind farm layout optimization: A comparative study”. In: *Journal of Energy Resources Technology* 144.7 (2022), p. 070904.

[79] Frederik Zahle et al. *Definition of the IEA Wind 22-Megawatt Offshore Reference Wind Turbine*. Tech. rep. DTU Wind Report E-0243, https://doi.org/10.11581/DTU.00000317. Technical University of Denmark, International Energy Agency, 2024.

[80] L. Zhan, S. Letizia, and G. V. Iungo. “Optimal tuning of engineering wake models through lidar measurements”. In: *Wind Energy Science* 5.4 (2020), pp. 1601–1622. DOI: 10.5194/wes-5-1601-2020. URL: https://wes.copernicus.org/articles/5/1601/2020/.

[81] Haohua Zong and Fernando Porté-Agel. “A momentum-conserving wake superposition method for wind farm power prediction”. In: *Journal of Fluid Mechanics* 889 (2020), A8. DOI: 10.1017/jfm.2020.77.

A

Wind velocity field

A.1. Flow field with baseline conditions and different incoming wind speeds

Velocity field from LES

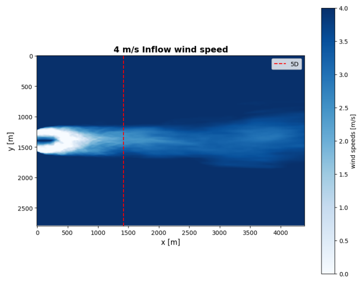

(a) LES incoming wind speed = 4 m/s

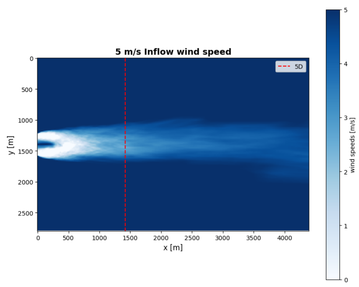

(b) LES incoming wind speed = 5 m/s

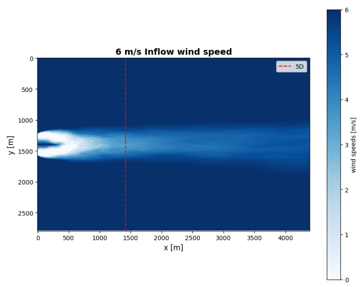

(c) LES incoming wind speed = 6 m/s

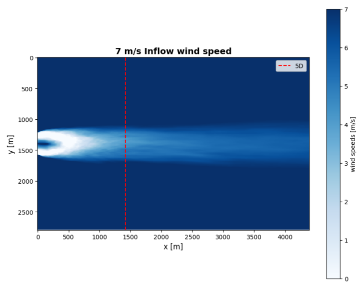

(d) LES incoming wind speed = 7 m/s

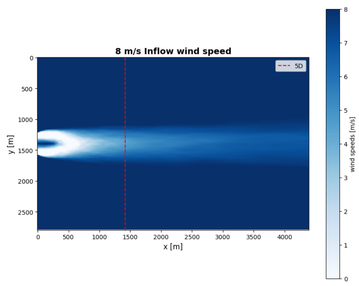

(e) LES incoming wind speed = 8 m/s

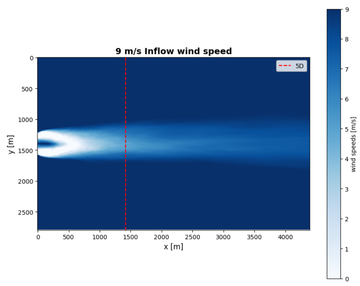

(f) LES incoming wind speed = 9 m/s

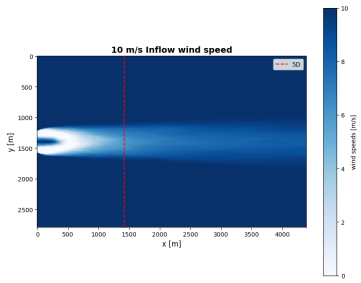

(g) LES incoming wind speed = 10 m/s

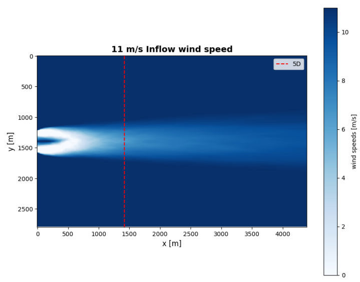

(h) LES incoming wind speed = 11 m/s

Figure A.1: LES wake representation for different incoming wind speed - baseline simulation (no dynamic control)

Velocity field from PyWake after the calibration process

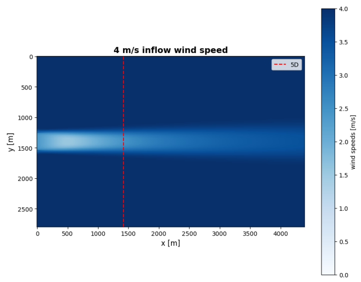

(a) Incoming wind speed = 4 m/s

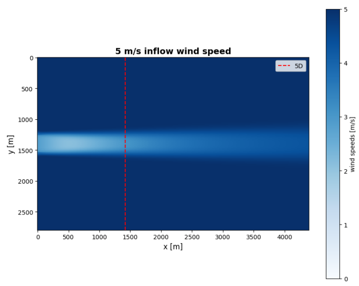

(b) Incoming wind speed = 5 m/s

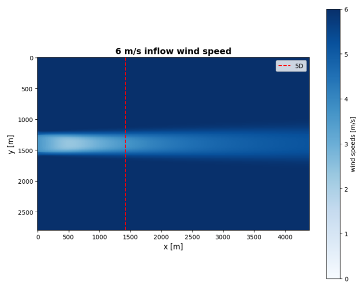

(c) Incoming wind speed = 6 m/s

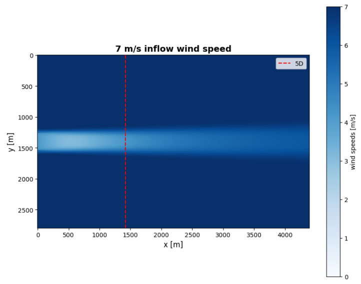

(d) Incoming wind speed = 7 m/s

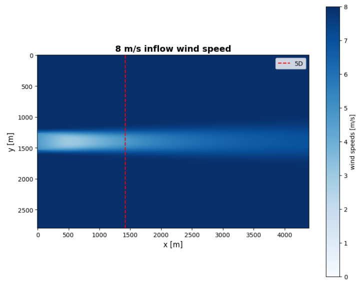

(e) Incoming wind speed = 8 m/s

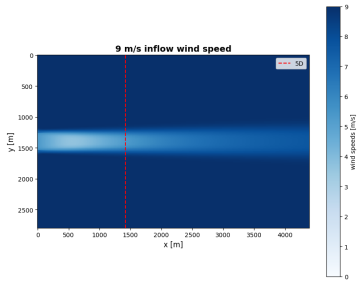

(f) Incoming wind speed = 9 m/s

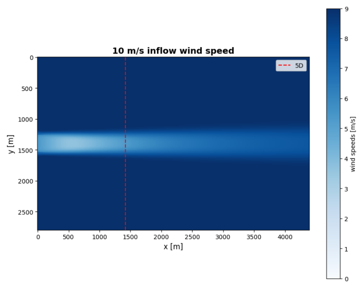

(g) Incoming wind speed = 10 m/s

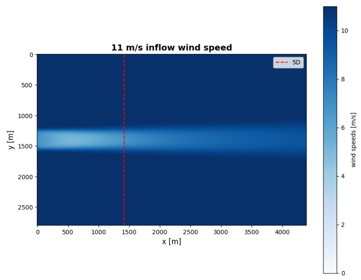

(h) Incoming wind speed = 11 m/s

Figure A.2: Wind field wake representation of SuperGaussian model calibrated for different inflow wind speeds

A.2. Flow field with helix approach applied

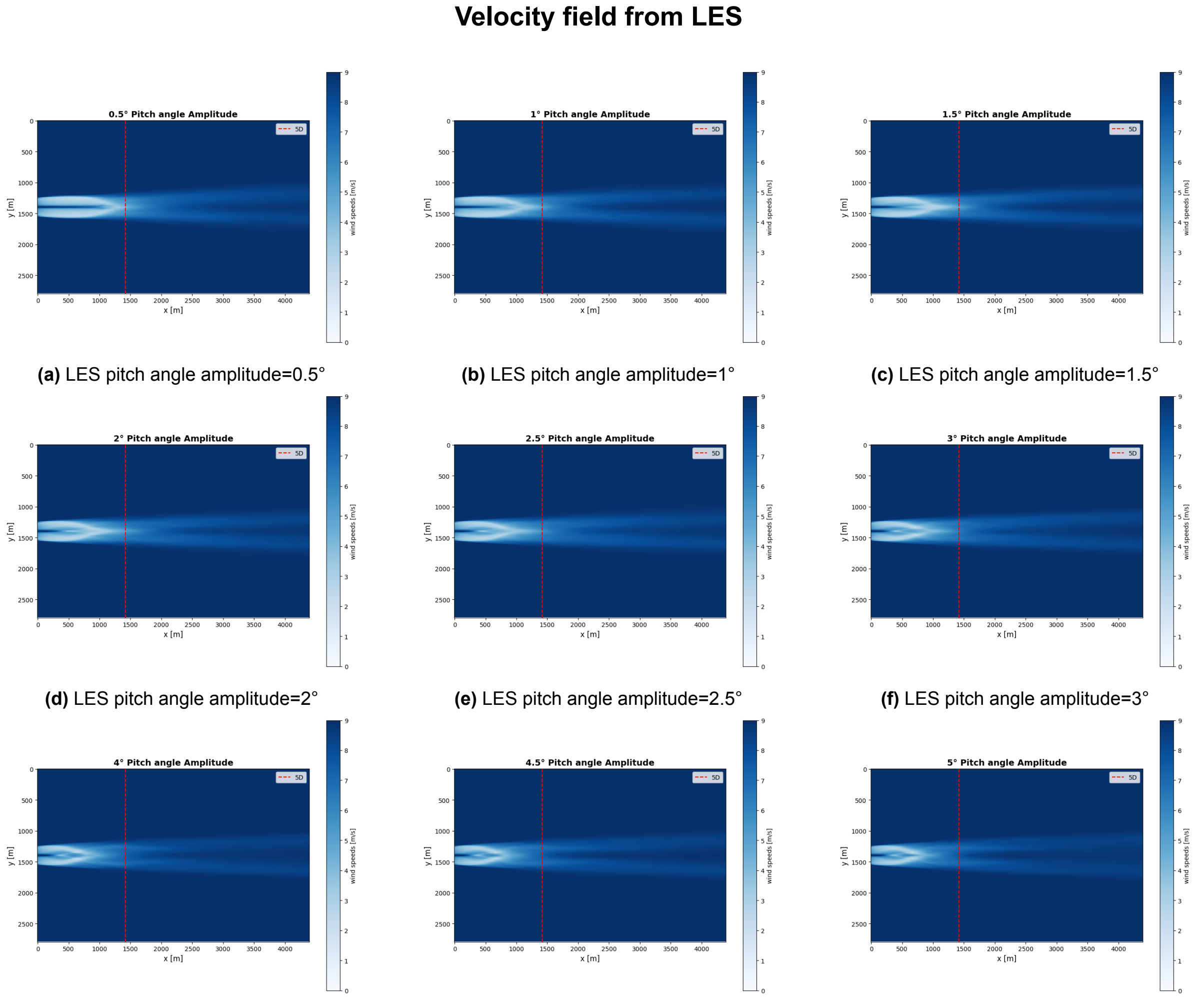

(a) LES pitch angle amplitude=0.5°

(b) LES pitch angle amplitude=1°

(c) LES pitch angle amplitude=1.5°

(d) LES pitch angle amplitude=2°

(e) LES pitch angle amplitude=2.5°

(f) LES pitch angle amplitude=3°

(g) LES pitch angle amplitude=4°

(h) LES pitch angle amplitude=4.5°

(i) LES pitch angle amplitude=5°

Figure A.3: LES wake representation for different pitch angle amplitudes of helix control

Velocity field from PyWake after the calibration process

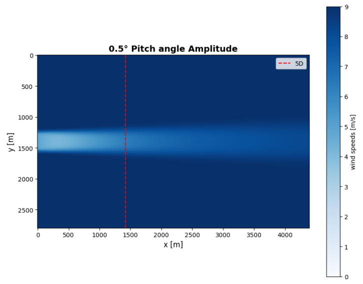

(a) Pitch angle amplitude=0.5°

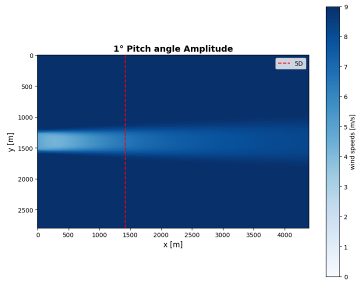

(b) Pitch angle amplitude=1°

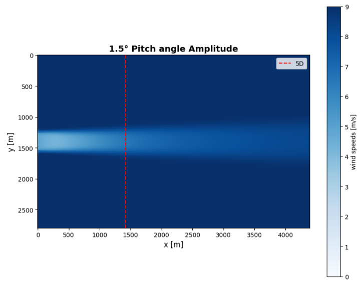

(c) Pitch angle amplitude=1.5°

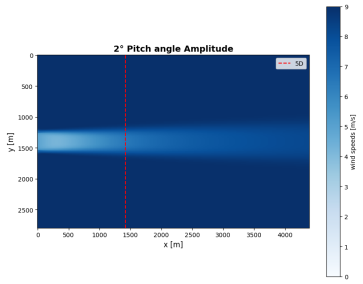

(d) Pitch angle amplitude=2°

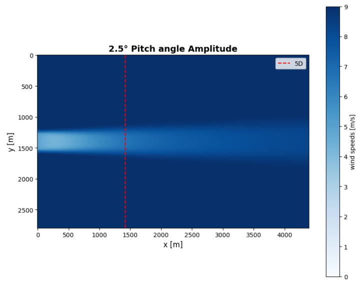

(e) Pitch angle amplitude=2.5°

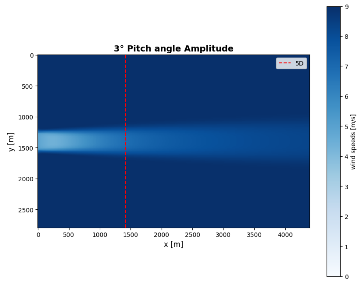

(f) Pitch angle amplitude=3°

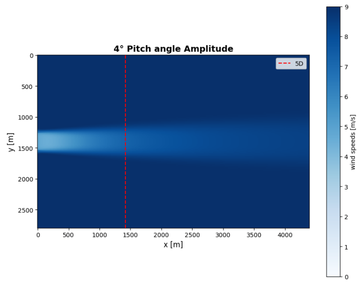

(g) Pitch angle amplitude=4°

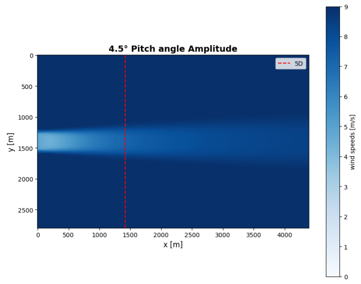

(h) Pitch angle amplitude=4.5°

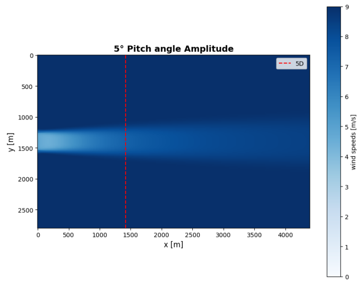

(i) Pitch angle amplitude=5°

Figure A.4: Wind field wake representation of SuperGaussian model calibrated for different pitch angle amplitudes of helix control

B
OpenFast

This section provides insight into the modeling of the wind turbine's behavioral response to inflow wind using OpenFast. The turbine has been modelled as a rigid body and the incoming wind as steady throughout the entire analysis. The simulation time has been set to 700 seconds with time steps of 0.01 seconds. Additional simulation time is unnecessary; the key is to reach a stable response, disregarding the initial transient adjustment period. The aim of this analysis is to accurately model the turbine response in order to obtain the correct power and thrust coefficient curves, which are essential for representing the turbine's behavior and performance in PyWake. To achieve this, OpenFast simulations are conducted at multiple wind speeds (with a higher number of speeds providing better results). The resulting data is then used to interpolate a curve that accurately fits the output values.
Since the control objectives differ between the normal operation of wind turbines (referred to as "baseline") and the application of the helix approach control, the turbine response must be modeled accordingly. Section B.1 focuses on the modeling of baseline conditions, while Section B.2 introduces the effects of the helix approach.

B.1. Baseline Simulation

To illustrate the turbine's response, only four representative wind speeds have been selected. The following Table details these wind speeds and their respective operational regions.

Wind Speed [m/s]	Operational Region
6.15	Partial Load region
9.02	Partial Load region
11.17	Rated Conditions (transition from partial load to full load)
17.67	Full Load Region

The Partial Load Region occurs before the rated wind speed. In this mode, the goal is to maximize power output by keeping the power coefficient at its optimal value. This requires maintaining the blade pitch angle at an optimal, constant setting. The thrust coefficient also remains constant at its maximum value in this region, which ensures the highest energy extraction. When rated conditions are reached at 11 m/s, the power is constrained to its rated value to prevent mechanical and electrical damage. This is achieved by adjusting the blade pitch away from the optimal energy extraction configuration. As a result, both the power and thrust coefficients decrease. These effects are illustrated in the following plots.

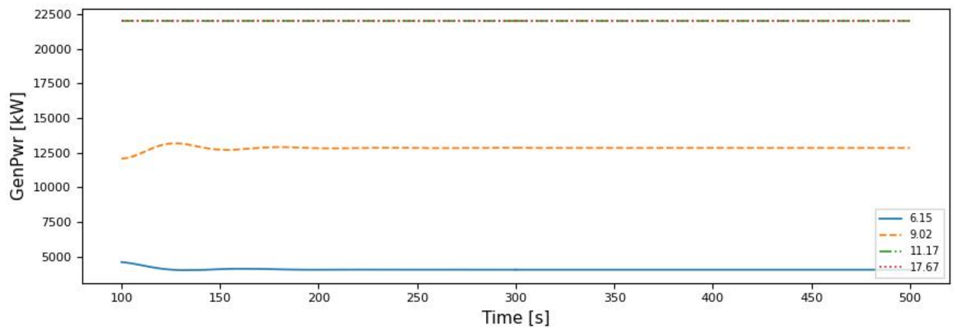

Figure B.1: OpenFast Simulation output (Power Produced [kW]) for wind speeds= [6.15,9.02,11.17,17.67]. Time interval 100-500 s.

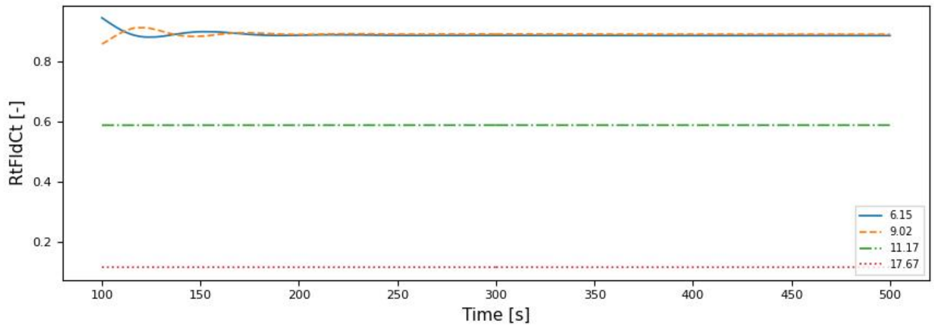

Figure B.2: OpenFast Simulation output (Thrust Coefficient [-]) for wind speeds= [6.15,9.02,11.17,17.67]. Time interval 100-500 s.

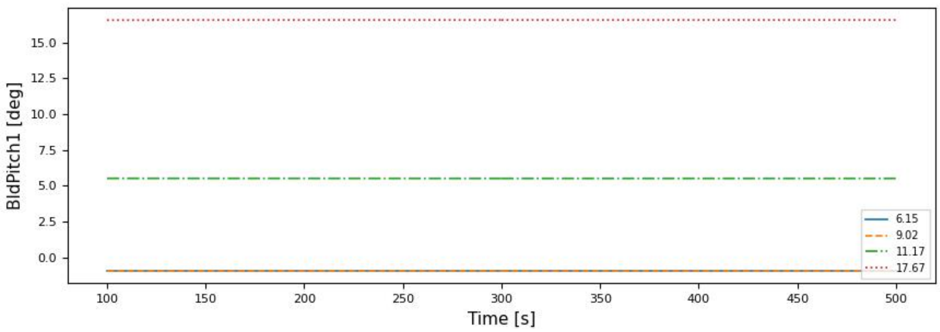

Figure B.3: OpenFast Simulation output (Pitch Angle [deg]) for wind speeds= [6.15,9.02,11.17,17.67]. Time interval 100-500 s.

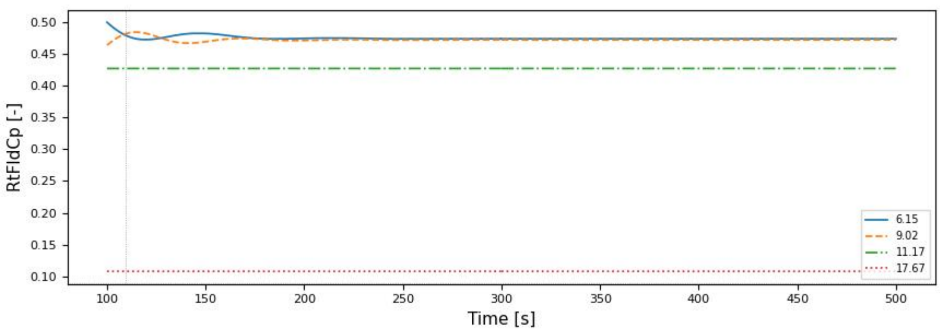

Figure B.4: OpenFast Simulation output (Power Coefficient [-]) for wind speeds= [6.15,9.02,11.17,17.67]. Time interval 100-500 s.

B.2. Helix Approach Simulation

When the helix approach is implemented, the blade pitch angles exhibit a sinusoidal variation with specific frequency and amplitude. Figure B.5 illustrates the sinusoidal behavior of the pitch angle for one blade at a wind speed of 6.97 m/s, showcasing different amplitudes with a fixed frequency.

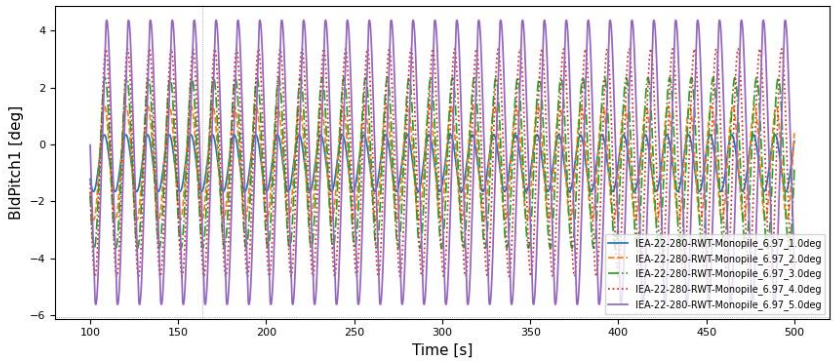

Figure B.5: OpenFast Simulation output (Pitch Angle [deg]) for pitch angle amplitudes= [1,2,3,4,5] and incoming wind speed=6.97 m/s. Time interval 100-500 s.

As the amplitude of the sinusoidal variation increases, the effect of the control becomes more pronounced, leading to greater wake mixing. However, with a larger amplitude, the turbine moves further from its optimal energy production configuration, resulting in increased power losses. Figure B.6 depicts the decrease of the power produced with increasing pitch amplitude.

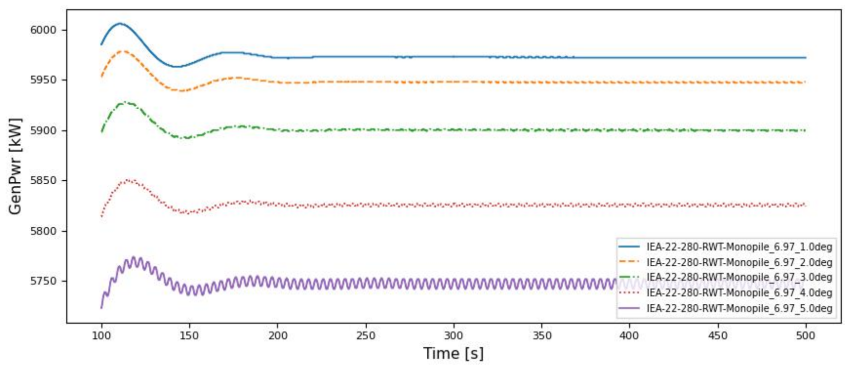

Figure B.6: OpenFast Simulation output (Power Produced [kW]) for pitch angle amplitudes= [1,2,3,4,5] and incoming wind speed=6.97 m/s. Time interval 100-500 s.

The same behaviour can be observed for other wind speeds.